UNIVERSITY OF CALIFORNIA,
IRVINE

Passive and Semi-Active Control of Civil Structures

DISSERTATION

submitted in partial satisfaction of the requirements
for the degree of

DOCTOR OF PHILOSOPHY

in Mechanical and Aerospace Engineering

by

Shant Aram Danielian

Dissertation Committee:
Professor Faryar Jabbari, Chair
Professor Farzin Zareian
Professor Mark Walter

2023

DEDICATION

To Mom and Dad

TABLE OF CONTENTS

LIST OF FIGURES

ACKNOWLEDGMENTS

I would like to first thank my advisor and dissertation committee chair Professor Faryar Jabbari for his guidance, support and understanding throughout my PhD program. I also like to thank my unofficial co-advisor and dissertation committee member, Professor Farzin Zareian, for his suggestions, discussions, and expertise in structural control. I also like to thank Professor Mark Walter for serving on my dissertation committee. I would also like to thank Professor Natascha Buswell for reigniting my passion for teaching and providing guidance and advice in education research. I would like to also thank the countless professors and mentors I have had throughout my studies from undergraduate until now. I grateful to have had so many fantastic teachers that have provided me with the tools I needed to succeed.

I would also like to thank the GAANN fellowship for providing me financial support, which greatly contributed to my success as a graduate student.

Most importantly, I would like to thank my family and friends for supporting me throughout my academic journey. In particular, I would like to thank my parents, Anahid and Varoujan, and brother, Tadeh, for their continued love, support, and understanding throughout my PhD program. I would also like to thank my friends Matt, Phil, Serj, and Lorik for their words of encouragement and support.

VITA

Shant Aram Danielian

EDUCATION

Doctor of Philosophy in Mechanical and Aerospace Engineering **2023**
University of California, Irvine *Irvine, CA*

Master of Science in Mechanical and Aerospace Engineering **2020**
University of California, Irvine *Irvine, CA*

Master of Science in Applied Mathematics **2015**
California State Polytechnic University, Pomona *Pomona, CA*

Bachelor of Science in Civil Engineering and Applied Mathematics **2013**
California State Polytechnic University, Pomona *Pomona, CA*

TEACHING EXPERIENCE

Lecturer

Advanced Engineering Mathematics **Fall 2015–2022**
California State Polytechnic University, Pomona *Pomona, CA*

Applied Probability Concepts in Civil Engineering **Fall 2022**
California State Polytechnic University, Pomona *Pomona, CA*

Mechanics of Materials **Spring/Fall 2021-2022**
California State Polytechnic University, Pomona *Pomona, CA*

Engineering Statics **Fall 2022**
California State Polytechnic University, Pomona *Pomona, CA*

Computer Programming and Numerical Methods **Fall 2021**
California State Polytechnic University, Pomona *Pomona, CA*

Graduate Teaching Assistant

Dynamics **Winter 2018–2019**
University of California, Irvine *Irvine, CA*

Mechanics of Materials (Lecture/Lab) **Fall/Spring/Summer 2016–2019**
University of California, Irvine *Irvine, CA*

INDUSTRY EXPERIENCE

Associate Structural Engineer **2016-2018**
Aujaghian & Associates Consulting Engineers *Newport Beach, CA*

FELLOWSHIPS AND AWARDS

Chancellors Doctoral Incentive Program Fellowship **2020**
Division of Teaching Excellence and Innovation (DTEI) Travel Grant **2019**
Graduate Presidential Fellowship **2014**
President's Council Scholarship **2014**
Edison Scholar **2014**
Dr. Emil R. Herzog Scholarship **2014**

JOURNAL PUBLICATIONS

Danielian, S.A., Jabbari, F., Zareian, F., Effects and distribution of semi-active resettable springs on the seismic response of asymmetric structures. (In Review)

Danielian, S.A., Jabbari, F., Zareian, F., Resettable semi-active tuned mass damper applied to base-isolation systems. (Work In Progress)

Danielian, S.A., Jabbari, F., Zareian, F., Performance and reliability of semi-active equipment isolation. (Work In Progress)

CONFERENCE PUBLICATIONS

Danielian, S.A., Arun, V.R., & Buswell, N.T. (2020, April), A thematic analysis of students' perspectives and opinions on the construction of exam support sheets Paper presented at Proceedings of the 2020 ASEE PSW Section Conference, canceled, Davis, California. https://peer.asee.org/36034

Danielian, S.A., Buswell, N.T. (2019, April), Do support sheets actually support students? A content analysis of student support sheets for exams Paper presented at 2019 Pacific Southwest Section Meeting, California State University, Los Angeles , California. https://peer.asee.org/31824

PROFESSIONAL TRAINING AND WORKSHOPS

Mentoring Excellence Program **2021**
Certificate of Course Design Program **2020**
Certificate of Teaching Excellence **2020**

ABSTRACT OF THE DISSERTATION

Passive and Semi-Active Control of Civil Structures

By

Shant Aram Danielian

Doctor of Philosophy in Mechanical and Aerospace Engineering

University of California, Irvine, 2023

Professor Faryar Jabbari, Chair

During the 20$^{\text{th}}$ century, over 1200 major earthquakes occurred, causing damage estimated to be upwards to $1 trillion worldwide. On average, 10,000 people have died annually from 1900 to 1999. Several studies have shown that nearly three-quarters of earthquake fatalities occurred due to building collapse. Consequently, an earthquake-resistant design philosophy was adopted by the earthquake engineering community. Two common strategies to reduce the displacement and acceleration response of the structure include base isolation, which separates the structure from the ground, and incorporating vibration suppression devices within the structure. For this dissertation, several different types of devices such as tuned mass dampers, inerters, and semi-active devices have been used in a variety of settings to provide further reduction of the response of civil structures. A tuned mass damper (TMD) is an auxiliary mass attached to the structure using spring and damper in parallel. The stiffness and damping are selected such that the first mode vibrations of the structure are reduced. Several studies have shown that TMDs are effective in reducing the response of a structure yet require a large mass and footprint to house the TMD. Inerters are devices that provide a force proportional to the relative acceleration of the two ends. They provide an apparent mass that is several times larger than the physical mass of the device. Both TMDs and inerters are broadly classified as passive devices since they require no power to operate. On the other hand, semi-active devices are those that require a small power source usually

provided by an on-site battery. These devices can alter the stiffness or damping properties of the structure. For this dissertation, a semi-active resettable spring (SRS) was used. This device provides continuous stiffness, while also dissipating energy by resetting its unstretched length. Both inerters and SRSs have been incorporated individually in tuned mass damper systems. Yet, a hybrid system incorporating both devices has not been studied before. One objective of this dissertation was to determine the effectiveness of incorporating a SRS and inerter within a tuned mass damper system, known as a semi-active tuned mass damper inerter (SATMDI). Single and multi-story structures were considered, and the results showed that the SATMDI can provide additional reductions to the displacement and acceleration responses, while also significantly reducing the required footprint to house the control system.

The selection of the stiffness and damping of a TMD is what is known as the tuning strategy. Several different tuning strategies for TMDs have been proposed that assume harmonic or white noise base excitations. Other strategies use the modal properties of the structure within the tuning strategy. Researchers have studied systems where an inerter is incorporated within a TMD, known as a tuned mass damper inerter (TMDI). The tuning strategies for TMDIs are based on those used for TMDs. In this dissertation, an alternative tuning strategy for a tuned mass damper inerter (TMDI) is proposed. This tuning strategy is also based on that of a TMD, yet instead uses the modal properties of the structure to tune the TMDI. The results of this alternative tuning strategy show that significant improvements in reducing the displacement and acceleration responses can be achieved for a significantly smaller TMD mass and inerter. Moreover, the footprint required to house the TMDI is much smaller as compared with other tuning strategies.

Base-isolation has been shown to be effective in reducing the response of a structure by separating the structure from the ground. The isolators provide lateral flexibility, reducing the amount of energy transferred to the structure. While these devices provide adequate protection, there is some evidence to suggest otherwise. To remedy this, researchers have

proposed hybrid systems, where TMDs are attached to the base. In particular, a non-traditional TMD (NT-TMD), which attaches the spring, mass, and damper in series has been proposed. It has been shown that the NT-TMD can provide reductions in the displacement, while also reducing the footprint to house the NT-TMD. In this dissertation, a novel NT-TMD is introduced, known as a non-traditional semi-active TMD (NT-SATMD). The results of this work show that the NT-SATMD can provide the same level of performance as a NT-TMD for a significantly smaller mass. Moreover, the footprint required to house the NT-SATMD is comparable to that of a NT-TMD.

The single and multi-story structures considered assume only lateral motion, which occurs if the distribution of the mass and/or stiffness of the structure is uniform. In cases where this is not possible, an eccentricity is developed between the center of resistance and center of mass, coupling the lateral and rotational motion. Buildings that have this property are called asymmetric. In this dissertation, the SRS has been used to reduce the lateral and rotational response of an asymmetric structure. A parametric study over a wide range of structure periods was considered in addition to studying rotational stiff, flexible, and strongly coupled structures. Two strategies for determining the optimal placement for the devices were proposed, both leading to roughly the same performance. It was found that distributing the semi-active devices such that it produces an eccentricity equal in magnitude, but opposite in sign to the structure's eccentricity lead to the greatest reductions in the flexible and stiff edges. Guidelines and limitations on the selection of the device distribution were also provided for design purposes.

Chapter 1

Introduction

1.1 Background and Motivation

It is generally accepted that strong earthquakes cause significant structural and economic damage if proper precautions are not taken. From 1900 to 1999, a total of 1248 major earthquakes occurred, causing damage estimated to be upwards of $1 trillion worldwide [21]. On average 10,000 people have died annually during that same time span [12]. Some contemporary examples include the 1988 Armenian earthquake which killed 25,000 people and caused damage in excess of $200 million [61], the 1994 Northridge earthquake that killed 60 people and caused $311 million in damages [29], and the 2019 Ridgecrest earthquake causing nearly $4 billion in damages [14]. Investigations into earthquake fatalities have shown that three-quarters of deaths occurred due to building collapse [22]. Consequently, an earthquake-resistant design philosophy has been adopted by the earthquake engineering community worldwide. To this aim, various types of earthquake protection strategies have been proposed. The most common are to increase the structural stiffness, isolate the structure from the ground, or use vibration suppression devices. Several hybrid systems combining the

three strategies have also been implemented. The first strategy alters the natural frequency of the structure by increasing the stiffness. Thus, the natural frequency of the structure is higher than the predominate earthquake frequency. The second strategy completely separates the structure from the ground by using base-isolators, thereby minimizing the amount of energy transferred to the structure in the event of a strong earthquake. The third strategy reduces the response of the structure by using devices that dissipate energy from the structure or alter the structural properties in real-time.

From the three strategies stated above, base-isolation is most widely used in practice, due to its simplicity in design, installation, and maintenance. Base-isolators consists of rubber and steel layers, where the rubber provides horizontal flexibility while the steel layers are used to prevent bulging due to vertical loading [74]. The application of base-isolators are commonly used for critical structures, such as hospitals or power plants. This is because of the monetary cost to manufacture and install the base-isolators, which is justified due to the level of importance of the structure to remain operational after a strong earthquake [24].

Vibration suppression devices can be categorized as passive, active, or semi-active. As the name suggests, passive devices provide vibration suppression without the use of external energy. Some examples include base-isolation or tuned mass dampers. On the other hand, active devices are those which require external power source to operate. Active devices can be used over a wider range of operation since their properties can be adjusted in real-time. However, it is difficult to ensure the power requirements in the event of a strong earthquake. Semi-active devices are those which combine principles from both passive and active control. The parameters of the device can be adjusted using significantly less power than active control. Moreover, semi-active devices provide a fail-safe, where in the event of power loss, they can still provide some passive control. Due to the limitations of active control, passive and semi-active control are considered in this dissertation.

There are numerous examples of structures implementing passive control. A well-known

example is the Taipei 101 structure. In this structure, a tuned mass damper (TMD) is used to reduce vibrations caused by wind or earthquakes [82]. The TMD consists of a mass that is suspended by cables with viscous dampers attached for energy dissipation. The TMD is typically placed where the response is largest, that is, near the top of the structure. The TMD requires a tuning strategy for selecting the stiffness and damping of the TMD so to minimize a specific response (e.g., displacement or acceleration) of the structure. The performance of TMDs has been extensively studied [78, 13, 42, 111]. The study done by Villaverde and Koyoma [111] showed that the performance of TMDs was subject to the ground motion characteristics and only had a narrow frequency band where suppression was achieved. Considerably large masses are necessary to provide sufficient response reduction. In addition, the TMD system may also require a large stroke, that is, the relative displacement between the TMD and structure. The footprint requirement to house the TMD can also lead to issues when choosing to implement or retrofit in a structure.

In 1997, a device comprised of a spring in parallel with flywheels and a geared rod was patented in Japan by Okumura Atsushi [77]. The resisting force provided by the device is proportional to the relative acceleration between the terminal ends. In other words, the device provides an inertial force that is multiple times larger than the actual mass of the device. The term "inerter" was first coined by Smith in 2002 [93]. Since then, three physical realizations of inerters were developed, namely, ball-screw inerters [44], rack-and-pinion [93], [94] and fluid inerters [113]. Applications of inerters have also been studied in various settings within civil [92, 35, 129, 119], mechanical [114, 115], and aerospace engineering [67, 66]. In these various contexts, inerters were combined with other mechanical elements, such as springs and dampers. Three different types of configurations have been proposed: (1) tuned inerter dampers (TID) proposed by Lazar et al. [62], (2) tuned mass damper inerter (TMDI) put forward by Marian et al. [70] and (3) tuned viscous mass dampers (TVMD) first introduced by Saito et al. [88]. For this dissertation, the first two configurations will be studied.

Semi-active devices were developed to combine the best components of passive and active control, or at least, mitigate their less desirable qualities. Semi-active devices avoid using large external energy, while performing better than passive control. Typically, semi-active devices do not add mechanical energy to the structural system, and so stability is guaranteed [10]. Due to the low power requirements and large force capacity, semi-active devices are an attractive alternative to active control. Several different implementations of semi-active control have been proposed. Examples include variable-orifice fluid dampers [53, 120], controllable friction devices [1, 2] and variable-stiffness [11, 48, 75]. For this dissertation, the semi-active resettable spring first proposed by Bobrow et al. [11] will be used extensively. Applications of this device within tuned mass damper systems has been studied by Chey et al. [19]. In that study, a portion of the structure was used as the mass of the TMD. This was done by isolating the upper stories with rubber bearings and connected with the semi-active resettable spring. A parametric study was conducted over a wide range of ground motions showcasing the efficacy of using the semi-active device within a tuned mass damper system.

The term hybrid control refers to combining a passive and active device or passive and semi-active device. A hybrid system using active devices supplements and improves the performance of a passive control system, whereas passive control is used with active control to alleviate some of energy needs [102]. One of the earliest examples is the active tuned mass damper (AMD), which incorporates an active actuator within a passive TMD system [76]. Later studies then combined an AMD within another TMD system, known as hybrid mass damper (HMD) [47]. Other hybrid systems have also been proposed where the passive control is taken to be base-isolation and either other passive [106, 121, 26], active [124] or semi-active devices [127, 122] incorporated in various configurations. Due to having multiple devices operating, hybrid control systems can provide higher performance levels while also easing some of the restrictions and limitations that exist with each control device acting separately.

The research proposed in this dissertation studies the control of single-story, multi-story, and asymmetric structures. The latter structure is one where an imbalance in the stiffness and/or mass distribution causes the structure to rotate under lateral ground motion. This rotation is due to an eccentricity between the center of mass and the center of rigidity of the structure. For single and multi-story structures, a novel configurations of the semi-active resettable spring (SRS) within other existing control systems are proposed and studied. Each new system is evaluated to determine the effectiveness in reducing the structural response under ground motions. One such configuration is to incorporate an SRS within a TMDI system. In addition, an alternative tuning strategy is proposed for a TMDI system in a damped multi-story structure. With regards to base-isolated structures, a novel hybrid system incorporating SRS within a TMD system will be proposed. For asymmetric structures, the effects of including SRSs within the structure will be studied extensively. Guidelines for the use and placement of SRSs will also be proposed.

1.2 Objectives and Scope

The primary objective of this research is to evaluate the effectiveness of the semi-active resettable spring (SRS) in a variety of existing control strategies. Performance will be evaluated by comparing the response of the controlled system to that of the uncontrolled system, typically being a structure without any control devices used. Two sets of ground motions representing rock-site and pulse-like earthquakes will be used. Basic statistical methods will be used to evaluate the performance. The structural system considered in this work will focus on the response of moment resisting frames and the scope will cover the following:

1. To investigate the efficacy of semi-active resettable springs within a TMDI system in reducing the response of single and multi-story structures.

2. To investigate the efficacy of using a semi-active resettable spring within a hybrid base-isolation and TMD system and propose an ad-hoc tuning strategy.

3. To introduce an alternative tuning strategy for a TMDI within a multi-story structure.

4. To study the effects and distribution of resettable semi-active springs in controlling the seismic response of a one-story asymmetric structure.

1.3 Outline

Following this chapter, Chapter 2 presents a literature review, which introduces the control devices and systems used in this dissertation. These include the semi-active resettable spring (SRS), inerter, tuned mass damper (TMD), and base-isolation systems (BISs). Combinations of these, also known as hybrid control systems, will also be introduced. In Chapter 3, a brief introduction on the two ground motion sets used in this work is presented. The general characteristics and properties of the ground motions are discussed.

In Chapter 4, several different types of control strategies for lightly damped one-story structures are introduced. The control strategies incorporate SRSs, inerters, TMDs and BISs. In particular, the tuned mass damper inerter (TMDI) and semi-active TMDI (SATMDI) are introduced. The latter of which is a novel configuration proposed in this work. Tuning strategies for each control system are introduced. Hybrid control is also considered, where the response of a one-story structure equipped with a BIS is studied. The control strategy is to attach a traditional TMD (T-TMD) or non-traditional TMD (NT-TMD) to a BIS. The NT-TMD is one where the spring, mass, and damper are in series, that is, the damper grounds the TMD mass. A new configuration is also proposed, where the SRS is used to ground the mass of a traditional TMD system. Tuning strategies for each of the hybrid control systems are presented. For each of the control strategies in this chapter, the response of

the system under the two ground motion sets is studied.

In Chapter 5, the TMDI and SATMDI systems are applied to a lightly damped multi-story structure. Modified tuning strategies for the TMDI and SATMDI are introduced. In addition, an alternative tuning strategy is proposed for the TMDI system. Comparisons between each control strategy were performed for a three-story structure under the two ground motion sets.

In Chapter 6, SRSs are used in the bracing of an asymmetric structure, that is, a structure which has an eccentricity caused by an imbalance in the mass and/or stiffness. An extensive parametric study was done studying the optimal placement and stiffness distribution of the SRSs. Two methods are proposed and the limitations of each are discussed. General guidelines for implementation are also discussed.

In Chapter 7, a summary and the contributions of this dissertation are presented. Future work and possible avenues for further research are also proposed based on the work presented herein and preliminary results.

Chapter 2

Literature Review

2.1 Introduction

Reducing the response of structures under strong earthquakes has been the primary focus of researchers concerned with mitigating the damage caused by strong earthquakes. Typically, the displacement and acceleration responses are related to the damage in the structural and non-structural components of a building. Some common approaches include strengthening the structure by adding additional bracing or incorporating energy dissipating devices. This dissertation focuses on using passive and semi-active devices to reduce the response of the structure. In Chapter 2, a review of the vibration suppression devices and various configurations are presented. These devices included the semi-active resettable spring, inerter, tuned mass dampers, and base-isolation. Hybrid systems combining one or more of the vibration suppression devices is also introduced.

2.2 Vibration Suppression Devices

2.2.1 Semi-active Resettable Springs

Semi-active devices combine the benefits of active and passive control, while attempting to mitigate their drawbacks. Semi-active devices avoid the large power requirements of active control, while also being able to modify their mechanical properties in real-time, leading to perform better than passive control. Moreover, similar to passive systems, semi-active devices provide a fail-safe in the event of power loss. Since energy can only be extracted from the building, semi-active devices will not cause instability to the structural system [10]. Semi-active devices have been extensively studied in theoretical, numerical, and experimental contexts [11, 10, 48, 125, 64, 63].

In a semi-active control system, the mechanical properties of the device can be altered in real-time through the use of sensors, feedback measurements, and a control law which modifies the mechanical properties of the device [63, 64]. The control forces developed are based on the structure response, or at least, the structure response local to the device. In the latter case, the control law would be considered decentralized [48]. Studies have shown that using semi-active devices have significantly better performance than passive systems, and at times, performance comparable to active systems [28]. Semi-active control was first used in civil structures by Hrovat et al. in 1983 [43]. Since then several researchers have investigated the performance of semi-active devices in the seismic protection of single and multi-story structures [30, 10, 28, 71, 72, 126].

The nonlinear nature of semi-active devices requires careful selection on the control law so to employ the full capabilities of the device when used in practice. Several nonlinear control laws have been developed, for example, bang-bang control, clipped optimal control [50], resetting logic [10, 11, 48], fuzzy control [20], and genetic algorithm [3].

In this dissertation, the semi-active resettable spring (SRS) will be used. This device was first introduced by Bobrow et al. [11]. The device components are a double-acting cylinder, piston, and valve. A schematic of the device is shown in Figure 2.1a. When the valve is

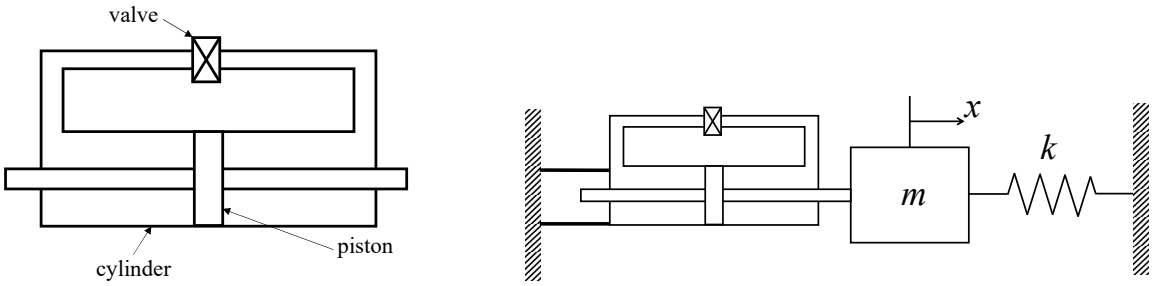

Figure 2.1: (a) Schematic of resettable semi-active spring (SRS), (b) single-degree-of-freedom system with attached resettable semi-active spring.

closed, the cylinder compresses the fluid through piston movement. After the value opens, the energy stored in the fluid is dissipated by heat and fluid slushing. For a single-degree-of-freedom system, as shown in Figure 2.1b, the energy dissipated when the value opens is given by the equation

$$E(t) = \frac{1}{2} k_d (x(t) - x_r)^2 \tag{2.1}$$

where k_d is the SRS stiffness, x is the displacement of the mass, and x_r is a piece-wise constant denoting the zero force position of the SRS [11]. The control law or resetting logic is then chosen so to extract the maximum energy, that is, when $\dot{E}(t) = 0$. More explicitly,

$$\dot{E}(t) = \dot{x}(t) k_d (x(t) - x_r) \tag{2.2}$$

To extract energy from the system, $E(t) \neq 0$, which from (2.1), requires $x(t) \neq x_r$. Thus, $\dot{E}(t) = 0$ whenever $\dot{x} = 0$ and the control law is defined as

$$\text{set } x_r = x \text{ whenever } \dot{x} = 0 \tag{2.3}$$

The term reset indicates that the stored energy of the SRS is dissipated after opening the valve. Based on the work by Bobrow et al. [11, 10], the stored energy is released when the velocity of the piston is zero (see (2.3)). Since the time it takes for the stored energy to dissipate is short [63], the SRS provides constant stiffness to the system. Therefore, the SRS acts as a spring element that resets its unstretched length at local maximum strain energy. A typical force-displacement graph showing a single cycle (three resets) is presented in Figure 2.2. The area enclosed is the work absorbed by the SRS, that is, the total energy dissipated in one cycle. Based on the prior discussion, the SRS behaves similar to a spring element,

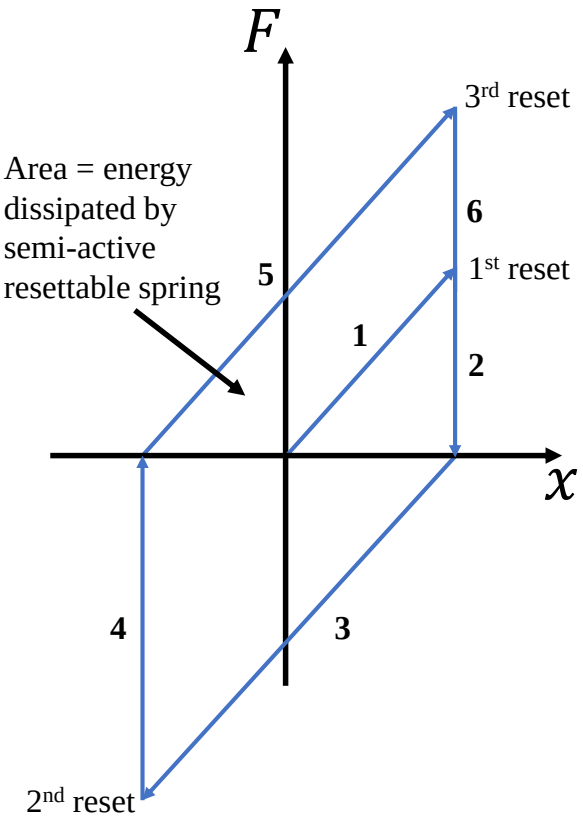

Figure 2.2: Generic force-displacement curve of SRS showing one cycle (three resets).

where k_d is the SRS stiffness and x_r is the piece-wise constant defined by (2.3). The SRS stiffness has been shown [11] to be

$$k_d = \frac{4A\beta}{s} \tag{2.4}$$

where A is the piston area, β is the bulk modulus of the fluid, and s is the stroke of the piston. By selecting the bulk modulus, stroke, and stiffness, a piston area can be calculated. Prior experimental studies have verified the effectiveness of SRSs in both small-scale [11, 48] and full-scale [125, 63] testing. Due to the relatively easy and inexpensive construction, multiple SRSs can be used in parallel to satisfy large force and stiffness requirements.

The control law for the SRS is a resetting technique often denoted as 1-4, since all four quadrants of the force-displacement diagram are engaged. The control force provided by the SRS is given by

$$F = k_d(x - x_r) \tag{2.5}$$

where k_d is the stiffness of the device and x_r is a piece-wise constant defined in (2.3). To understand the effect the SRS has on a dynamical system, consider the single-degree-of-freedom system shown in Figure 2.1b. The equation of motion is given $m\ddot{x}+kx+k_d(x-x_r) = 0$, and so the SRS adds k_d amount of stiffness in addition to having a forcing function equal to $k_d x_r$, where x_r is defined by equation (2.3). It is worth noting that although the additional stiffness provided by the SRS increases the natural frequency of the system, resonance is not possible due to the additional term $k_d x_r$. This term acts as a type of forcing function on the system driving the system to equilibrium, that is, to zero displacement [10].

2.2.2 Inerters

In 1997, Okumura Atsushi was issued a patent in Japan for a device comprised of a spring in parallel with flywheels and a geared rod [77]. This so-called gyro-mass consisted of two disks which rotated the gears in such a way that the force generated was proportional to the relative acceleration of the terminal ends. Defining x_1 and x_2 to be the displacement of each terminal (see Figure 2.3b), this relationship between force and acceleration can be expressed

by

$$F = m_d(\ddot{x}_2 - \ddot{x}_1) \tag{2.6}$$

where

$$m_d = \frac{J}{r^2} \tag{2.7}$$

and where J is the moment of inertia of the disks, r is the distance from the center of the disk to the point of attachment of the rod, and m_d is the apparent (or virtual) mass created by the device. In 2002, Smith [93] proposed a rack-and-pinions device (see Figure 2.3a), which he called the inerter. Similar to the gyro-mass device, the inerter produces a force proportional to the relative acceleration of the terminal ends, defined by

$$F = b(\ddot{x}_2 - \ddot{x}_1) \tag{2.8}$$

where b is called the inertance. So far, three variants of physical realizations have been developed, namely, rack-and-pinion [93, 94], ball-screw [44], and fluid inerters [113], the schematic of each shown in Figure 2.3. Rack-and-pinion inerters [77, 93] and ball-screw inerters [44] provide inertance through linear motion of a rod which is converted to rotational motion of the flywheel through gearing. On the other hand, some fluid inerters achieve their inertance through fluid movement to cause the flywheel to rotate. In 2009, Glover et al. [94] was the first to patent a fluid based inerter, known as a hydraulic inerter. In 2011, Wang [113] proposed another variant of a hydraulic inerter, while in 2013 Swift et al. [100] introduced the helical inerter. The latter realization generated inertance from fluid moving through a helical channel. This realization is unique in that the fluid movement generates the inertance as opposed to flywheel rotation. Experimental studies have been done studying the helical design and nonlinear behavior accounting for fluid friction and viscosity [99, 18, 25].

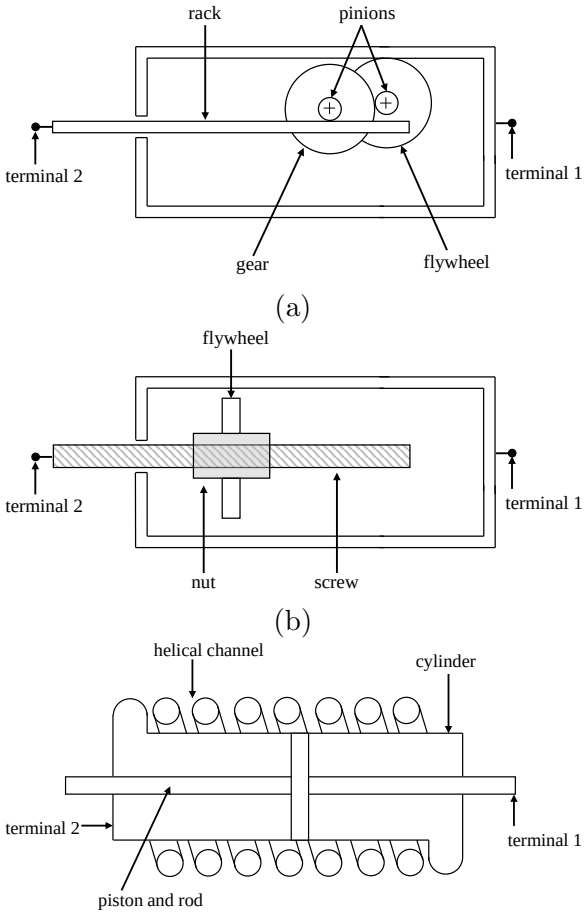

Figure 2.3: Schematic diagram of three physical realizations of inerter (a) rack-and-pinion, (b) ball-screw, and (c) fluid inerter.

Several applications of inerters to civil structures has been investigated. Wang et al. [112] studied the performance of structures equipped with inerters under ground motion and traffic loads. Other studies have been conducted evaluating the performance of inerters in reducing the response of multi-story structures under ground motion [103, 130, 131]. In the context of TMD systems, inerters have been used to either reduce [70] or replace [62] the mass of the TMD. To alleviate some of the mass requirements, an inerter is included within a TMD system, known as a tuned mass damper inerter (TMDI) [62], while the tuned inerter damper (TID) [70] entirely replaces the TMD mass by the inerter. Each of these systems will be discussed in detail in Section 2.3.

2.3 Tuned Mass Damper Systems

2.3.1 Tuned Mass Dampers

The key concept of tuned mass dampers is to attach an additional mass to the structure using mechanical devices, such as springs and dampers, so to mitigate or entirely eliminate vibrations from the structural system, as shown in Figure 2.4. This is achieved by transferring the energy of the structure through the spring to the mass and dissipates the energy through the damper. The spring and damper properties are selected (or tuned) to reduce the response of the structure under wind or seismic excitations. In contrast, when considering a single-degree-of-freedom system, the TMD can also be used to change the phase of the system. Namely, by transforming a lightly damped first mode vibration into two coupled more heavily damped modes of vibration. A similar idea extends to multi-story structures [87]. The first

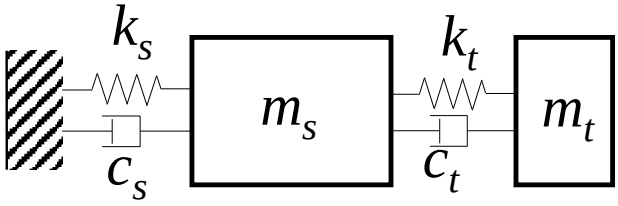

Figure 2.4: Tuned mass damper attached to single-degree-of-freedom system.

to introduce the idea of a TMD was Frahm in 1909. Frahm implemented a TMD to reduce the rolling motion of ships and hull vibrations [31]. The approach was to attach a small mass to the structure by a spring to reduce vibrations under harmonic loading. This idea was extended by Ormondroyd and Hartog by adding a viscous damper in parallel to the spring to dissipate energy [78, 27]. The tuning strategy for the spring and damper was first derived by Hartog, using what is now known as fixed-point theory [27]. The name of the approach comes from the fact that the frequency response curves of a single-degree-of-freedom system equipped with a TMD pass through two fixed points for any choice in the damping constant. The approach is to select a spring stiffness such that the two points have

equal magnitude, while the damping constant is selected so that the slope at both points is zero, that is, at peak values. It is worth noting that the structure is under harmonic force applied to the structure itself. By solving the algebraic equations, the following formulations for the optimal frequency and damping ratio have been found to be [78]

$$f = \frac{1}{1+\mu} \quad \text{and} \quad \zeta_t = \sqrt{\frac{3\mu}{8(1+\mu)}} \tag{2.9}$$

where $f = \omega_t/\omega_s$ is known as the frequency ratio, ω_s and ω_t are the natural frequencies of the structure and TMD under rigid motion, respectively, and $\mu = m_t/m_s$ where m_t is the TMD mass and m_s is the mass of the structure. The term ζ_t denotes the damping ratio of the TMD system. Since the early work of Ormondroyd and Hartog, several other researchers have developed new formulations for the frequency and damping ratio of the TMD. For example, Warburton [118] derived the frequency and damping ratio for a structure under white-noise base excitation

$$f = \frac{\sqrt{1-\mu/2}}{1+\mu} \quad \text{and} \quad \zeta_t = \sqrt{\frac{\mu(1-\mu/4)}{4(1+\mu)(1-\mu/2)}} \tag{2.10}$$

while Sadek et al. [87] selected the frequency and damping ratios such that the first two natural frequencies and damping ratios of the system are equal. Through extensive numerical work and curve fitting, the following equations were found for a single-degree-of-freedom system

$$f = \frac{1}{1+\mu}\left(1 - \zeta\sqrt{\frac{\mu}{1+\mu}}\right) \quad \text{and} \quad \zeta_t = \frac{\zeta}{1+\mu} + \sqrt{\frac{\mu}{1+\mu}} \tag{2.11}$$

where ζ is the critical damping ratio of the single-degree-of-freedom system. Note that the work by Sadek et al. accounted for damping of the structure, while Hartog's and Warburton's approach assumes no structural damping. More contemporary work by Leung and Zhang [65] used particle swarm optimization to select the frequency and damping ratios.

Explicit formulas were found from curve fitting for a damped structure under white noise base excitation,

$$f = \frac{\sqrt{1-\mu/2}}{1+\mu} + (-4.9453 + 20.2319\sqrt{\mu} - 37.9419\mu)\sqrt{\mu}\zeta + (-4.8287 + 25.0000\sqrt{\mu})\sqrt{\mu}\zeta^2 \quad (2.12)$$

and

$$\zeta_t = \sqrt{\frac{\mu(1-\mu/4)}{4(1+\mu)(1-\mu/2)}} - 5.3024\zeta^2\mu \quad (2.13)$$

Other variants of TMDs have also been proposed. One example is a non-traditional TMD (NT-TMD) first introduced by Ren [85]. In this configuration, instead of the spring and damper in parallel, the damper grounds the TMD, that is, the spring, mass, and damper are in series. Xiang and Nishitami [121] applied the NT-TMD to base-isolated structures (BISs). In each of those studies, the NT-TMD was shown to be more effective than a standard TMD system. In this work, an SRS will be incorporated within a TMD system, such that it will ground the TMD mass, thereby classifying it as non-traditional TMD system.

2.3.2 Tuned Mass Dampers with Inerters

Although TMDs have been shown to be effective in reducing the response of a structure under wind and ground motion, the need for a large mass and/or large stroke inhibits implementation in several scenarios [98]. One way researchers have mitigated the large mass requirement of TMDs is to incorporate inerters within the tuned mass damper system. The first variant of a inerter based TMD was proposed by Saito et al. [88], which arranged the inerter and damper in parallel, while the spring was in series, shown in Figure 2.5a. This configuration was known as a Tuned Viscious Mass Damper (TVMD). Another type of physical realization was introduced by Ikago et al. [44] which used a ball-screw mechanism to convert translational motion to rotational motion through the flywheel. For this physical

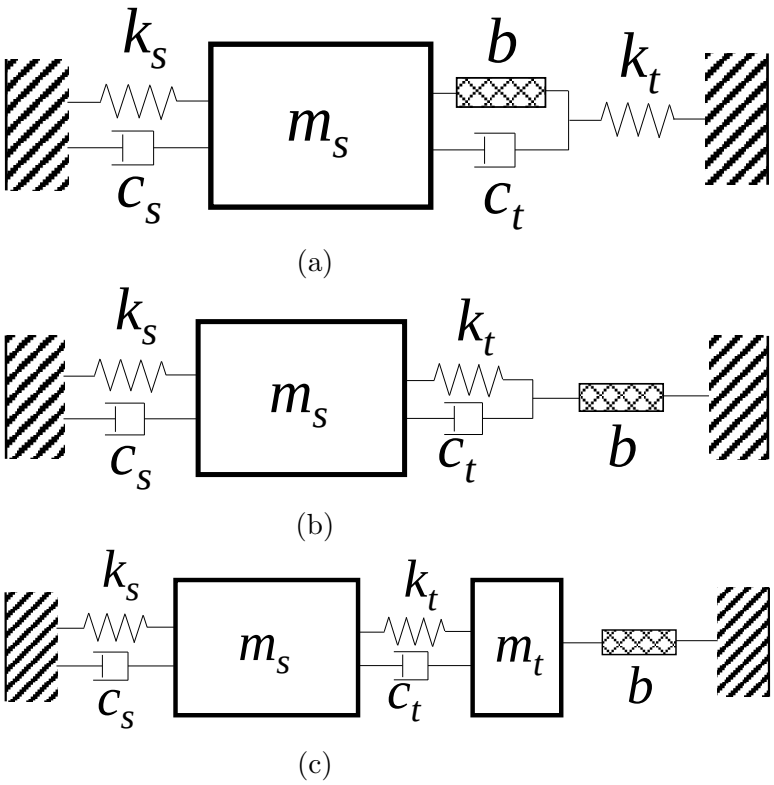

Figure 2.5: Schematic diagram of three physical realizations of inerter (a) ball-screw, (b) rack-and-pinion, and (c) fluid inerter.

realization, several studies have been done on the seismic performance, modal properties, and experimental testing [45, 6, 59]. Lazar et al. [62] proposed a different variant of an inerter based TMD known as the tuned inerter damper (TID), as shown in Figure 2.5b. In this configuration, the inerter entirely replaces the TMD mass. The tuning strategy used Hartog's approach, with the difference being that three fixed points in the frequency response curve would need to be accounted for. Modal analysis was performed for a multi-story structure and found that the TID performed as well as a TMD having an equivalent inertance, yet the TID was placed at the lower level of the structure as opposed to the upper story. Moreover, it was found that not only did the TID suppress vibration in the first mode of the structure, but in all modes [62].

Marian et al. [70] also introduced another variant called the tuned mass damper inerter (TMDI), as shown in Figure 2.5c. In this configuration, the inerter is used to supplement

additional mass, thereby requiring less physical mass as opposed to a standard TMD system. Similar to the TID system, the TMDI has the inerter grounded, while in multi-story structures it would be attached to the floor below. The tuning strategy followed Warburton's approach, where white-noise base excitation was assumed, and the structure was undamped. For a single-degree-of-freedom system, the following frequency, and damping ratios where derived

$$f = \frac{1}{1+\beta+\mu}\frac{\sqrt{\beta(\mu-1)+(2-\mu)(1+\mu)}}{\sqrt{2(1+\mu)}} \tag{2.14}$$

$$\zeta_t = \frac{\sqrt{\beta+\mu}\sqrt{\beta(3-\mu)+(4-\mu)(1+\mu)}}{2\sqrt{2(1+\beta+\mu)[\beta(1-\mu)+(2-\mu)(1+\mu)]}} \tag{2.15}$$

where $\beta = b/m_1$ is denoted as the inertance ratio. Note that by setting $\beta = 0$ the frequency and damping ratio found by Warburton's tuning strategy (see 2.10) are recovered. Damped multi-story structures were also considered by running a numerical optimization minimizing a cost function related to the displacement of the upper story [70, 33]. The results of the studies found that by the TMDI provides a significant reduction in the required physical (or real) mass, yet for very large TMD masses, the standard TMD outperforms the TMDI, aligning with engineering intuition.

2.4 Base-isolation Systems

The earliest known development of base isolation was in 1868 by the Scottish engineer David Stevenson, where he published the paper "Notice of Aseismatic Arrangements, adapted to Structures in Countries subject to Earthquake Shocks" [69]. The key concept Stevenson recognized was by separating the structure from the ground, much of the force (or shock)

from the ground motion will be negated. In other words, creating a break in the continuity of the rigid parts of the structure prevents the propagation of the shock to the structure [69]. The designed mechanism was a rolling-bearing device, called an aseismatic joint, comprised of metal balls set between two plates with hallowed out cups [15]. Figure 2.6 shows a section of the lamp table equipped with the aseismatic joint. For unknown reasons, Stevenson did

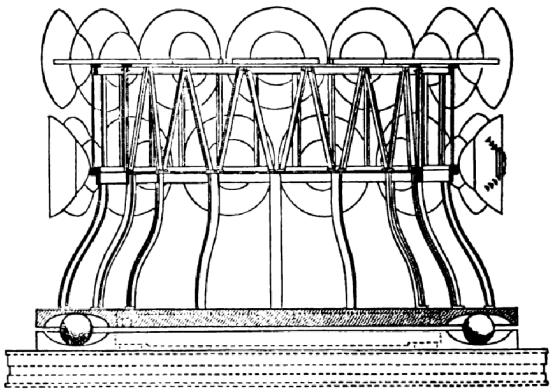

Figure 2.6: Schematic of lamp table with aseismatic joint.

not patent his invention, and instead, Jules Touaillon was the first to be issued a US patent in 1870 [105]. Only two weeks after Touaillon patented his device, A.F. Cooper patented a system which incorporated rubber bearings with the intention of reducing the force (or shock) due to ground motion [15]. Figures 2.7a and 2.7b show Touaillon and Cooper's patent designs, respectively. The key concept each of these inventors recognized was that by separating the structure from the ground, a significant portion of the force produced by the ground motion can be negated. This is accomplished by allowing the base to absorb much of the displacement demand. The function of the base-isolator is then to support the structure while providing significant lateral flexibility. Consequently, the fundamental frequency of the system is significantly increased, which leads to increased deformation of the base-isolator. Several examples of isolators have since been developed, for example, friction devices [73, 117], elastometric rubber bearings [56], lead-rubber bearings [23, 86]. For analysis, the elastometric or lead-rubber bearings can be modelled as either a linear or nonlinear spring and damper in parallel [91]. Kelly [57] provided an introduction to the

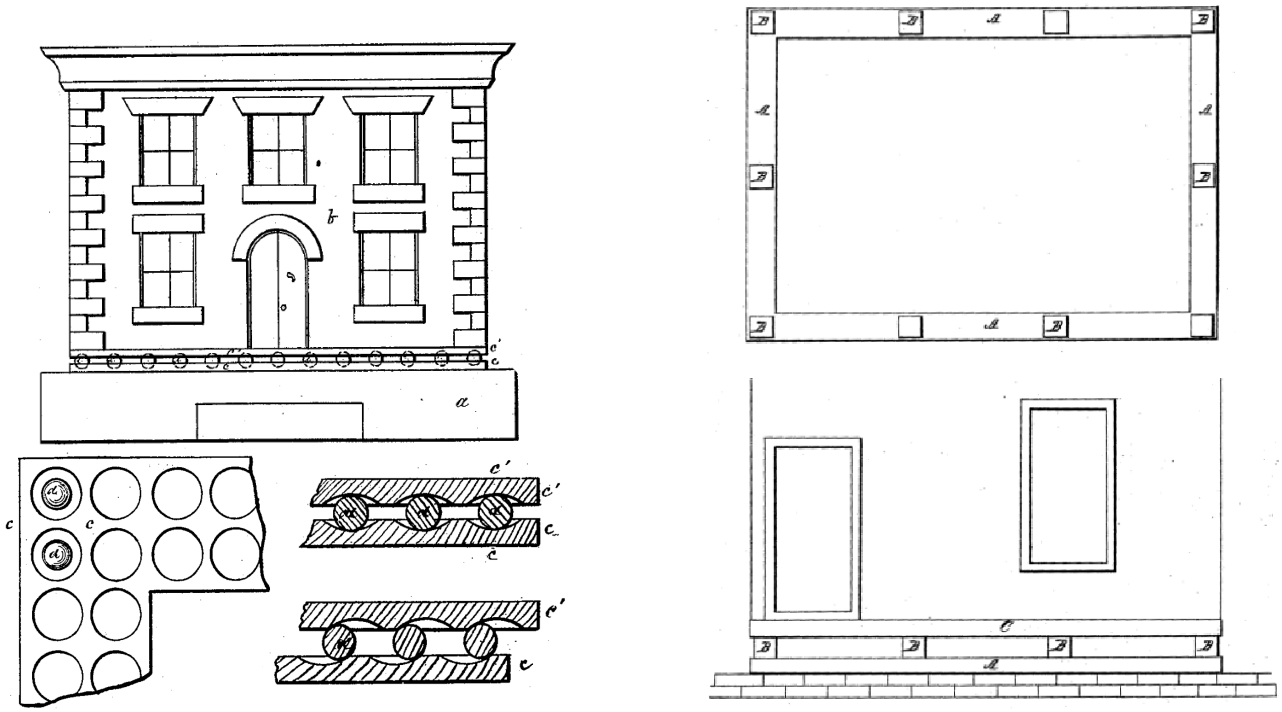

(a) (b)

Figure 2.7: Base-isolated structure using (a) Touaillon [105] and (b) Cooper's patent design [69].

dynamic behavior of base-isolated structures using a simplified two-degree-of-freedom model, where the system is assumed to remain in the elastic region.

There have been several applications of base-isolation worldwide, including U.S., Europe, Japan, and New Zealand [74]. The first base-isolated structure in the U.S. (and first in the world to use high-damping natural rubber) was the Foothills Communities Law and Justice Center, located in Rancho Cucamonga, California [74]. The largest base-isolated structure in the world is the West Japan Postal Computer Center, located in Sanda, Kobe Prefecture. This is a six-story structure supported on 120 elastometric isolators, with several additional steel and lead-core rubber bearings isolators [74]. A notable example is the University of Southern California (USC) teaching hospital, which was the only hospital in Los Angeles to have minimal damage during the 1994 Northridge earthquake, giving testament to the effectiveness of base-isolation [107]. While the base-isolation systems(BISs) have generally

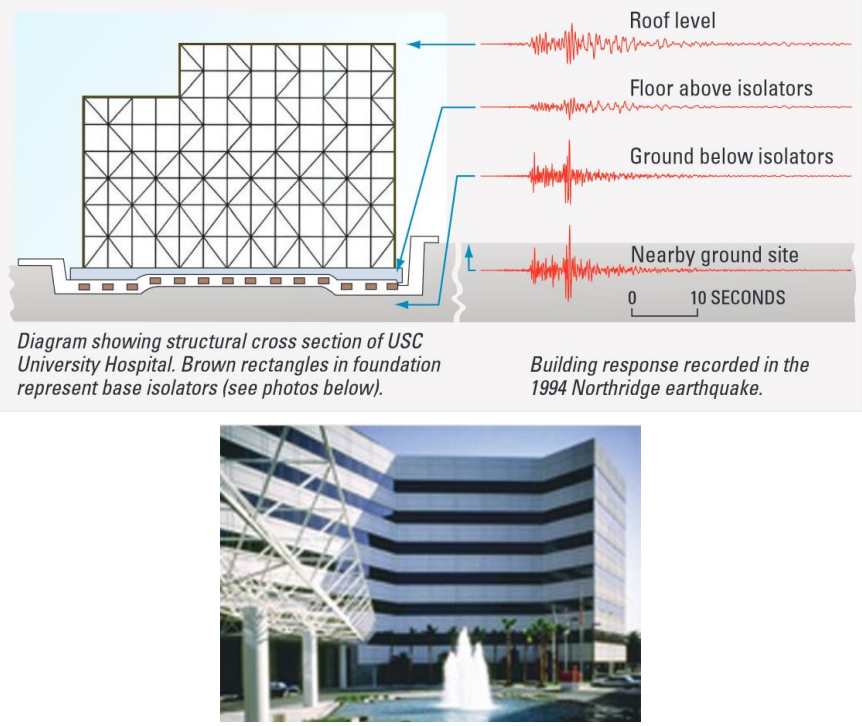

Figure 2.8: Base-isolation of USC teaching hospital [107].

provided adequate protection, there is some evidence to suggest otherwise. Some concerns include localized buckling of the isolator or collapse of the structure due to excessive lateral displacement [74]. In addition, it has been shown that BISs are insufficient to protect structures against near-source, pulse-like earthquakes [52, 97]. Similar studies have shown that near-fault ground motions can cause excessive base displacements [38, 40, 55, 58]. Moreover, utility connections must also be flexible enough to not be damaged [58] and the distance between adjacent buildings must also be considered to avoid structural pounding [4]. Due to these drawbacks of BISs, researchers began developing hybrid control strategies combining a BIS with other energy dissipative devices, with the most common approach of connecting a tuned mass damper (TMD) to a BIS.

2.5 Hybrid Control Systems

The term hybrid control in civil engineering typically refers to the combination of either passive and active control or passive and semi-active control [102]. The idea of hybrid control is to supplement passive devices with other devices so to increase the performance of the overall system. In [97], an exhaustive review of control schemes for various civil structures was done. In that paper, 40 buildings and ten bridges used active or hybrid control strategies, some of which include, semi-active TMD, variable orifice dampers, variable friction dampers.

As mentioned prior, BISs are prone to excessive displacements under long-period and long-duration ground motions. A hybrid system comprised of a TMD and BIS has been shown to be effective in mitigating large displacements. Studies [106, 104, 79, 80] have shown that TMDs used in conjunction with BISs are effective in reducing displacement at the base of the structure. However, attaching a TMD to a BIS results in reduced isolator displacement, adequate performance requires large stroke and/or TMD mass [7]. The work of Xiang et al. [121] proposed attaching a non-traditional TMD [85] to a BIS. The results of that study showed that the NT-TMD greatly reduces, stroke, yet large masses are still necessary for sufficient response reduction. In summary, although a TMD system does reduce the response of a structure, the drawbacks are that it typically requires a large footprint in the building, that is, a stroke, and/or a large mass so to properly reduce the response.

2.6 Summary

In this chapter, several control devices used in reducing the response of a structure were introduced. Some of these devices provide energy dissipation, such as the semi-active re-settable spring (SRS) or increase the apparent mass of the system by using an inerter. In addition, the tuned mass damper (TMD) system and base-isolation systems (BISs) were

presented. Incorporating an inerter within a TMD system in several different configurations was introduced. Lastly, hybrid control systems, which attach a TMD system to a BIS to mitigate the displacement of the base structure were shown. One such hybrid control system was the non-traditional TMD (NT-TMD), which arranges the spring, mass, and damper in series, where the damper grounds the TMD mass. The NT-TMD was shown to be effective in reducing the BIS displacement while also having a significantly reduced stroke.

In this dissertation, the control of a single-story structure is studied using the control devices presented in this chapter. A new type of TMDI system which incorporates the SRS device, called the semi-active TMDI (SATMDI) is presented, and the performance is compared with the TMDI system. For BISs, a new configuration of a TMD system using the SRS device is introduced. This configuration, called the NT-SATMD, attaches an SRS to a TMD system, where the SRS grounds the TMD mass. Tuning strategies for both of the new configurations is also introduced.

For multi-story structures, an alternative tuning strategy for the TMDI system based on the work of Sadek et al. [87] is proposed. This new tuning strategy is compared with a TMDI having a tuning strategy based on white noise input. In addition, the SATMDI system is used within a multi-story structure and the performance is evaluated.

Chapter 3

Ground Motions

3.1 Introduction

The ground motions used in this study were taken from the Pacific Earthquake Engineering Research (PEER) Ground Motion Selection Project [54]. The goal of that study was to introduce techniques for selecting sets of ground motions to be used in a variety of structural and geotechnical systems located in earthquake-prone regions of California. The results were four different ground motion sets, two which were used in this work, namely, the broad-band rock-site and pulse-like ground motion sets. These two sets were selected based on having larger magnitudes, near-fault, and pulse characteristics. Each set of ground motions comes in three components. For this work, only the normal component was considered as it typically has the largest magnitude. In this chapter, we will briefly introduce the defining properties of the two ground motion sets used in this dissertation.

3.2 Broad-band Rock-site Ground Motion Set

The broad-band rock-site ground motion set contains 40 unscaled three-component ground motions. The ground motions were selected such that their response spectra match median and log standard deviations for a magnitude 7 earthquake at a distance of 10 km. Since the ground motions were meant to represent rock sites for the response analysis, the site V_{s30} was assumed to be 760 m/s. Figure 3.1 shows the spectral acceleration of each ground motion and the median value.

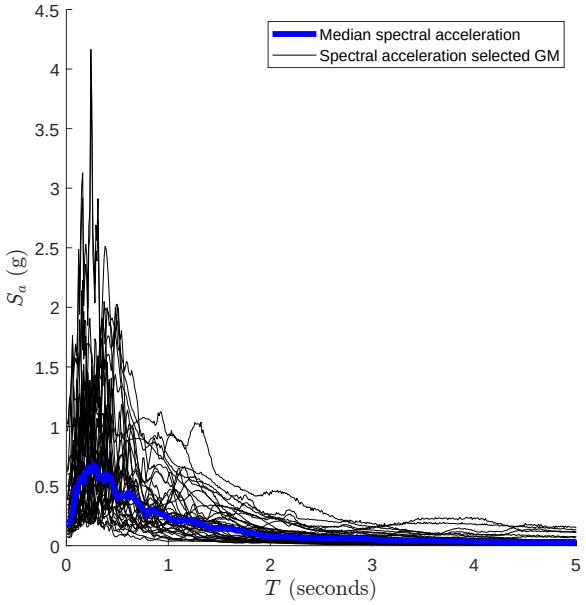

Figure 3.1: Spectral acceleration of 40 rock-site ground motions and median response spectrum.

3.3 Pulse-like Ground Motion Set

The pulse-like ground motion set contains 40 unscaled three-component ground motions containing strong velocity pulses of varying periods. The directivity effects of the near-fault ground motions cause strong velocity pulses. In particular, the ground motions have strong velocity pulses in the strike-normal direction, as shown by the the work done by Baker [8].

The pulse-period varies across the 40 ground motions since the relative period between the structure and pulse-period affects the structural response. The pulse-periods ranged from 1 to 12.9 seconds having a mean of 5.5 seconds. Figure 3.2 shows the spectral acceleration of each ground motion and the median value.

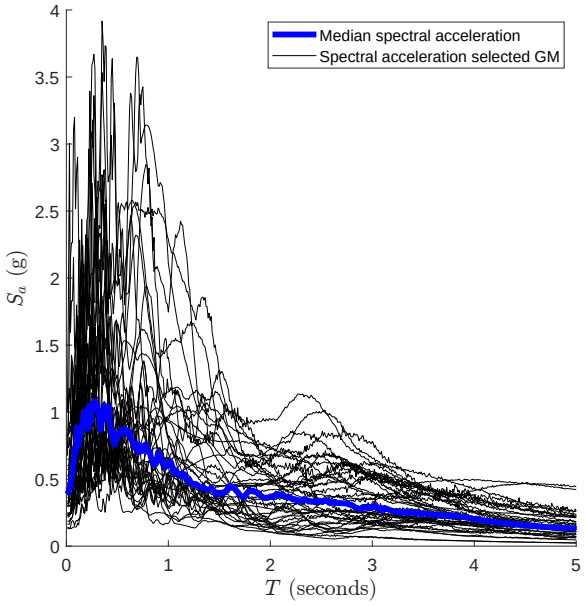

Figure 3.2: Spectral acceleration of 40 pulse-type ground motions and median response spectrum.

3.4 Summary

In this chapter, two ground motion sets, known as the rock-site and pulse-like ground motion sets, were introduced. These ground motion sets were selected based on having near-fault or pulse-like characteristics, the latter of which is known to cause significant increase in the response of the structure. Spectral acceleration plots of each ground motion set were also presented.

Chapter 4

Control of Single-story Structures

4.1 Introduction

Vibration control of civil engineering structures is an integral part of the design process, particularly structures subjected to earthquakes. Well known approaches include base isolation, [96, 84], energy dissipation, [101, 30], and tuned mass dampers (TMDs) [31, 42]. Tuned mass dampers have seen extensive use in civil structures, due to their simplicity and robustness. Since the early work of Ormondroyd and Hartog [78], there has been a variety of applications of TMDs to civil structures, such as bridge decks [16], tall buildings [128], and wind turbine towers [5]. Extensive analytical and experimental investigations have been conducted to measure the effectiveness of TMDs in vibration control [87, 116]. However, vibration control of the structure has been shown to be insufficient if the mass ratio of the TMD mass to the structure is significantly lower than 1% [7].

In Section 4.2, a new configuration of a TMD is introduced using a passive device and resettable semi-active spring (SRS). The passive device is taken to be an inerter, first introduced by Smith [93], and the SRS is a resettable spring element, put forward by Bobrow et al.

[11, 48]. The inerter is placed between the ground and the TMD, while the SRS is placed between the structure and TMD. This configuration will be known as a Semi-Active Tuned Mass Damper Inerter (SATMDI).

4.2 Semi-Active Tuned Mass Damper Inerter (SATMDI)

This section will investigate the use of a SATMDI in reducing displacement and acceleration responses of a single-story structure. The relative displacement between the structure and TMD, otherwise known as the stroke, will be compared between the SATMDI and TMDI systems. The response values will be normalized by the uncontrolled system, that is, a structure with no TMD system attached. The amount of virtual mass provided by the inerter, and stiffness provided by the SRS will also be studied.

Performance between the SATMDI and TMDI was evaluated using the median (50^{th} percentile). To measure the dispersion (or variation) in the responses, the median absolute deviation (MAD) was used. The results of this investigation will show that the SATMDI provides equal or better performance in reducing the the responses of the structure for a TMD system with a significantly smaller physical mass and can be housed in less area than a traditional TMD. Thus, the SATMDI will provide performance comparable to that of a large mass TMD, yet potentially without the additional costs and design complications for implementing a large mass TMD.

4.2.1 Equations of Motion

The equations of motion for the system shown in Figure 4.1 are given as,

$$\begin{bmatrix} m_s & 0 \\ 0 & m_t + b \end{bmatrix} \begin{bmatrix} \ddot{x}_1 \\ \ddot{x}_2 \end{bmatrix} + \begin{bmatrix} c_t + c_s & -c_s \\ -c_s & c_s \end{bmatrix} \begin{bmatrix} \dot{x}_1 \\ \dot{x}_2 \end{bmatrix} + \begin{bmatrix} k_s + k_t & -k_t \\ -k_t & k_t \end{bmatrix} \begin{bmatrix} x_s \\ x_t \end{bmatrix}$$

$$+ \begin{bmatrix} k_d & -k_d \\ -k_d & k_d \end{bmatrix} \begin{bmatrix} x_s \\ x_t \end{bmatrix} - \begin{bmatrix} k_d & -k_d \\ k_d & k_d \end{bmatrix} \begin{bmatrix} x_{sr} \\ x_{tr} \end{bmatrix} = - \begin{bmatrix} m_s \\ m_t \end{bmatrix} \ddot{x}_g. \tag{4.1}$$

In the above equations, m_s and m_t are the masses of structure and TMD, respectively, while

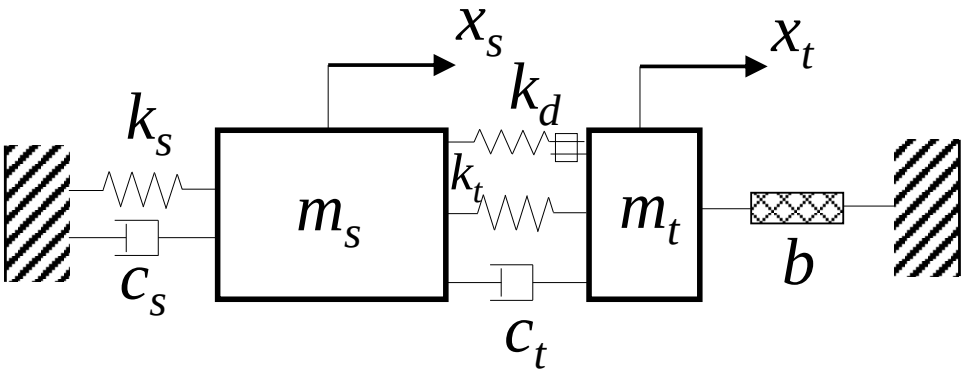

Figure 4.1: Semi-Active Tuned Mass Damper Inerter proposed in this paper.

b is taken to be the inertance (virtual mass) provided by the inerter. In addition, c_t and c_s are the damping coefficients of the structure and TMD, respectively, k_s and k_t are the stiffness of the structure and TMD, respectively, and k_d is the stiffness provided by the SRS. The displacement of the structure and TMD is measured relative to the ground displacement and denoted as x_s and x_t, respectively. The terms x_{sr} and x_{tr} are the values x_s and x_t at the last reset time, that is,

$$\text{set} \begin{bmatrix} x_{sr} \\ x_{tr} \end{bmatrix} = \begin{bmatrix} x_s \\ x_t \end{bmatrix} \text{ whenever } \dot{x}_s - \dot{x}_t = 0. \tag{4.2}$$

The ground acceleration is denoted by $\ddot{x}_g$. In this configuration, the inerter is attached directly to the ground, adding b amount of virtual mass to the the TMD system. This configuration is done to illustrate the effect an inerter has when incorporated within a TMD system. For multi-degree-of-freedom systems the inerter would instead be attached to the floor below, which has been studied by previous researchers [33].

Similar to previous work [31, 42], equation (4.1) is non-dimensionalized to reveal pertinent the parameters of the system, shown in (4.3).

$$\begin{bmatrix} \frac{1}{\mu+\beta} & 0 \\ 0 & 1 \end{bmatrix} \begin{bmatrix} \ddot{x}_1 \\ \ddot{x}_2 \end{bmatrix} + \begin{bmatrix} \frac{2\omega_s\zeta_s}{\mu+\beta} + 2\omega_t\zeta_t & -2\omega_t\zeta_t \\ -2\omega_t\zeta_t & 2\omega_t\zeta_t \end{bmatrix} \begin{bmatrix} \dot{x}_1 \\ \dot{x}_2 \end{bmatrix} + \begin{bmatrix} \frac{\omega_s^2}{\mu+\beta} + \omega_t^2 & -\omega_t^2 \\ -\omega_t^2 & \omega_t^2 \end{bmatrix} \begin{bmatrix} x_s \\ x_t \end{bmatrix}$$

$$- \begin{bmatrix} \omega_d^2 & -\omega_d^2 \\ -\omega_d^2 & \omega_d^2 \end{bmatrix} \begin{bmatrix} x_{sr} \\ x_{tr} \end{bmatrix} = - \begin{bmatrix} \frac{1}{\mu+\beta} \\ \frac{\mu}{\mu+\beta} \end{bmatrix} \ddot{x}_g. \tag{4.3}$$

The mass ratio μ and the inertance ratio β are defined as

$$\mu = \frac{m_t}{m_s} \text{ and } \beta = \frac{b}{m_s} \tag{4.4}$$

where the definition for β is consistent with previous studies for an inerter in TMD [70, 62]. We denote ω_s, ω_t, and ω_d as

$$\omega_s = \sqrt{\frac{k_s}{m_s}}, \quad \omega_t = \sqrt{\frac{k_t + k_d}{m_t + b}} \text{ and } \omega_d = \sqrt{\frac{k_d}{m_t + b}}. \tag{4.5}$$

It is worth noting that setting $b = k_d = 0$, reduces to the dimensionless ratios first defined by Hartog [78], where ω_s and ω_t were called the natural frequencies of the structure and TMD,

respectively. We also denote ζ_s and ζ_t, structure and TMD damping ratios, as

$$\zeta_s = \frac{c_t}{2m_s\omega_s} \text{ and } \zeta_t = \frac{c_s}{2m_t\omega_t}. \tag{4.6}$$

4.2.2 Tuning Strategy for SATMDI

The tuning strategy for a SATMDI system is based on the tuning strategy of a TMDI subject to white noise base excitation. This was due to its ease of use to demonstrate the effectiveness of the SATMDI system. A similar approach was done in [19], which incorporated a SRS within a TMD system using closed-form equations developed in [87].

As typically done in literature [70, 19, 27], consider the dimensionless frequency ratio f expressed by

$$f = \frac{\omega_t}{\omega_s} \tag{4.7}$$

where ω_s and ω_t are defined by in (4.5). To gauge the effect the SRS, we define the stiffness ratio κ, which is the ratio of the SRS stiffness to the total TMD stiffness,

$$\kappa = \frac{k_d}{k_t + k_d}. \tag{4.8}$$

For $\kappa = 1$, the SRS would completely replace the TMD spring, that is, $k_t = 0$. For $\kappa = 0$, the SRS provides no stiffness, and for $0 < \kappa < 1$, both the TMD spring and SRS contribute to the total stiffness. For this study, fixed values of κ ranging from 0 to 1 with increments of 0.25 are selected. The stiffness ratio values chosen are not optimized and are only used to show feasibility of the SATMDI system.

To tune the SATMDI, the equations from Marian et al. [70] are adopted to find the frequency

ratio f and damping ratio ζ_t, given by equations (4.9) and (4.10), respectively.

$$f = \frac{1}{1+\beta+\mu}\frac{\sqrt{\beta(\mu-1)+(2-\mu)(1+\mu)}}{\sqrt{2(1+\mu)}} \tag{4.9}$$

$$\zeta_t = \frac{\sqrt{\beta+\mu}\sqrt{\beta(3-\mu)+(4-\mu)(1+\mu)}}{2\sqrt{2(1+\beta+\mu)[\beta(1-\mu)+(2-\mu)(1+\mu)]}} \tag{4.10}$$

The above closed-form equations for the frequency and damping ratios were derived for an undamped single-degree-of-freedom system under white noise base excitation. The structure considered in this paper is lightly damped yet using equations (4.9) and (4.10) to tune the SATMDI will be adequate to show the effectiveness of using an SRS within a TMDI system.

4.2.3 Results

Using the two ground motion sets presented in Chapter 3, peak responses of the displacement, acceleration and stroke were found. The structure mass and stiffness were chosen to achieve a natural period of $T = 1$ second. The mass ratios used were $\mu = 0, 0.01, 0.05$. To gauge the performance of the TMD systems, the following reduction factors are introduced,

$$R_D = \frac{\text{Peak displacement of controlled structure}}{\text{Peak displacement of uncontrolled structure}} \tag{4.11}$$

$$R_A = \frac{\text{Peak acceleration of controlled structure}}{\text{Peak acceleration of uncontrolled structure}} \tag{4.12}$$

$$R_S = \frac{\text{Peak stroke of the SATMDI system}}{\text{Peak stroke of the TMDI system}} \tag{4.13}$$

and are called the displacement, acceleration, and stroke reduction factors, respectively. In (4.11) and (4.12) the controlled structure refers to the structure equipped with a SATMDI or TMDI system. The uncontrolled structure refers to the structure without either control device. Having $R_D < 1$ or $R_A < 1$ would indicate that the controlled system is effective in reducing the structure displacement and acceleration. When $R_S < 1$, the SATMDI system has less stroke than the TMDI system. The median of the reduction factors over ground motions from each set is used to compare the systems.

Figures 4.2-4.7 show the median displacement, acceleration, and stroke reduction factors for the rock-site and pulse-like ground motion set. Each figure displays the results using mass ratios $\mu = 0, 0.01$, and 0.05.

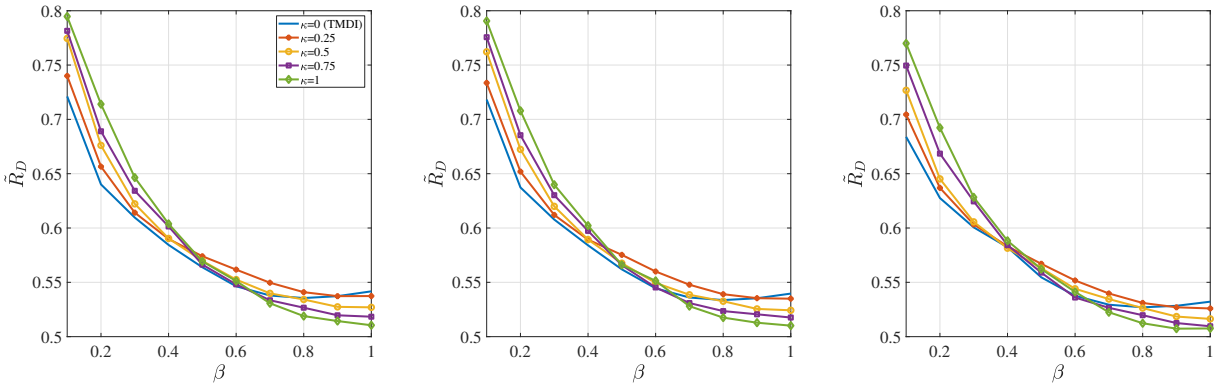

(a) (b) (c)

Figure 4.2: Rock-site ground motion set for displacement reduction factor $\bar{R}_D$ where (a) $\mu = 0$, (b) 0.01, and (c) 0.05.

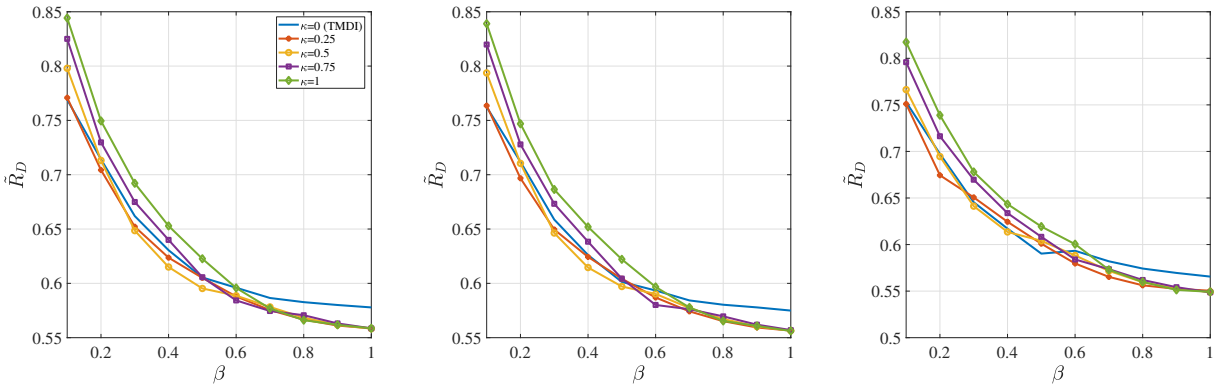

(a) (b) (c)

Figure 4.3: Pulse-like ground motion set for displacement reduction factor $\bar{R}_D$ where (a) $\mu = 0$, (b) 0.01, and (c) 0.05.

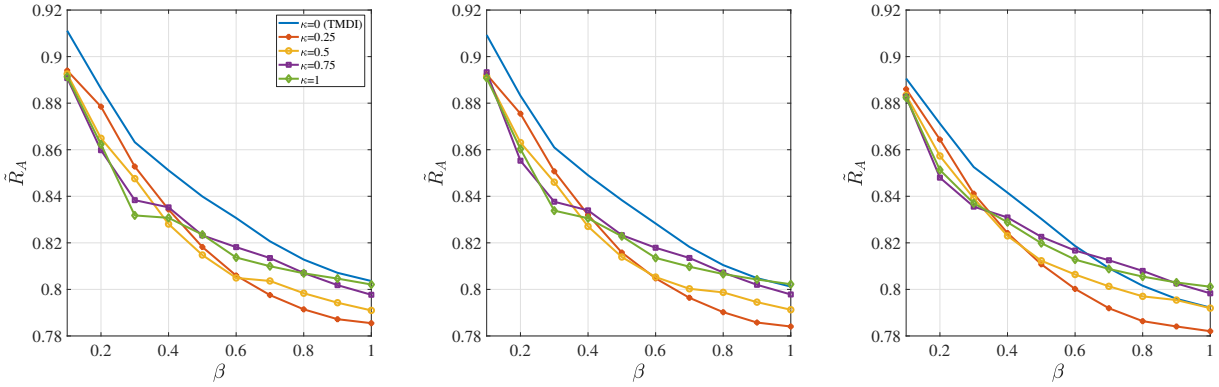

(a) (b) (c)

Figure 4.4: Rock-site ground motion set for acceleration reduction factor $\bar{R}_A$ for (a) $\mu = 0$, (b) 0.01, and (c)0.05.

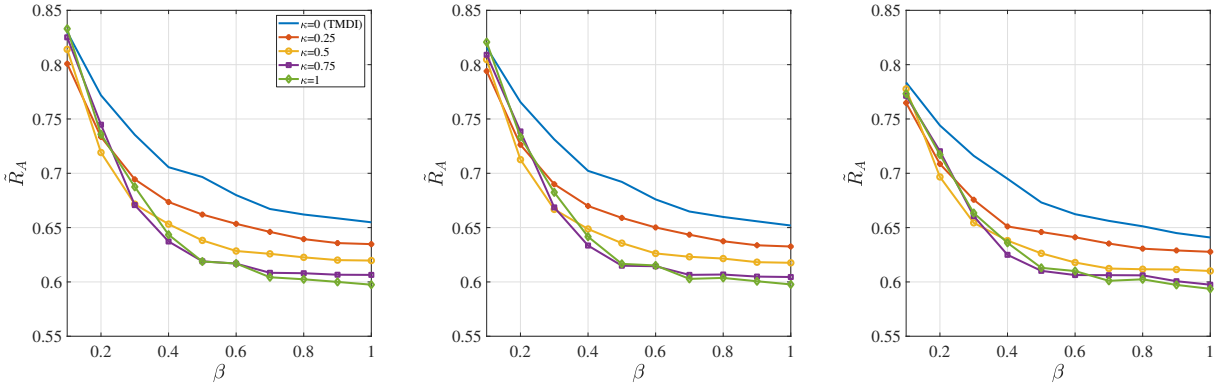

(a) (b) (c)

Figure 4.5: Pulse-like ground motion set for acceleration reduction factor $\bar{R}_A$ for (a) $\mu = 0$, (b) 0.01, and (c)0.05.

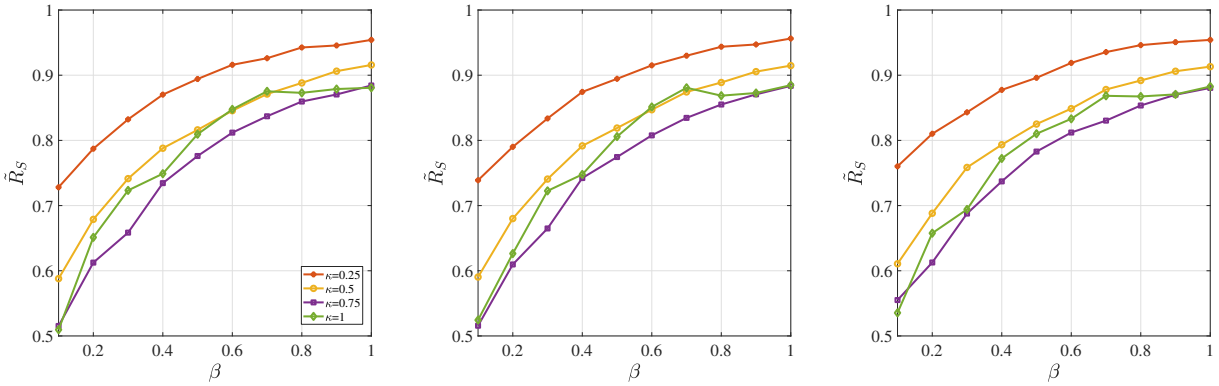

(a) (b) (c)

Figure 4.6: Rock-site ground motion set for stroke reduction factor $\bar{R}_S$ for (a) $\mu = 0$, (b) 0.01, and (c)0.05.

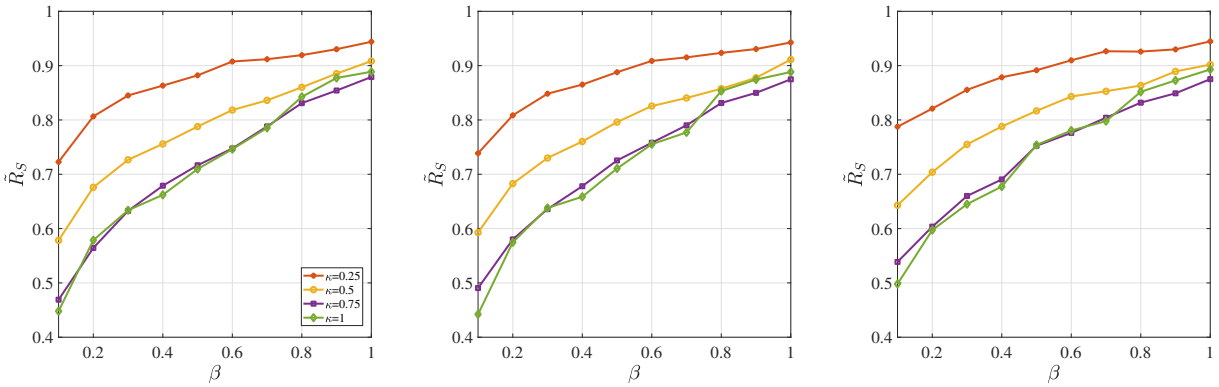

(a) (b) (c)

Figure 4.7: Pulse-like ground motion set for Stroke reduction factor $\bar{R}_s$ for (a) $\mu = 0$, (b) 0.01, and (c)0.05.

4.2.4 Discussion

Figures 4.2 and 4.3 show that the SATMDI and TMDI are effective in reducing the displacement response for all mass ratios and each ground motion set. By increasing the inertance β, the responses decrease. Similarly, by increasing the mass ratio, the responses decrease. For the rock-site ground motion set, Figures 4.2a-4.2c show that increasing the stiffness ratio κ when $\beta < 0.4$ leads to worse performance, while the reverse occurs for $\beta > 0.4$. The pulse-like ground motion set has a similar behavior, yet instead of the reversal in performance, the lines coalesce. The reason the SATMDI performs worse as the stiffness ratio is increased can be explained by the tuning strategy of the TMDI system and the resetting of the SRS. The TMDI was tuned to minimize displacement while the spring remains linear. For the SATMDI, the force provided by the SRS is nonlinear. In particular, the force vanishes at reset (see (2.5)), which adversely affects the displacement response. For the rock-site ground motion set, only after increasing the inertance past 0.4 is there an improvement in performance. The results presented are consistent with those found in a previous study [19] incorporating an SRS within a TMD system, where a portion of the structure is used as the TMD mass, that is, where the mass ratio $\mu > 0.4$.

For the acceleration (Figures 4.4 and 4.5), the SATMDI provides better performance than the TMDI. Specifically, there is considerable reductions in acceleration for the pulse-like ground motion set when using a SATMDI system. As for the stroke (Figures 4.6 and 4.7), as much as a 50% reduction occurs for small values of inertance, yet for larger inertance there is less improvement. This behavior is also present for the displacement and acceleration responses as the inertance is increased. Thus, the reductions in the response are mainly due to a larger inerter than those provided from the SRS device.

The reductions in the acceleration and stroke of the SATMDI can be attributed to the energy dissipative property of the SRS. Since the SRS is placed between the structure and TMD,

energy transfer can occur from the structure to the SRS, providing reduced acceleration. A similar effect occurs for the stroke. In fact, it has been shown [11, 48] for an SRS placed between two masses where the control law is given by (4.2) that the SRS does not provide direct reductions in the displacement of a single mass. Since the control law is based on the relative velocity of the ends, the relative displacement between the masses is reduced. Thus, an SRS placed between a structure the TMD mass, it is the stroke that is directly reduced, while reducing the structure displacement indirectly.

From the results shown, for inertance values greater than 0.4, there is considerable reductions in the acceleration of the structure. This is especially important in the event of a strong ground motion, where the occupants and/or delicate equipment within the structure experience reduced forces. For inertance values between 0.2-0.4, there is a good balance between reducing the displacement, acceleration, and stroke responses. For smaller values of inertance there is a large reduction in the stroke. Therefore, depending on which response is critical, the SATMDI parameters can be chosen to accommodate the requirement.

When $\mu = 0$, there is an addition benefit, where the inerter replaces the TMD mass. The displacement, acceleration, and stroke responses show marginally improved performance than nonzero μ. Therefore, by using an SRS within a TMDI system where $\mu = 0$, the SATMDI has nearly equal or better performance in reducing displacements, while having additional reductions in the acceleration and stroke. More importantly, by replacing the TMD mass by the inerter, the SATMDI acts as a miniaturized large mass TMD, yet can be housed in a smaller area of the structure due to the reduced mass and stroke. Thus, the SATMDI can provide the performance of a large mass TMD, yet at a potentially reduced monetary cost and retrofitting complications.

4.3 Base-isolation

Base-isolation systems (BISs) have been extensively used in practice to mitigate the damage in structures caused by strong earthquakes. This is accomplished by providing sufficient lateral flexibility at the base level to absorb the displacement demand. This results in several large base-isolators. To ease the displacement demand, tuned mass dampers (TMDs) have been attached to the base structure in various configurations. In the following sections, two common approaches are presented. In addition, a new configuration incorporating a SRS is proposed.

4.3.1 Traditional and Non-traditional Tuned Mass Dampers

Several researchers [106, 104, 85, 121] have studied various configurations of TMD systems attached to the base structure to reduce the response. This study investigated the use of a traditional TMD (T-TMD) and non-traditional TMD (NT-TMD) attached to a BIS, shown in Figures 4.8a and 4.8b, respectively. The T-TMD and NT-TMD was compared to the new one proposed in this paper, called the non-traditional SATMD (NT-SATMD), shown in Figure 4.8c.

For each system in Figure 4.8, the center of mass displacement of the superstructure, base, and TMD are denoted by x_s, x_b, and x_t, with each having mass m_s, m_b, and m_t, respectively. The superstructure stiffness and damping are denoted as k_s and c_s, and the stiffness and damping of the BIS are denoted as k_b and c_b. The stiffness and damping of the TMD system are denoted as k_t and c_t, while k_d denotes the stiffness of the SRS. The ground displacement is denoted as x_g.

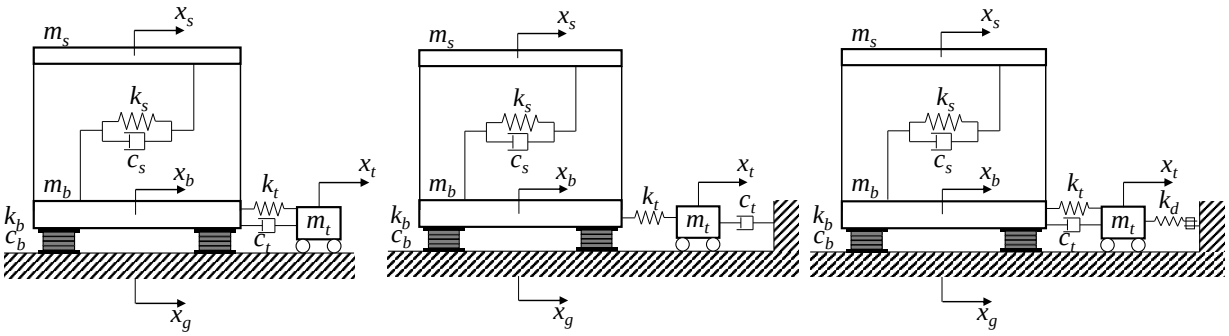

Figure 4.8: Idealized 3DOF system using lead-plug rubber bearings as the base isolation system equipped with a (a) T-TMD, (b) NT-TMD, and (c) NT-SATMD system.

4.3.2 Equations of Motion of T-TMD and NT-TMD

The equations of motion for the T-TMD and NT-TMD are shown in (4.14) where $\boldsymbol{u} = \begin{bmatrix} u_{sb} & u_b & u_t \end{bmatrix}^T$ and $\boldsymbol{r} = \begin{bmatrix} 0 & 1 & 1 \end{bmatrix}^T$, and a dot denotes a derivative with respect to time. The mass and stiffness matrices for each system are defined in (4.15), while the damping matrix for the T-TMD is given in (4.16), and for NT-TMD in (4.17).

$$\boldsymbol{M}\ddot{\boldsymbol{u}} + \boldsymbol{C}\dot{\boldsymbol{u}} + \boldsymbol{K}\boldsymbol{u} = -\boldsymbol{M}\boldsymbol{r}\ddot{x}_g \tag{4.14}$$

$$\boldsymbol{M} = \begin{bmatrix} m_s & m_s & 0 \\ m_s & m_s + m_b & 0 \\ 0 & 0 & m_t \end{bmatrix}, \boldsymbol{K} = \begin{bmatrix} k_s & 0 & 0 \\ 0 & k_b + k_t & -k_t \\ 0 & -k_t & k_t \end{bmatrix} \tag{4.15}$$

$$\boldsymbol{C}_{T-TMD} = \begin{bmatrix} c_s & 0 & 0 \\ 0 & c_b + c_t & -c_t \\ 0 & -c_t & c_t \end{bmatrix} \tag{4.16}$$

$$\boldsymbol{C}_{NT-TMD} = \begin{bmatrix} c_s & 0 & 0 \\ 0 & c_b & 0 \\ 0 & 0 & c_t \end{bmatrix} \tag{4.17}$$

4.3.3 Non-traditional Semi-Active Tuned Mass Damper

The non-traditional semi-active tuned mass damper (NT-SATMD) is show in Figure 4.8c. In this arrangement, the linear spring and damper, TMD mass, and SRS are placed in series. The parallel spring and damper attach the TMD mass to the base structure, while the SRS is placed between the TMD mass and ground. In the following sections, the equations of motion and tuning strategy are presented for the NT-SATMD.

4.3.4 Equations of Motion of NT-SATMD

The equations of motion for a BIS equipped with an NT-SATMD (Figure 4.8c) is shown in (4.18) where the mass, damping, and stiffness matrices are given by (4.15) and (4.16). The sparse stiffness matrix associated with the SRS is defined in (4.19).

$$\boldsymbol{M\ddot{u}} + \boldsymbol{C\dot{u}} + (\boldsymbol{K} + \boldsymbol{K_d})\boldsymbol{u} - \boldsymbol{K_d u_r} = -\boldsymbol{M r}\ddot{x}_g \tag{4.18}$$

$$\boldsymbol{K_d} = \begin{bmatrix} 0 & 0 & 0 \\ 0 & 0 & 0 \\ 0 & 0 & k_d \end{bmatrix} \tag{4.19}$$

The piece-wise constant $\boldsymbol{u_r}$ is defined by (4.20) and is analogous to the control law in (2.3), yet since there is ground motion, the velocity across the SRS must be considered. The approach is similar to prior studies [11, 48] using an SRS within a multi-story structure. In the context of this paper, the velocity across the SRS is the velocity of the TMD mass relative to the ground, that is, $\dot{u}_t = \dot{x}_t - \dot{x}_g$.

$$\text{set } \boldsymbol{u_r} = \boldsymbol{u} \text{ whenever } \dot{u}_t = 0 \tag{4.20}$$

In (4.18), setting $k_d = 0$, reduces to the equations of motion for a BIS equipped with a T-TMD system [106], while further setting $k_t = c_t = 0$ the equations of motion of a BIS is recovered [74].

As typically done in previous studies of TMDs [74, 121], non-dimensionalizing (4.18) gives the critical parameters of the system used in the tuning strategy for the TMD. This leads to the following dimensionless mass, stiffness, and damping matrices.

$$\boldsymbol{M} = \begin{bmatrix} 1 & 1 & 0 \\ \frac{1}{1+\mu_b} & 1 & 0 \\ 0 & 0 & 1 \end{bmatrix} \tag{4.21}$$

$$\boldsymbol{K} = \begin{bmatrix} \omega_s^2 & 0 & 0 \\ 0 & \omega_b^2 + \omega_t^2 \left(\frac{\mu_t}{1+\mu_b}\right) & -\omega_t^2 \left(\frac{\mu_t}{1+\mu_b}\right) \\ 0 & -\omega_t^2 \left(\frac{\mu_t}{1+\mu_b}\right) & \omega_t^2 \end{bmatrix}, \boldsymbol{K_d} = \begin{bmatrix} 0 & 0 & 0 \\ 0 & 0 & 0 \\ 0 & 0 & \omega_d^2 \end{bmatrix} \tag{4.22}$$

$$\boldsymbol{C}_{NT-SATMD} = \begin{bmatrix} 2\omega_s\zeta_s & 0 & 0 \\ 0 & Y & -Z \\ 0 & -Z & Z \end{bmatrix} \tag{4.23}$$

where

$$Y = 2\omega_b\zeta_b + 2\omega_t\zeta_t\left(\frac{\mu_t}{1+\mu_b}\right), \tag{4.24}$$

$$Z = 2\omega_t\zeta_t\left(\frac{\mu_t}{1+\mu_b}\right). \tag{4.25}$$

The dimensionless parameters in (4.21)-(4.25) are given by

$$\mu_b = \frac{m_b}{m_s}, \mu_t = \frac{m_t}{m_s} \tag{4.26}$$

$$\omega_s = \sqrt{\frac{k_s}{m_s}}, \zeta_s = \frac{c_s}{2m_s\omega_s} \tag{4.27}$$

$$\omega_b = \sqrt{\frac{k_b}{m_s+m_b}}, \zeta_b = \frac{c_b}{2(m_s+m_b)\omega_b} \tag{4.28}$$

$$\omega_t = \sqrt{\frac{k_t+k_d}{m_t}}, \zeta_t = \frac{c_t}{2m_t\omega_t}, \omega_d = \sqrt{\frac{k_d}{m_t}}. \tag{4.29}$$

For this study, the mass of the super and base structures were taken as $m_s = 1\times10^6$ kg and $m_b = 5\times10^5$ kg, respectively. The stiffness of the super and base structures are selected to achieve natural periods of $T_s = 1$ and $T_b = 4$ seconds, and with damping ratios $\zeta_s = 0.02$ and $\zeta_b = 0.05$. The choices on the damping ratios were to model a lightly damped structure having a moderately damped BIS.

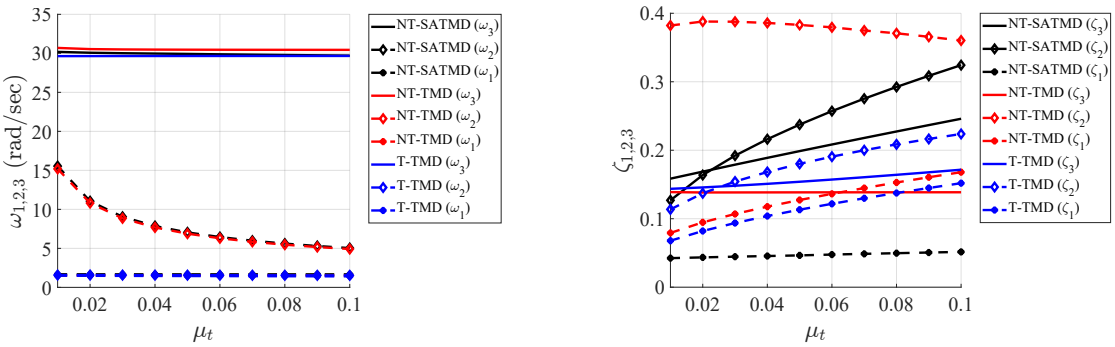

(a) (b)

Figure 4.9: Selection of (a) damping ratio ζ_t and (b) stiffness ratio κ for mass ratios (μ_t) ranging from 0.01-0.1.

The terms in (4.26) are the mass ratios of the base and TMD, respectively. In (4.27)-(4.28), the parameters ω_s and ζ_s are the natural frequency and damping ratio of the fixed base structure without a BIS, while ω_b and ζ_b are the natural frequency and damping ratio of the BIS where the superstructure and BIS experience rigid motion. For (4.29), ω_t and ζ_t are the natural frequency and damping ratio of the TMD system, assuming the BIS and superstructure remains stationary. The non-dimensional parameters ω_s, ω_b, and ω_t are typically referred to as the natural frequencies super and base structure, and TMD [74, 106]. These are not the actual natural frequencies of the system, but is merely done to simplify exposition. Similar dimensionless parameters can be derived for the T-TMD and NT-TMD systems, but are left out for brevity. The actual natural frequencies and damping ratios versus the μ_t are shown in Figure 4.9. Based on these results, the natural frequencies of each system are relatively equal, while the damping ratios vary greatly. This is a consequence of the tuning strategy of each system, which will be described in detail in the following section.

4.3.5 Tuning Strategy for NT-SATMD

When tuning a TMD system, the dimensionless frequency ratio f [106], defined as

$$f = \frac{\omega_t}{\omega_b} \tag{4.30}$$

is used where ω_b and ω_t are defined in (4.28) and (4.29). Based on the tuning strategy of NT-TMD applied to BISs [121], the frequency ratio for this study is taken to be

$$f = \frac{1}{\sqrt{\mu_t}} \tag{4.31}$$

For T-TMD systems, the frequency ratio is found to be less than one due to the results of a closed-form equation [27, 9] or by the constraints set when solving numerically [89, 87]. For a NT-TMD, the numerical optimization done by Xiang et al. [121] instead set the upper bound on the frequency ratio to be $1/\sqrt{\mu_t}$, which was done to find the global minimum of the maximum magnitude of frequency transfer function of acceleration. It was found that setting the frequency ratio to be as large as possible led to the greatest response reductions. For base-isolated structures, it is possible to set $f = 1/\sqrt{\mu_t}$. The frequency ratio is greater than one for $\mu_t < 1$, which leads to having a larger spring stiffness for a NT-TMD and NT-SATMD as compared with the T-TMD systems. This can seen by writing $k_t + k_d$ in terms of k_b using (4.28) and (4.29) in (4.30), where the frequency ratio is squared. A portion of the stiffness for the NT-SATMD is provided by the SRS. Since the energy absorbed increases for larger stiffness (see (2.1)), by having a larger stiffness for the TMD system, the SRS can become more beneficial.

The damping ratio ζ_t is taken from the work of Sadek et al. [87], defined in (4.32), since it

allows for simple damper tuning with desirable performance.

$$\zeta_t = \Phi \left(\frac{\zeta_1}{1+\mu} - \sqrt{\frac{\mu}{1+\mu}} \right) \tag{4.32}$$

where μ is defined as

$$\mu = \frac{m_t}{\boldsymbol{\phi}_1^T \boldsymbol{M} \boldsymbol{\phi}_1} \tag{4.33}$$

where $\boldsymbol{M}$ is the mass matrix and $\boldsymbol{\phi}_1$ is the fundamental mode shape normalized to have unit participation factor. The first modal damping ratio of the system is denoted by ζ_1 and Φ is the amplitude of the normalized first mode shape at the location of the TMD. Prior studies [19] used an SRS with the resetting technique defined in (2.3). In that study, the SRS was placed between the structure and the TMD mass, and the damping ratio was selected using (4.32). Figure 4.10a shows the damping ratio for the T-TMD (black), NT-TMD (red), NT-SATMD (black), as a function of the mass ratio μ_t.

To capture the effect of the SRS, the dimensionless ratio, κ, so forth called as the stiffness ratio, is defined as

$$\kappa = \frac{k_d}{k_t + k_d} \tag{4.34}$$

For $\kappa = 1$, the SRS replaces the linear spring, while for $\kappa = 0$, the SRS is not used. For $0 < \kappa < 1$, both the linear spring and SRS are engaged. The selection of stiffness ratio was to minimize the peak displacement of the base structure subject to a series of harmonic base excitations having input frequencies varying from $0.3\omega_b$ to $2\omega_b$. The MATLAB Optimization Toolbox was used to find the stiffness ratio κ. The surrogate optimization function was employed due to having a computationally expensive objective function. Moreover, the objective function may be non-convex, yet surrogate optimization is derivative-free and can be used [37]. The mass ratios μ_t ranged from 0.01-0.1, and the base structure mass is taken

as 5% of the superstructure, which are comparable to other studies [121, 39].

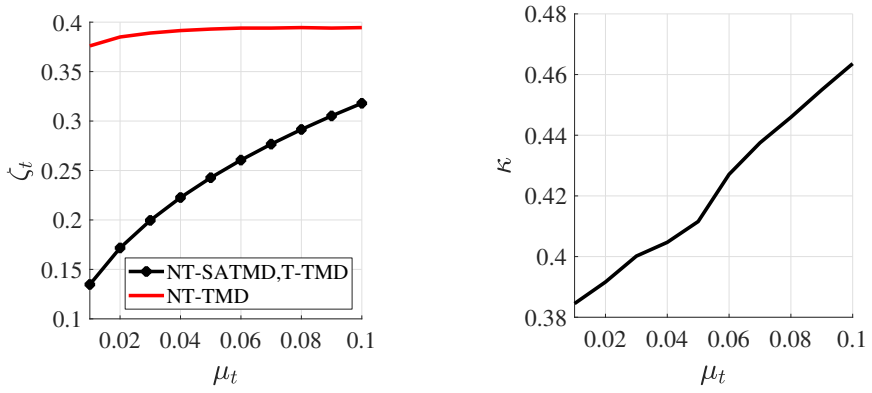

(a) (b)

Figure 4.10: Selection of (a) damping ratio ζ_t and (b) stiffness ratio κ for mass ratios (μ_t) ranging from 0.01-0.1.

Figure 4.10b shows the results of the optimization to find the stiffness ratio. Selecting the frequency ratio in (4.31) and damping ratio in (4.32) results in a nearly linear relationship between the stiffness ratio, κ, and mass ratio, μ_t, even though the SRS is a nonlinear device. This allows for an easier TMD design process since the selection of the frequency, damping, and stiffness ratios can be easily calculated. Previous studies [19] which incorporated a SRS within a TMD system chose stiffness ratios from 0 to 1 in varying increments, and similarly, used the tuning strategy of Sadek et al [87]. The results of that study showed that the using an SRS within a TMD system provided greater reductions in the displacement and acceleration responses as compared to a passive TMD system.

4.3.6 Results

To gauge the performance of each TMD system, the displacement and acceleration of the super and base structure are considered. The relative displacement between the super and base structure, and relative displacement between the base and TMD mass, otherwise known as the stroke, are considered. The ratio of each of these, to the uncontrolled values, are

denoted by

$$R_D = \frac{\text{Peak displacement (controlled)}}{\text{Peak displacement (uncontrolled)}} \tag{4.35}$$

$$R_A = \frac{\text{Peak acceleration (controlled)}}{\text{Peak acceleration (uncontrolled)}} \tag{4.36}$$

$$R_S = \frac{\text{Peak stroke (SA or passive control)}}{\text{Peak stroke (passive control)}} \tag{4.37}$$

and are called the displacement, acceleration, and stroke reduction factors, respectively. The controlled system refers to a structure with a BIS having a TMD attached, whereas the uncontrolled refers to a structure with only a BIS. For the T-TMD, NT-TMD, and NT-SATMD peak displacements and accelerations are normalized by the peak displacement and acceleration of the BIS system. For the stroke reduction factor, the peak stroke of the NT-TMD and NT-SATMD are normalized by the peak stroke of the T-TMD. To compare the performance of each TMD system under each ground motion set, the mean reduction factors, $\bar{R}_D, \bar{R}_A$, and $\bar{R}_S$ were used.

Figures 4.11-4.13 show the mean peak displacement reduction factors for the super and base structure, and relative displacement under the rock-site and pulse-like ground motions. Figures 4.14 and 4.15 show the mean peak acceleration reduction factors for the super and base structure under the rock-site and pulse-like ground motions. Figure 4.16 shows the stroke reduction factor under the rock-site and pulse-like ground motion sets. Each of these plots vary with mass ratios of 0.01-0.1 for the T-TMD, NT-TMD, and NT-SATMD systems.

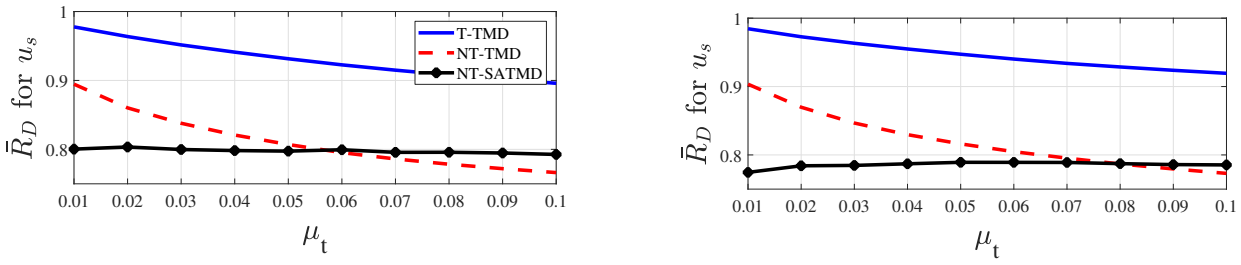

(a) (b)

Figure 4.11: Structure displacement, $\bar{R}_D$ of u_s for (a) rock-site and (b) pulse-like ground motion sets.

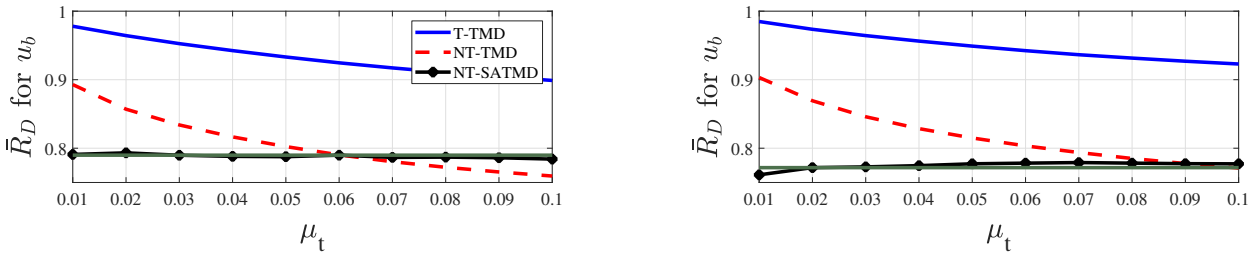

(a) (b)

Figure 4.12: Base displacement, $\bar{R}_D$ of u_b for (a) rock-site and (b) pulse-like ground motion sets.

4.3.7 Discussion

Figures 4.11-4.13 show the mean super and base structure, and relative displacement reduction factors for the rock-site and pulse-like ground motion sets. For either set of ground motions, the T-TMD and NT-TMD systems' performance improves for larger μ_t. For the NT-SATMD, the performance is nearly constant across all mass ratios (see Figures 4.11 and 4.12). In other words, the NT-SATMD effectiveness in reducing displacements is independent of the selection of the mass ratio. Moreover, the NT-SATMD is better in reducing the structure and base displacements for mass ratios less than 0.06. As for the relative displacement between the super and base structure (Figure 4.13), there is a small increase as compared with the BIS. Since the BIS already significantly reduces the relative displacement [74], this increase is negligible.

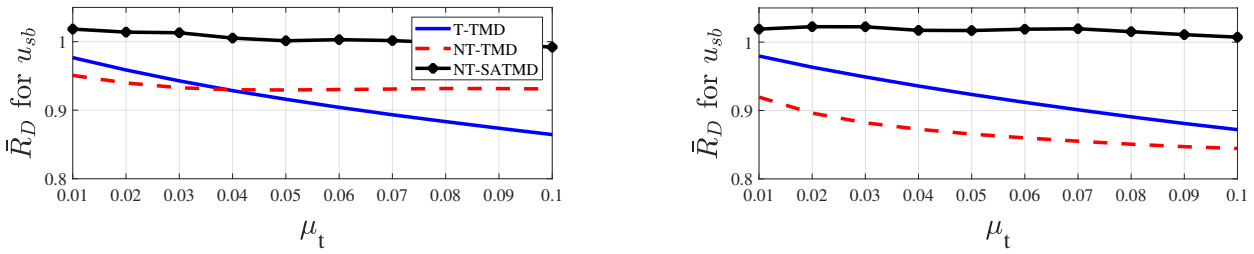

(a) (b)

Figure 4.13: Relative displacement, $\bar{R}_D$ of u_{sb} for (a) rock-site and (b) pulse-like ground motion sets.

Figures 4.14 and 4.15 show the mean super and base structure acceleration reduction factors for the rock-site and pulse-like ground motion sets. Similar to the displacement, the NT-SATMD is nearly constant for all mass ratios μ_t, with the only exception being the base acceleration for the pulse-like ground motion set. Specifically, for $\mu_t = 0.01$, there is a spike occurring, and should be avoided by selecting $\mu_t \geq 0.02$. The spike in acceleration is a consequence of the tuning strategy used, that is, choosing $f = 1/\sqrt{\mu_t}$. As described earlier, since $f \geq 1$, the stiffness of the NT-SATMD is larger than the T-TMD. This leads to a greater amount of force transmitted from the ground to the base. A similar result was found in previous work [30] using the SRS in a bracing system that added stiffness to a single-degree-of-freedom system. Note that the rock-site ground motion set (Figure 4.15a) also exhibits a spike at μ_t, yet due to the characteristics of the ground motion set, it is not as pronounced. The spike in the acceleration of the pulse-like ground motion set can also be attributed to the velocity pulse and generally intense ground motions used [30].

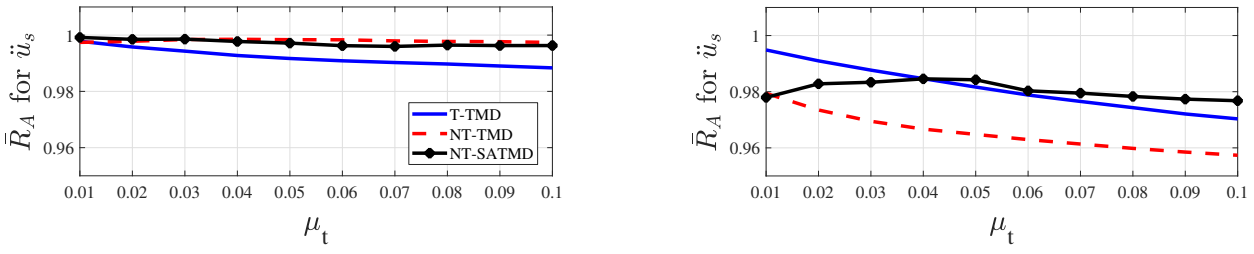

(a) (b)

Figure 4.14: Structure acceleration, $\tilde{R}_A$ of u_s for (a) rock-site and (b) pulse-like ground motion sets.

Figure 4.16 shows the stroke reduction factors for the rock-site and pulse-like ground motion sets. Both the NT-TMD and NT-SATMD provide considerable reductions in the stroke for small mass ratios. Increasing the the mass ratio has a diminishing effect on reducing stroke. The increase in $\bar{R}_S$ can be attributed to the T-TMD having less stroke for larger masses. Yet, even with $\mu_t = 0.1$, the NT-TMD provides nearly 70% reductions, while the NT-SATMD provides nearly 60%. The results are a direct consequence of the configurations of the NT-SATMD and NT-TMD, that is, by having the TMD mass grounded by either the SRS or damper, the displacement of the TMD mass is reduced, and in turn reducing the relative displacement between the base structure and TMD.

The main contribution of this section is demonstrating that using an NT-SATMD has an equal (or better) performance in reducing the super and base structure displacements for a mass ratio three to five times smaller. Observing Figure 4.12a (rock-site ground motion set), the NT-SATMD for $\mu_t = 0.02$ has an equal level of performance as a NT-TMD with $\mu_t = 0.06$. This is shown by the green line. Similarly, by considering Figure 4.12b, the NT-SATMD with $\mu_t = 0.02$ has equal performance as the NT-TMD with $\mu_t = 0.08 - 0.1$ under the pulse-like ground motion set. Moreover, the stroke of the NT-SATMD for $\mu_t = 0.02$ and a NT-TMD for $\mu_t = 0.06$ are within 5% as shown by difference between the green line and the black. Assessing the performance of three control systems having equal mass ratios ($\mu_t = 0.02$), the NT-SATMD has greater reductions in the super and base structure

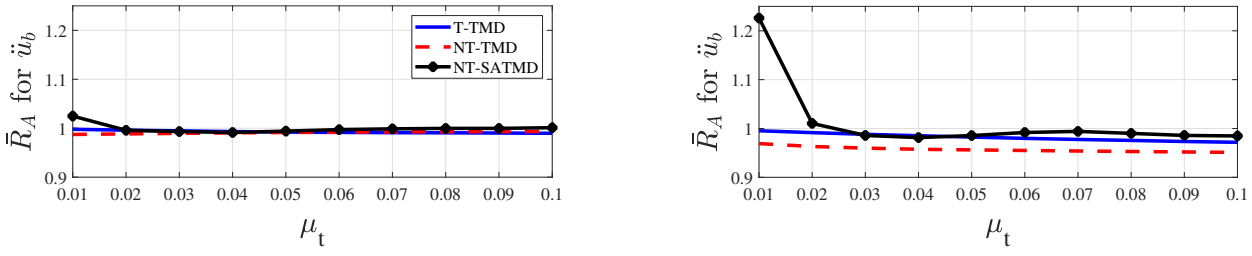

(a) (b)

Figure 4.15: Base acceleration, $\bar{R}_A$ of u_b for (a) rock-site and (b) pulse-like ground motion sets.

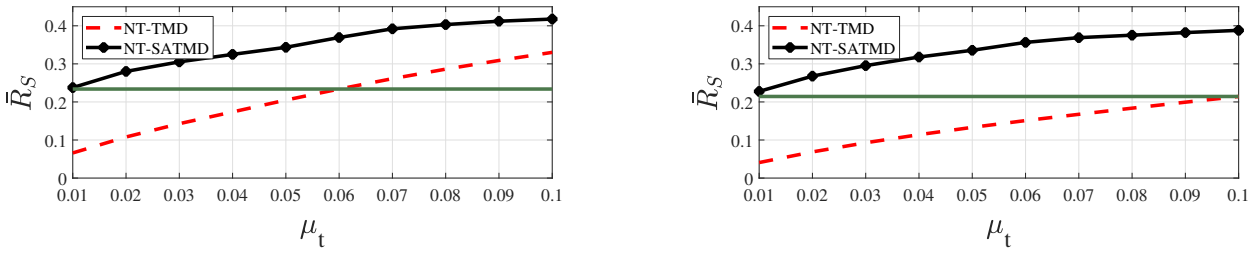

(a) (b)

Figure 4.16: Stroke, $\bar{R}_s$, for (a) rock-site and (b) pulse-like ground motion sets.

displacements (see Figures 4.11 and 4.12). The acceleration performance is approximately the same for the three control systems (see Figures 4.14 and 4.15).

The negative effect of using a NT-SATMD is having an increase of no more than 2.5% in the relative displacement between the super and base structure (Figures 4.13a and 4.13b). In addition, the super and base structure accelerations (Figures 4.14 and 4.15) are also larger for some choices in μ_t. To address the former negative effect, since the BIS already greatly reduces the relative displacement between the super and base structure [74], the small increase will likely have no considerable effect. For the latter effect, using mass ratios $\mu_t \geq 0.02$ also avoids the large base structure accelerations for pulse-like ground motions. For a NT-SATMD where $\mu_t = 0.02$, there is considerably smaller super and base structure displacements as compared with a T-TMD having a large mass ($\mu_t \geq 0.05$). By having a reduced stroke, the footprint required to house the NT-SATMD is much smaller than a T-TMD. As for comparing the NT-SATMD with $\mu_t = 0.02$ to a NT-TMD with $\mu_t = 0.06$, the NT-SATMD has equal performance in reducing the displacements as a NT-TMD. Moreover, the stroke of a NT-SATMD with $\mu_t = 0.02$ is comparable to that of a NT-TMD with $\mu_t = 0.06$. Given that the NT-SATMD has equal or better performance with a smaller mass, there is potentially reduced monetary costs in construction and installation.

4.4 Summary

In this chapter, a new type of hybrid control system for BIS was introduced. A resettable semi-active spring (RSS) was used to ground a TMD mass that is attached to the base structure of a BIS. In this configuration, called the NT-SATMD, the performance was compared against a NT-TMD and T-TMD. When comparing equal level mass ratios, the results showed that the NT-SATMD outperforms the T-TMD and NT-TMD in reducing the super and base structure displacements. More interestingly, the NT-SATMD can provide equal (or better) performance in reducing the super and base structure displacements with a mass that is considerably smaller. For a small mass ($\mu_t = 0.02$), the NT-SATMD provides nearly equal performance of a large mass ($\mu_t = 0.06$) NT-TMD, and better performance than a large mass T-TMD. Consequently, using an NT-SATMD provides equal or better reductions in the structure responses, while also being housed in a smaller area of the structure, which can potentially lead to cheaper costs in the construction and installation.

Chapter 5

Control of Multi-story Structures

5.1 Introduction

In this chapter, the control techniques presented in Chapter 4 are extended to multi-story structures. The control systems considered are the tuned mass damper inerter (TMDI) and the semi-active tuned mass damper inerter (SATMDI). The equations of motion for each configuration and the tuning strategies of each will be presented. The performance of each control system in reducing the response will be compared. In addition, an alternative tuning strategy for the TMDI will also be introduced and studied.

5.2 Tuned Mass Damper with Inerter

In Figure 5.1 a multi-story structure with a TMDI attached at the top story is shown. In this configuration, the inerter is attached to the floor below, which is consistent with literature on the application of TMDs to reduce the response of multi-story structures. In the following subsections the equations of motion and tuning strategy for a TMDI will be presented.

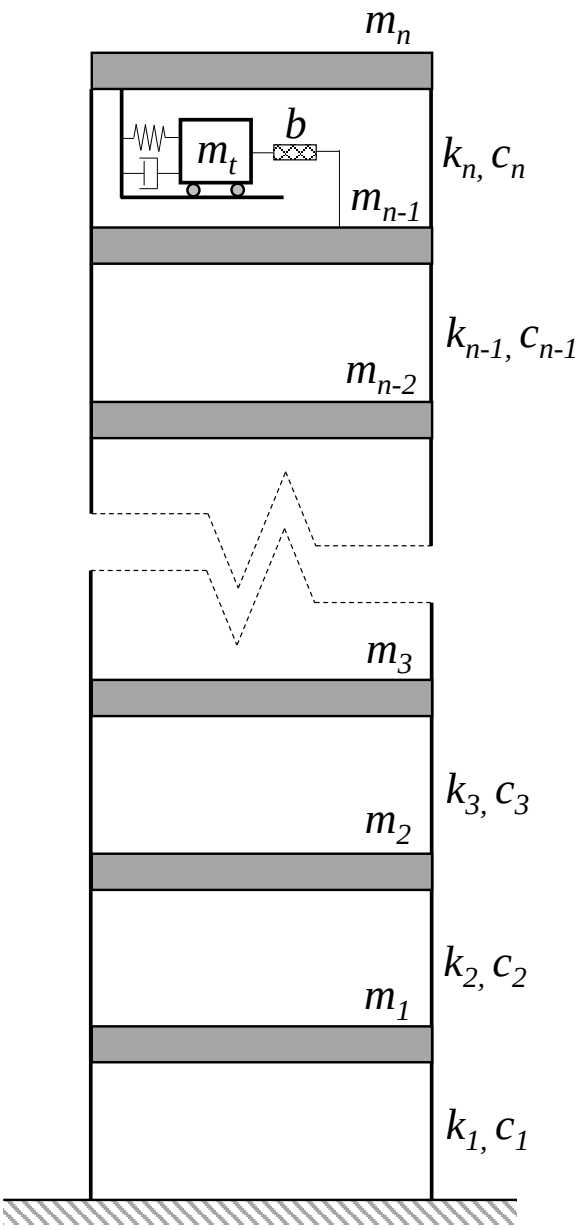

Figure 5.1: Multi-story structure with TMDI attached

5.2.1 Equations of Motion

To model a multi-story structure, a simplified shear-building model is adopted. The basic assumptions include that each floor is rigid, the mass of each floor is lumped at the center of mass, the motion in each lateral direction is decoupled, and that the system remains linear elastic. Due to these assumptions, the building can be modeled as a column with masses

lumped at each floor height. The equations of motion are then found by applying equilibrium of each floor along the horizontal direction. This leads to the following equations of motion, written in matrix form as,

$$\mathbf{M}\ddot{\mathbf{u}} + \mathbf{C}\dot{\mathbf{u}} + \mathbf{K}\mathbf{u} = -\mathbf{M}_\mathbf{m}\mathbf{r}\ddot{x}_g \tag{5.1}$$

In the above equation, the mass, damping, and stiffness matrices are defined by

$$\mathbf{M} = \begin{bmatrix} m_1 & 0 & 0 & \cdots & \cdots & \cdots & 0 \\ 0 & m_2 & 0 & \cdots & \cdots & \cdots & 0 \\ 0 & 0 & m_3 & \cdots & \cdots & \cdots & 0 \\ \vdots & \vdots & \vdots & \ddots & \cdots & \cdots & \vdots \\ 0 & 0 & 0 & \cdots & m_{n-1}+b & 0 & -b \\ 0 & 0 & 0 & \cdots & 0 & m_n & 0 \\ 0 & 0 & 0 & \cdots & -b & 0 & m_t+b \end{bmatrix}, \tag{5.2}$$

$$\mathbf{C} = \begin{bmatrix} c_1+c_2 & -c_2 & 0 & \cdots & \cdots & \cdots & 0 \\ -c_2 & c_2+c_3 & -c_3 & 0 & \cdots & \cdots & 0 \\ 0 & -c_3 & c_3+c_4 & -c_4 & 0 & \cdots & 0 \\ \vdots & \vdots & \vdots & \ddots & \cdots & \cdots & \vdots \\ \vdots & \vdots & \vdots & \cdots & \ddots & \cdots & \vdots \\ 0 & 0 & 0 & \cdots & -c_n & c_n+c_t & -c_t \\ 0 & 0 & 0 & \cdots & 0 & -c_t & c_t \end{bmatrix}, \tag{5.3}$$

$$\mathbf{K} = \begin{bmatrix} k_1+k_2 & -k_2 & 0 & \cdots & \cdots & \cdots & 0 \\ -k_2 & k_2+k_3 & -k_3 & 0 & \cdots & \cdots & 0 \\ 0 & -k_3 & k_3+k_4 & -k_4 & 0 & \cdots & 0 \\ \vdots & \vdots & \ddots & \ddots & \ddots & \cdots & \vdots \\ \vdots & \vdots & \vdots & \ddots & \ddots & \ddots & \vdots \\ 0 & 0 & 0 & \cdots & -k_n & k_n+k_t & -k_t \\ 0 & 0 & 0 & \cdots & 0 & -k_t & k_t \end{bmatrix}, \tag{5.4}$$

and

$$\mathbf{M_m} = \text{diag}(m_1, m_2, \ldots, m_n, m_t) \tag{5.5}$$

where m_i, c_i, and k_i for $i = 1, 2, \ldots, n$ are the mass, damping, and stiffness of each story. Moreover, m_t, c_t and k_t are the mass, damping, and stiffness of the TMD system, while b is the inertance. The vector $\mathbf{u}$ stores the displacement of each mass relative to the ground, that is,

$$\mathbf{u} = \begin{bmatrix} u_1 & x_2 & u_3 & \cdots & u_n & u_t \end{bmatrix}^T \tag{5.6}$$

where $u_i = x_i - x_g$ for $i = 1, 2, \ldots, n, t$. The vector $\mathbf{r}$, typically called the influence vector, is unit column vector. Note that when $b = 0$ equations (5.1) reduces to a multi-story structure with a traditional TMD system. It has been shown that the traditional TMD system suppresses the first mode of the structure, which in practice, contributes most to the displacement response of the structure under ground acceleration [83]. By including the inerter within the TMD system, the system remains linear and the total mass of the TMD system increases by b amount. Yet, unlike the single-story structure, the mass matrix is non-diagonal, leading to additional coupling between the TMD mass and the structure.

Since the structure remains linear, standard optimization techniques can be implemented in selecting the frequency and damping ratios. In the upcoming section on the tuning strategy of the TMDI, it will be more suited to consider the equations of motion in state-space form,

$$\dot{\mathbf{z}} = \mathbf{A}\mathbf{z} + \mathbf{B}\ddot{x}_g \tag{5.7}$$

where $\mathbf{z}$ is the state vector defined as

$$\mathbf{z} = \begin{bmatrix} \mathbf{u} \\ \dot{\mathbf{u}} \end{bmatrix} \tag{5.8}$$

and $\mathbf{A}$ and $\mathbf{B}$ are the system and input matrices, defined by

$$\mathbf{A} = \begin{bmatrix} \mathbf{0}_{n+1} & \mathbf{I}_{n+1} \\ -\mathbf{M}^{-1}\mathbf{K} & -\mathbf{M}^{-1}\mathbf{C} \end{bmatrix} \tag{5.9}$$

$$\mathbf{B} = \begin{bmatrix} \mathbf{0}_{n+1} \\ \mathbf{M}^{-1}\mathbf{M_m} \end{bmatrix} \tag{5.10}$$

where $\mathbf{0}_{n+1}$ and $\mathbf{I}_{n+1}$ are the zero and identity matrices, respectively.

5.2.2 Tuning Strategy for TMDI

The tuning strategy used in this section is based on the work done by Pietrosanti et al. [81], which assumed a white noise base excitation. The TMDI parameters were then selected to minimize the variance of the displacement response. A similar approach was also done by Marian and Giaralis [70, 34], yet a non-stationary input that is compatible, in the mean

sense, to the Eurocode 8 spectrum was used. This thesis chose the former approach for its simplicity and to be consistent with the tuning strategy done in Chapter 3 for a single-story structure.

As mentioned prior, the tuning strategy of the TMDI system will assume the ground acceleration to be a stationary stochastic process, namely, Gaussian white noise. This input has zero mean with finite variance. Moreover, each time instant is identically distributed and statistically independent and hence uncorrelated. By having zero mean, the response $\mathbf{z}(t)$ can be described by the covariance matrix [81], defined by

$$\mathbf{G}_{zz} = E[\mathbf{z}\mathbf{z}^T] \tag{5.11}$$

where $E[\cdot]$ denotes the expected value operator. It has been shown [123] that since $\mathbf{z}(t)$ is stationary, the covariance matrix, $\mathbf{G}_{zz}$, satisfies the differential equation

$$\dot{\mathbf{G}}_{zz} = \mathbf{A}\mathbf{G}_{zz} + \mathbf{G}_{zz}\mathbf{A}^T + 2\pi\mathbf{B}\mathbf{B}^T \tag{5.12}$$

Setting equation (5.12) equal to the zero gives the Lyapunov equation

$$\mathbf{A}\mathbf{G}_{zz} + \mathbf{G}_{zz}\mathbf{A}^T + 2\pi S_0\mathbf{B}\mathbf{B}^T = \mathbf{0}, \tag{5.13}$$

which can be solved numerically for the covariance matrix $\mathbf{G}_{zz}$. Similar to other tuning strategies for TMDs and TMDIs, the first mode (or fundamental mode) is considered, which corresponds to minimizing the variance of the displacement of the top story, denoted by $\sigma^2_{u_n}$. Similar to single-degree-of-freedom systems, the frequency ratio, f, is defined as

$$f = \frac{\omega_t}{\omega_1} \tag{5.14}$$

where ω_1 is the fundamental natural frequency and

$$\omega_t = \sqrt{\frac{k_t}{(m_t + b)}} \tag{5.15}$$

In addition, the TMDI damping ratio, ζ_t, is defined by

$$\zeta_t = \frac{c_t}{2m_t\omega_t} \tag{5.16}$$

In the same fashion to other studies [87, 81] of TMD and TMDI systems the mass ratio μ is given by

$$\mu = \frac{m_t}{\boldsymbol{\phi}_1^T \boldsymbol{M} \boldsymbol{\phi}_1} \tag{5.17}$$

where $\boldsymbol{\phi}_1$ is the fundamental mode shape normalized to have unit participation factor and $\boldsymbol{M}$ is the mass matrix of the structure only. The participation factor is a measure of how strongly a given mode contributes to the dynamic behavior of the system [110], and is defined by

$$\Gamma_1 = \frac{\boldsymbol{\phi}_1^T \boldsymbol{M} \mathbf{r}}{\boldsymbol{\phi}_1^T \boldsymbol{M} \boldsymbol{\phi}_1} \tag{5.18}$$

where $\boldsymbol{\phi}_1$ is the first mode, $\boldsymbol{M}$ is the mass matrix of the structure only, and $\boldsymbol{r}$ is the influence vector. Let us also define the inertance ratio, β, to be

$$\beta = \frac{b}{\boldsymbol{\phi}_1^T \boldsymbol{M} \boldsymbol{\phi}_1} \tag{5.19}$$

The parameters defining the optimization problem are given by μ, β, f, ζ_t and ζ_1, where ζ_1 is the first mode damping ratio. For a chosen μ and β and fixed ζ_1, the optimization problem

can be stated as

$$\begin{aligned} \min_{f,\,\zeta_t} \quad & \sigma^2_{u_n} \\ \text{subject to} \quad & 0 \leq f \leq 1 \\ & 0 \leq \zeta_t \leq 1 \end{aligned} \tag{5.20}$$

where the constraints on f and ζ_t were selected based on physical considerations. The results of optimization are given in Figures 5.2a and 5.2b for mass ratios, μ between 0.01 to 0.1 and inertance ratios, β, between 0 to 5.

5.2.3 Alternative Tuning Strategy for TMDI

In this section, an alternative tuning strategy is proposed for the TMDI system. This strategy was first introduced by Villaverde and Koyama [111] and further refined by Sadek et al. [87]. It is worth noting that this alternative tuning strategy has not previously been applied to TMDI systems. The work in the following sections will introduce the tuning strategy and discuss the performance of the alternative tuning strategy as compared with the white noise input from the prior section.

The alternative tuning strategy relies on determining the roots of the characteristic equation,

$$\det(\lambda \mathbf{I} - \mathbf{A}) = 0 \tag{5.21}$$

In this case, the state matrix $\mathbf{A}$ is defined for a multi-story structure equipped with the TMDI system. Due to the damping of the structure, t has been shown [111], the roots of

the characteristic equation come in complex conjugate pairs

$$\lambda_{i,i+1} = -\omega_i\zeta_i \pm i\omega_i\sqrt{1-\zeta_i^2}, \quad i = 1, 3, \ldots, m-1 \tag{5.22}$$

The notation $\lambda_{i,i+1}$ indicates that the eigenvalues come in pairs, where where ω_i and ζ_i are the natural frequency and damping ratio in the ith mode, and m is the number of degrees of freedom of the structure equipped with the TMDI system. Since i only takes on odd values, the second mode natural frequency and damping ratio would correspond to ω_3 and ζ_3, respectively.

Villaverde [111] first showed that for a TMD to be effective, the damping ratios in the two complex modes, ζ_1 and ζ_3, should be approximately equal to the average of the damping ratios of the structure and TMD, that is,

$$\zeta_1 \approx \zeta_3 \approx \frac{\zeta_{1,s} + \zeta_t}{2} \tag{5.23}$$

where $\zeta_{1,s}$ is the first mode damping ratio of the structure without a TMD and ζ_t is the damping ratio of the TMD. From extensive analytical work [111, 109], it was shown that the TMD should be in resonance with the structure, that is, $f = 1$, and the damping ratio in the first two modes should satisfy equation (5.23). However, numerical results performed by Sadek et al. [87] showed that such a requirement was only effective for TMDs having mass ratios smaller than 0.005. In fact, for larger mass ratios, the damping ratios in the first two modes were larger than what was found using (5.23).

To remedy the shortcoming of requiring small mass ratios, the optimal values of f and ζ_t for a given mass ratio μ were selected such that the first two modes natural frequency and damping ratios were equal [87]. This was accomplished by computing the eigenvalues of the state matrix and by using equation (5.22), the first and second mode natural frequency and damping ratios are determined. The optimal values for f and ζ_t are when $\omega_1 \approx \omega_3$ and

$\zeta_1 \approx \zeta_3$, for a given μ and $\zeta_{1,s}$. Note that for a multi-story structure equipped with a TMDI system, this same procedure was performed while also providing a given inertance ratio, β. Figures 5.3a and 5.3b show the optimal values for f and ζ_t for different mass and inertance ratios where $\zeta_{1,s} = 0.02$.

5.2.4 Results

In section 5.2.2, a tuning strategy for the TMDI system based on white noise input was introduced. The approach selected the frequency ratio f and damping ratio ζ_t so to minimize the variance of the displacement response of the top-story. Figures 5.2a and 5.2b show the results of the optimization. Section 5.2.3 introduced an alternative tuning strategy for the TMDI. This alternative tuning strategy has not been considered for TMDI systems prior to this work. The alternative tuning strategy selects the frequency ratio f and damping ratio ζ_t when the first two modes natural frequency and damping ratios are approximately equal. The results of the optimization are shown in Figures 5.3a and 5.3b.

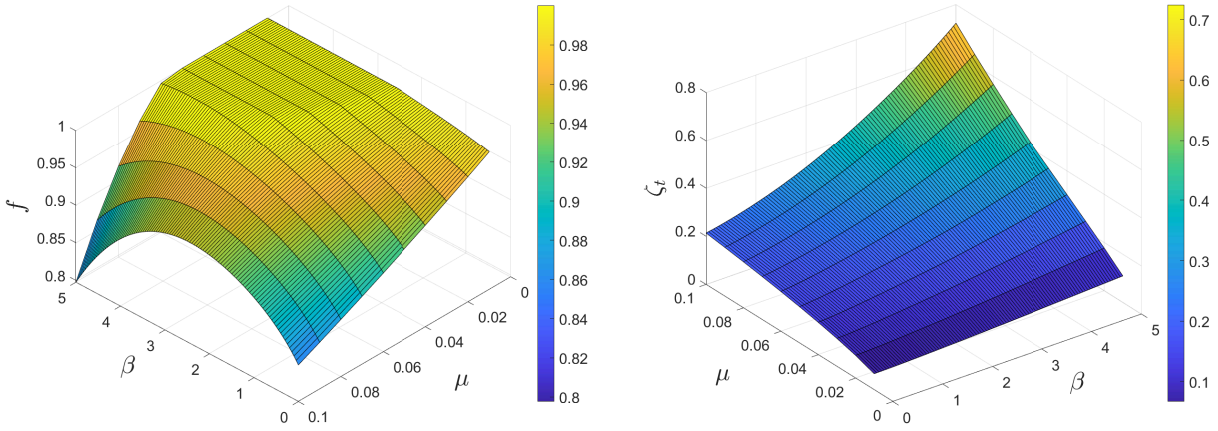

(a) (b)

Figure 5.2: (a) The frequency ratio f and (b) damping ratio ζ_t for various values mass ratios μ and inertance ratios β.

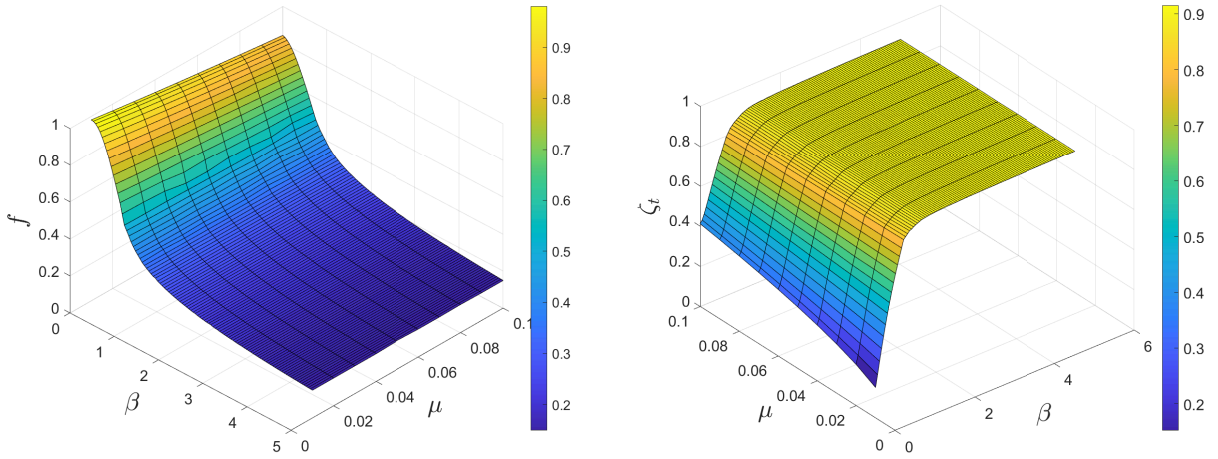

(a) (b)

Figure 5.3: (a) The frequency ratio f and (b) damping ratio ζ_t for various values mass ratios μ and inertance ratios β where $\zeta_{1,s} = 0.02$.

The result of each optimization show that the tuning strategies produce vastly different results in the selection of the frequency and damping ratios. In particular, the white noise tuning strategy produces larger frequency ratios for large inertance values, while the alternative tuning strategy has much smaller frequency ratios (see Figures 5.2a and 5.3a). This would imply that the TMDI spring stiffness is larger for the white noise tuning, while it is much smaller for the alternative tuning strategy. This relationship between the TMDI spring stiffness and frequency ratio can be determined by substituting (5.15) into (5.14) and solving for the TMDI spring stiffness k_t. When considering the damping ratios for the white noise and alternative tuning strategies, shown in Figures 5.2b and 5.3b, respectively, the alternative tuning strategy produces much larger damping ratios over most mass and inertance ratios, as compared with the white noise tuning strategy.

Using the two ground motion sets presented in Chapter 3, peak responses of the displacement and acceleration of each floor were found. The stroke of each TMDI system was also computed. The system considered was a three-story structure having a fundamental period of $T = 0.5$ seconds and first mode critical damping ratio $\zeta_1 = 0.02$. Moreover, the structure

has a soft top story, where the stiffness of the top-story was approximately 60% less stiff than the stiffness of the stories below. This is similar to what is done in practice, where column stiffness of each floor decreases for each additional story. Moreover, it has been shown in prior work that TMDIs perform significantly better when with soft top story [33, 90]. This is since greater flexibility at the top-story allows for more energy dissipation to be provided by the TMDI system. The mass ratios considered ranged from 0.01 to 0.1 at various inertance ratios. To gauge the performance of each TMDI system, the following reduction factors are introduced,

$$R_D = \frac{\text{Peak displacement of controlled structure}}{\text{Peak displacement of uncontrolled structure}} \tag{5.24}$$

$$R_A = \frac{\text{Peak acceleration of controlled structure}}{\text{Peak acceleration of uncontrolled structure}} \tag{5.25}$$

$$R_S = \frac{\text{Peak stroke of the TMDI with alternative tuning}}{\text{Peak stroke of the TMDI with white noise tuning}} \tag{5.26}$$

and are called the displacement, acceleration, and stroke reduction factors, respectively. In (5.24) and (5.25) the controlled structure refers to the structure equipped TMDI system. The uncontrolled structure refers to the structure without any control device. Having $R_D < 1$ or $R_A < 1$ would indicate that the controlled system is effective in reducing the structure displacement and acceleration. When $R_S < 1$, the TMDI system with the alternative tuning strategy has less stroke than the TMDI system using the white noise tuning strategy. The mean of the reduction factors over ground motions from each set is used to compare the tuning strategies.

Figures 5.4-5.5 show the displacement reduction factor of the first floor under the rock-site

and pulse-like ground motion sets. Similarly, Figures 5.6-5.7 and Figures 5.8-5.9, show the displacement reduction factor for the second and third floors, respectively. For each figure, the left plot corresponds to the alternative tuning strategy, while the right plot corresponds to the white noise tuning strategy. Figures 5.10-5.11 show the acceleration reduction factor of the first floor under the rock-site and pulse-like ground motion sets. Similarly, Figures 5.12-5.13 and Figures 5.14-5.15, show the acceleration reduction factor for the second and third floors, respectively. Figure 5.16 shows the stroke reduction factor under the rock-site and pulse-like ground motion sets.

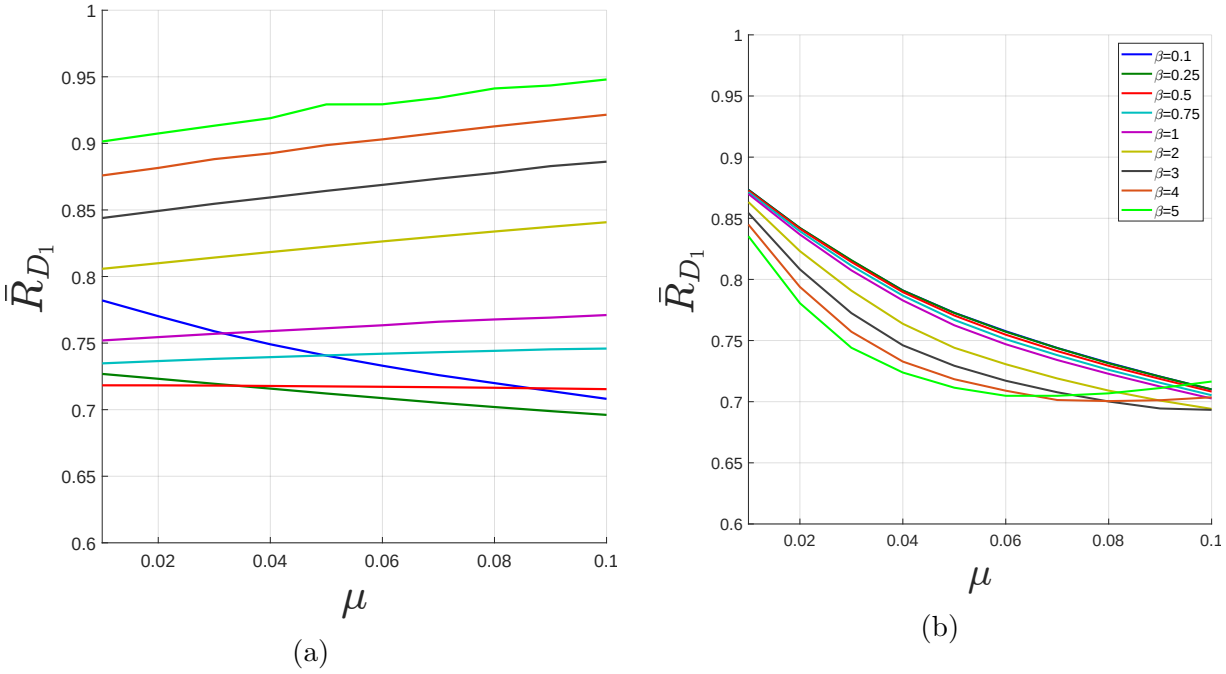

(a) (b)

Figure 5.4: First floor displacement reduction factor for (a) alternative tuning strategy and (b) white nose tuning strategy under the rock-site ground motion set.

5.2.5 Discussion

Figures 5.4-5.9 show the displacement reduction factors under both tuning strategies and show that each strategy provides reductions in the response. Yet, the alternative tuning strategy outperforms the white noise tuning strategy in reducing the response of the top-

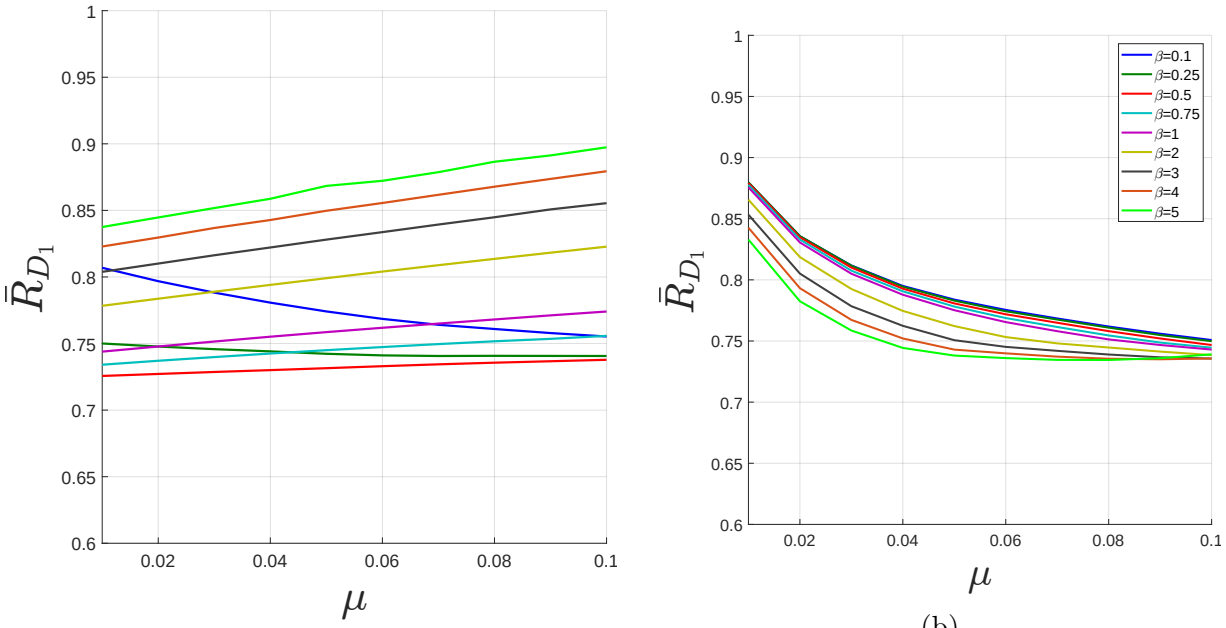

(a) (b)

Figure 5.5: First floor displacement reduction factor for (a) alternative tuning strategy and (b) white nose tuning strategy under the pulse-like ground motion set.

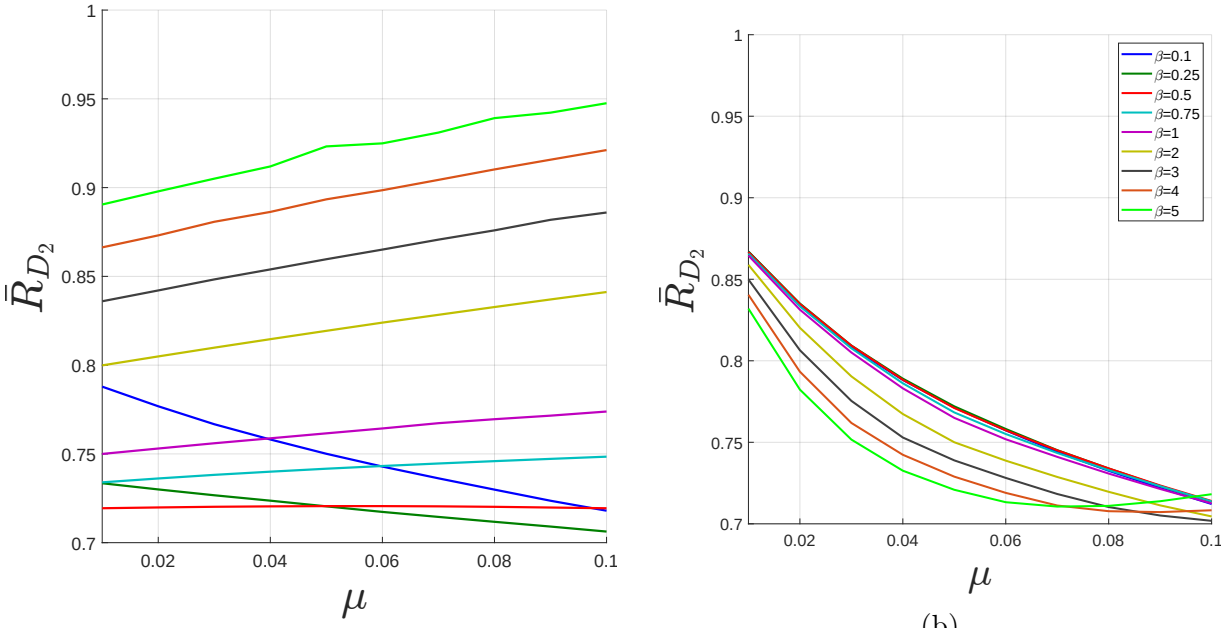

(a) (b)

Figure 5.6: Second floor displacement reduction factor for (a) alternative tuning strategy and (b) white nose tuning strategy under the rock-site ground motion set.

story. When considering the top-floor, Figures 5.8a, 5.9a and Figures 5.8b and 5.9b, show that increasing the inertance for a fixed mass ratio decreases the displacement response. As

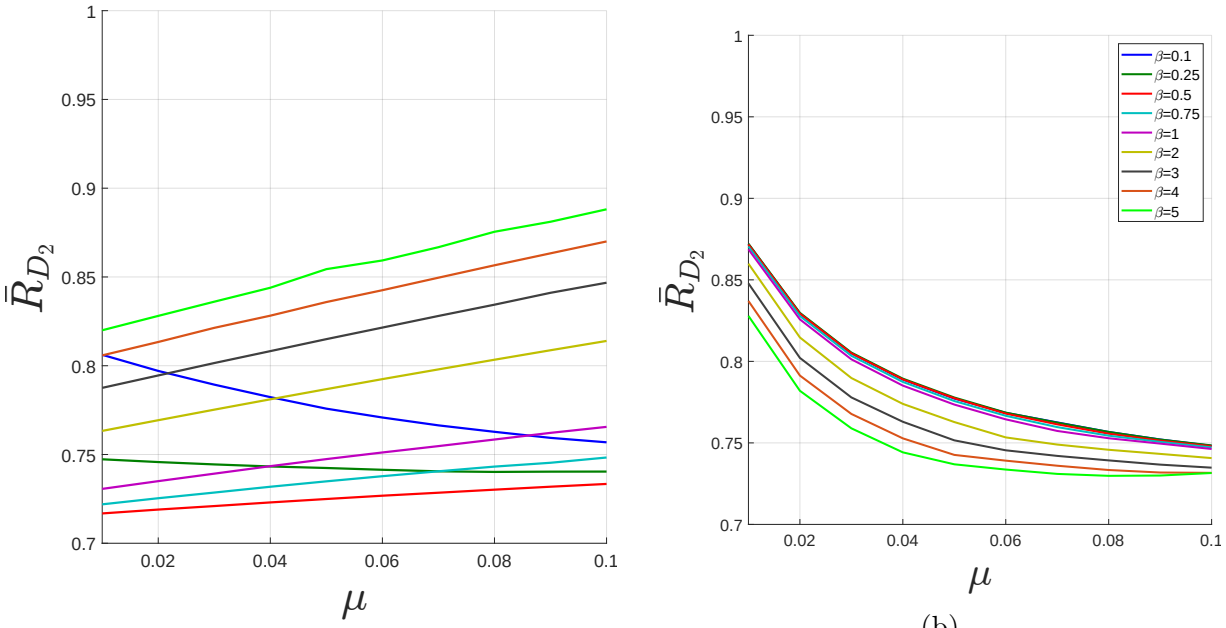

(a) (b)

Figure 5.7: Second floor displacement reduction factor for (a) alternative tuning strategy and (b) white nose tuning strategy under the pulse-like ground motion set.

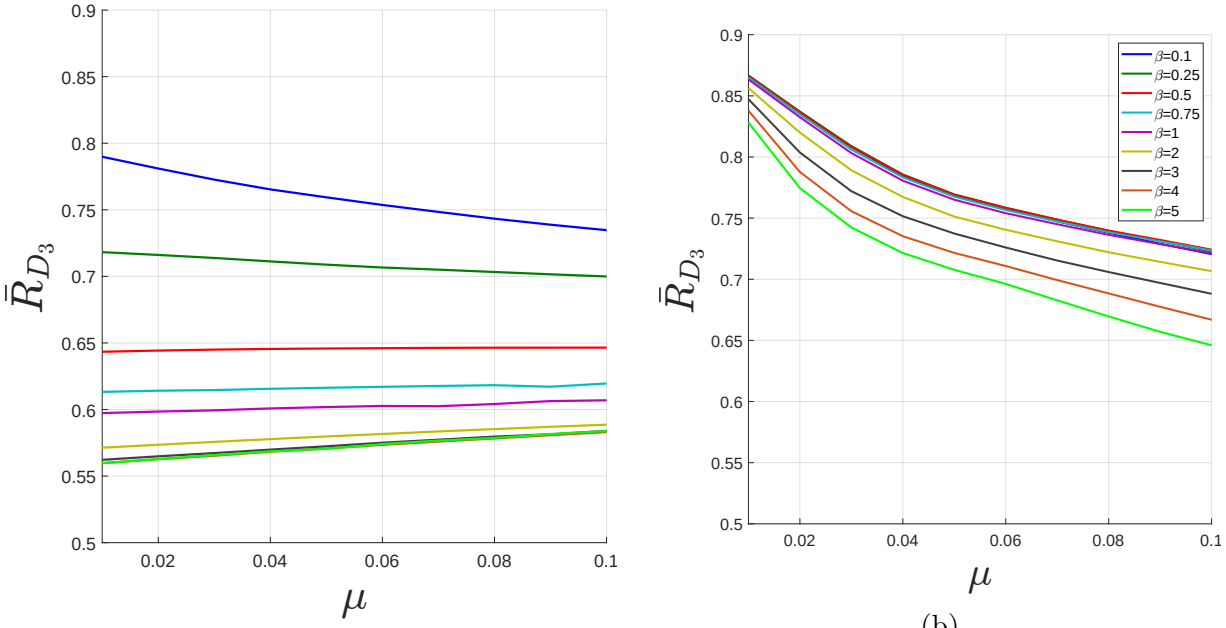

(a) (b)

Figure 5.8: Third floor displacement reduction factor for (a) alternative tuning strategy and (b) white nose tuning strategy under the rock-site ground motion set.

shown in Figure 5.8a and 5.9a, the alternative tuning strategy provides up to 45% reduction in displacement for small mass ratios, while the white nose tuning strategy provides no

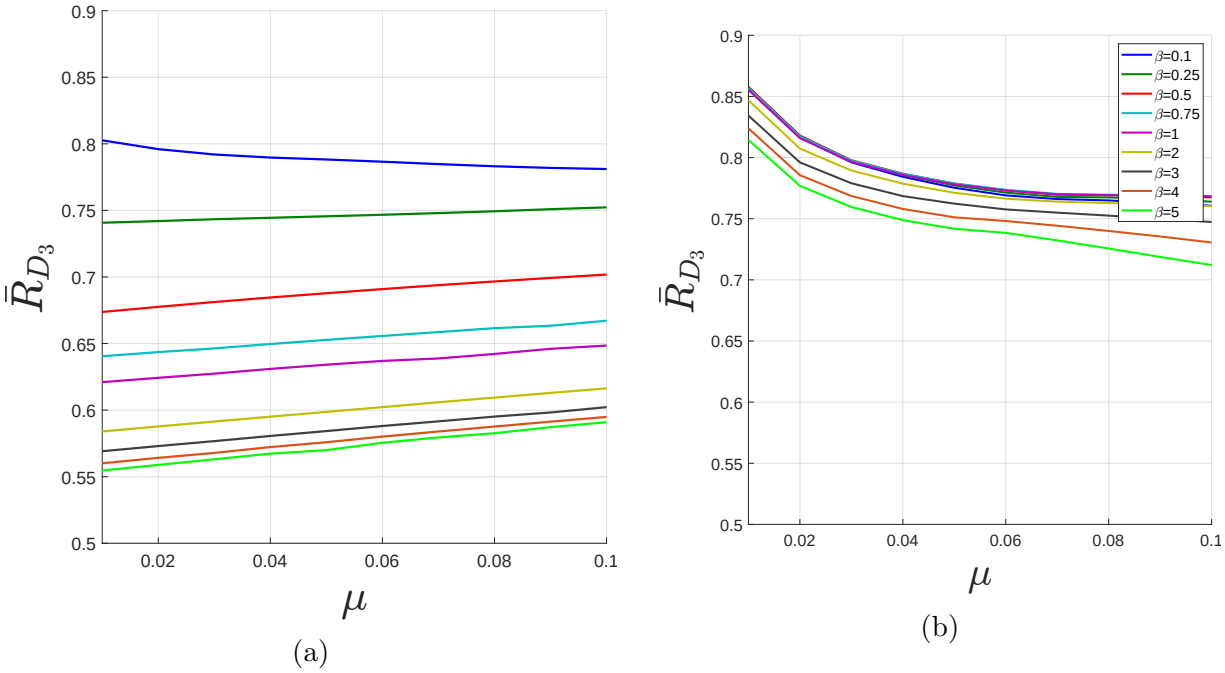

Figure 5.9: Third floor displacement reduction factor for (a) alternative tuning strategy and (b) white nose tuning strategy under the pulse-like ground motion set.

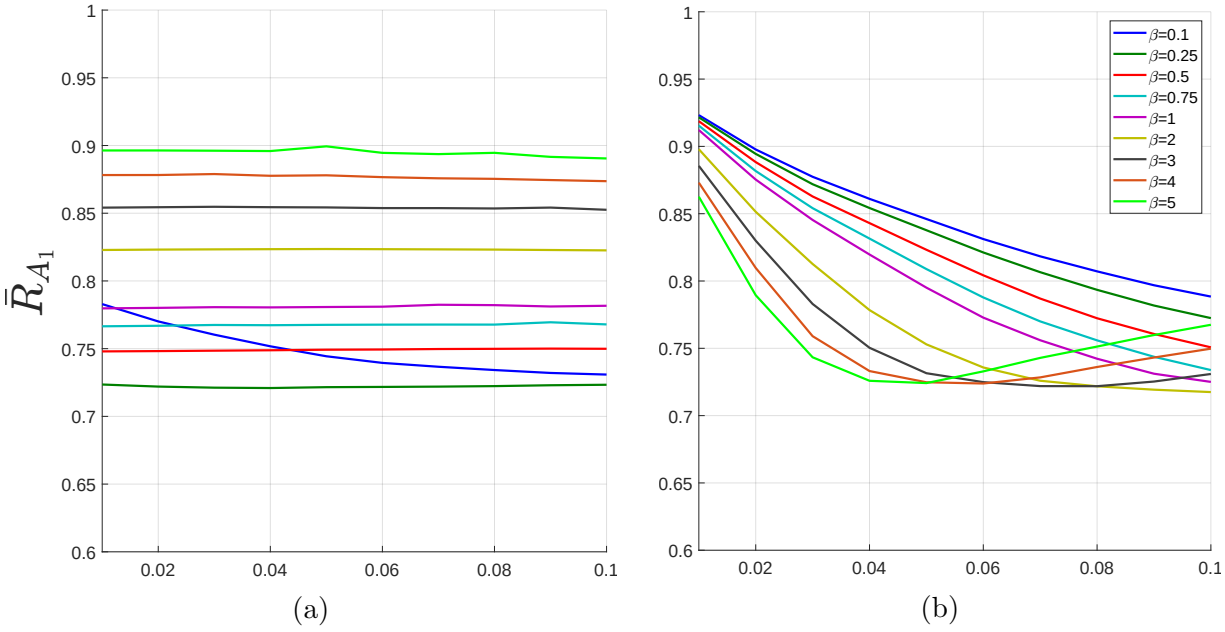

Figure 5.10: First floor acceleration reduction factor for (a) alternative tuning strategy and (b) white nose tuning strategy under the rock-site ground motion set.

more than 18%. In fact, a TMDI with a mass ratio of 0.01 and inertance of 0.1 has better performance tuned using the alternative strategy, than with one with a larger mass and

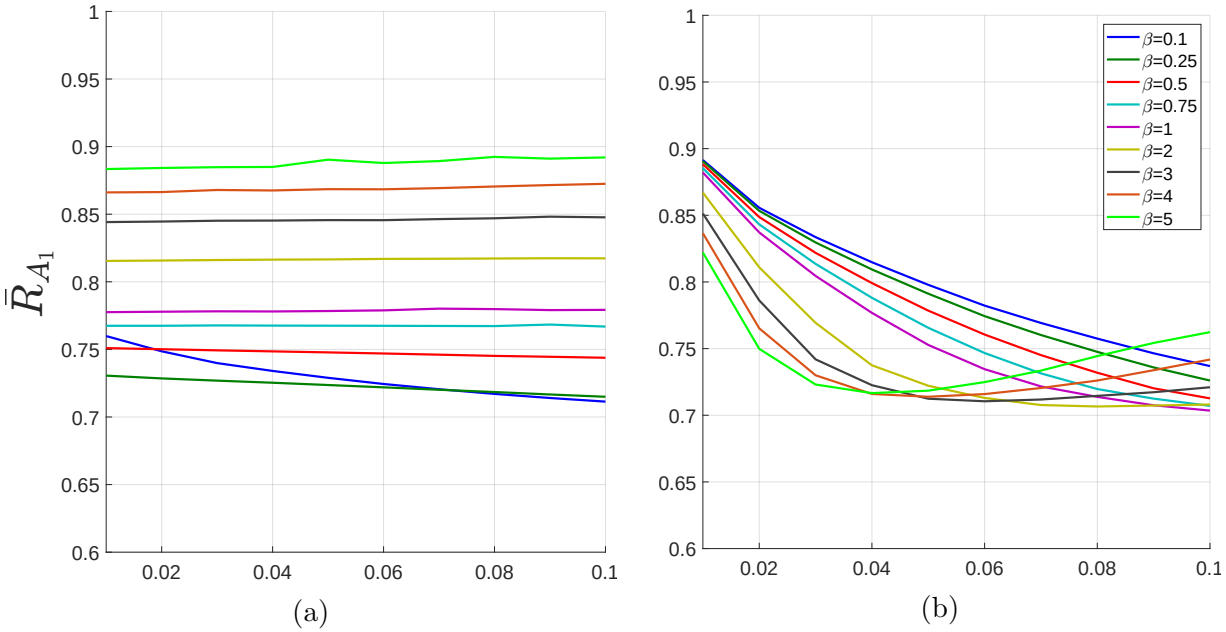

Figure 5.11: First floor acceleration reduction factor for (a) alternative tuning strategy and (b) white nose tuning strategy under the pulse-like ground motion set.

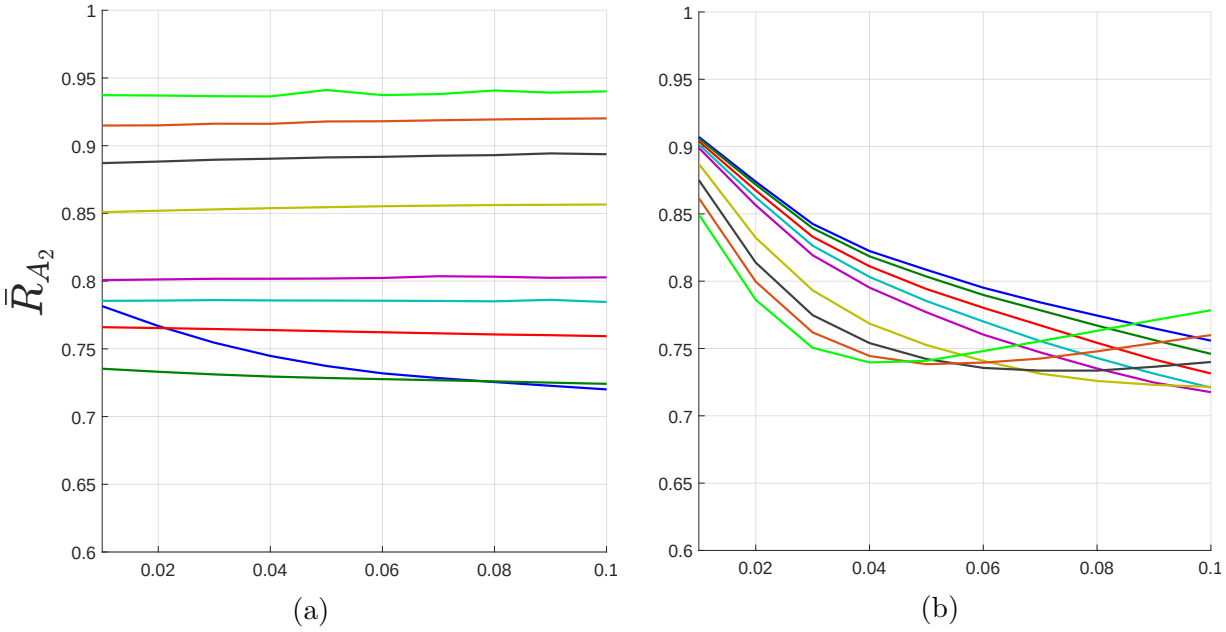

Figure 5.12: Second floor acceleration reduction factor for (a) alternative tuning strategy and (b) white nose tuning strategy under the rock-site ground motion set.

inertance using the white noise tuning strategy. This performance increase can be attributed to the fact that for small mass ratios and large inertance, the TMDI is tuned to have a larger damping ratio as opposed to one with the white noise tuning strategy. This can be seen by

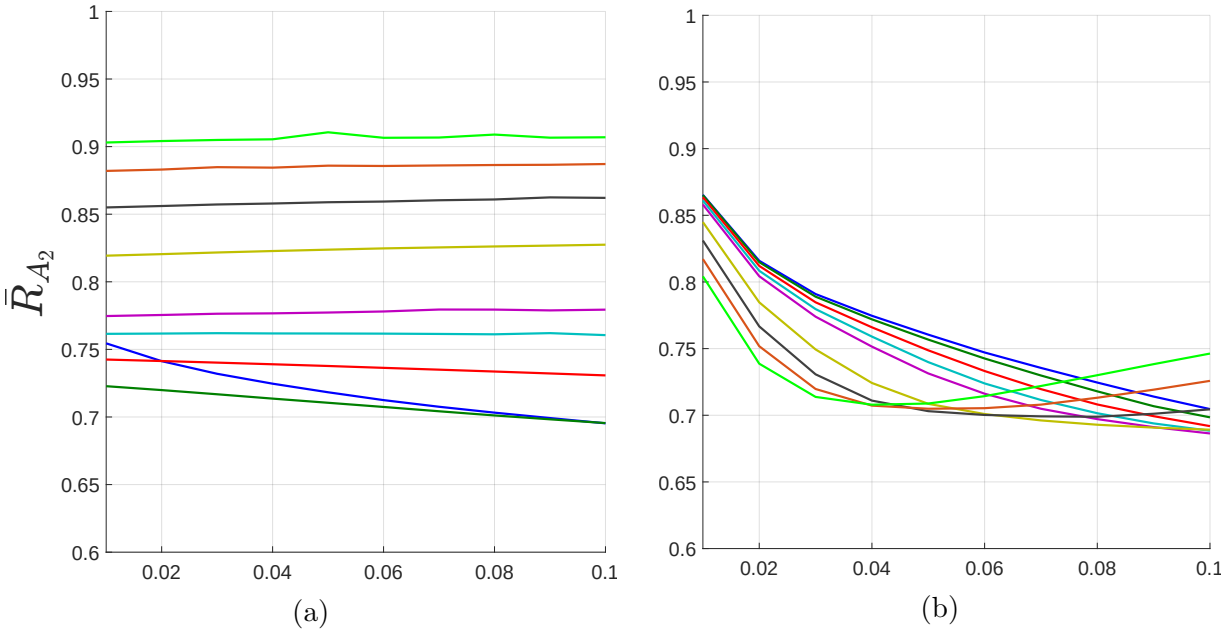

Figure 5.13: Second floor acceleration reduction factor for (a) alternative tuning strategy and (b) white nose tuning strategy under the pulse-like ground motion set.

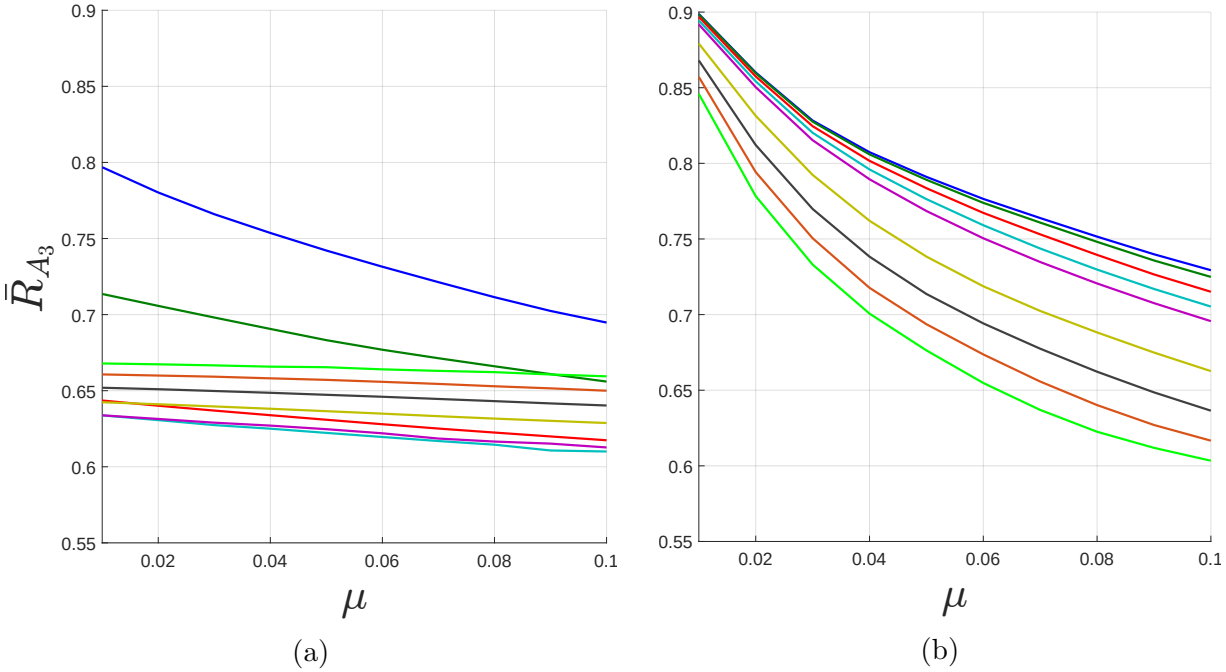

Figure 5.14: Third floor acceleration reduction factor for (a) alternative tuning strategy and (b) white nose tuning strategy under the rock-site ground motion set.

comparing the damping ratios of each tuning strategy (see Figures 5.2b and 5.3b).

For the lower floors of the structure, there is a similar behavior in the performance of the

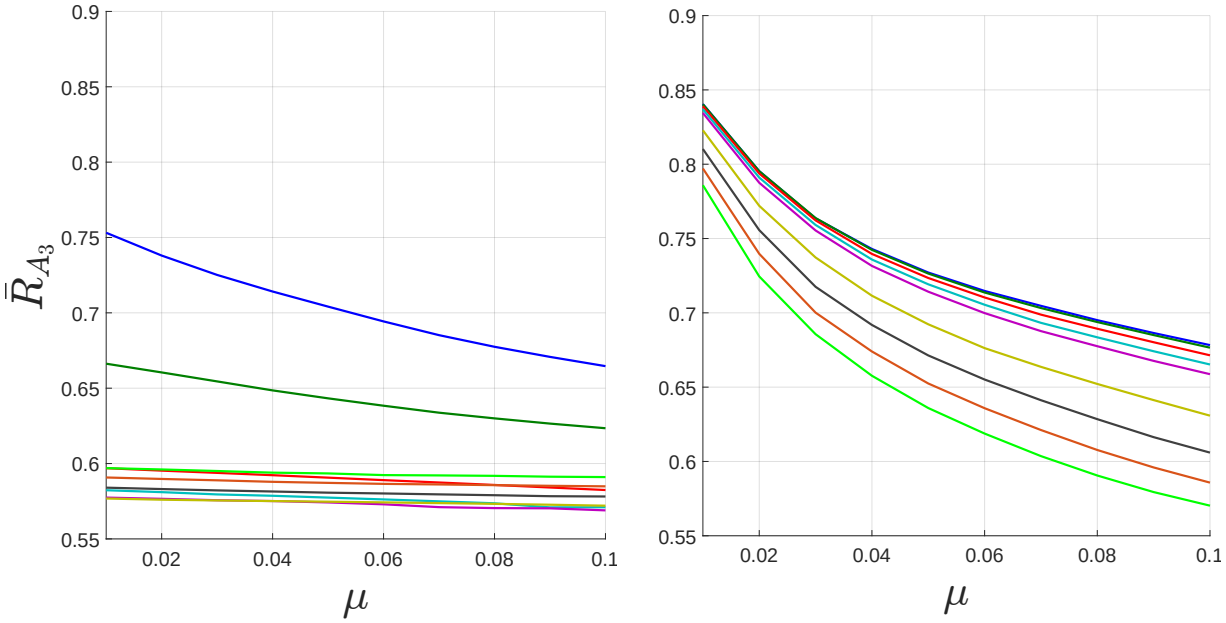

Figure 5.15: Third floor acceleration reduction factor for (a) alternative tuning strategy and (b) white nose tuning strategy under the pulse-like ground motion set.

TMDI with white nose tuning strategy, whereby increasing the inertance leads to better performance (Figures 5.6, 5.7 and Figures 5.8, 5.9). Yet, for the TMDI with the alternative tuning strategy, worse performance is found for larger inertance values, as shown in Figures 5.4a,5.6a and 5.5a and5.7a. For inertance value less than one, the pattern of decreased response for increased inertance occurs. This behavior is likely due to the coupling effects of the TMDI to the lower floors and the tuning strategy. Because of the increase in performance, this requires further inquiry to investigate why the performance drop occurs at the lower stories for higher inertance values.

The acceleration response reduction factor for the first, second, and third floor under the two ground motion set are shown in Figures 5.10-5.15. The behavior of the alternative tuning strategy is similar to the displacement response. The top story follows the pattern of increased inertance decreases the response. Moreover, increasing the mass ratio also decreases the response, yet is more pronounced for smaller inertance values. In addition, the lower stories also have a similar behavior to the displacement response, whereby larger

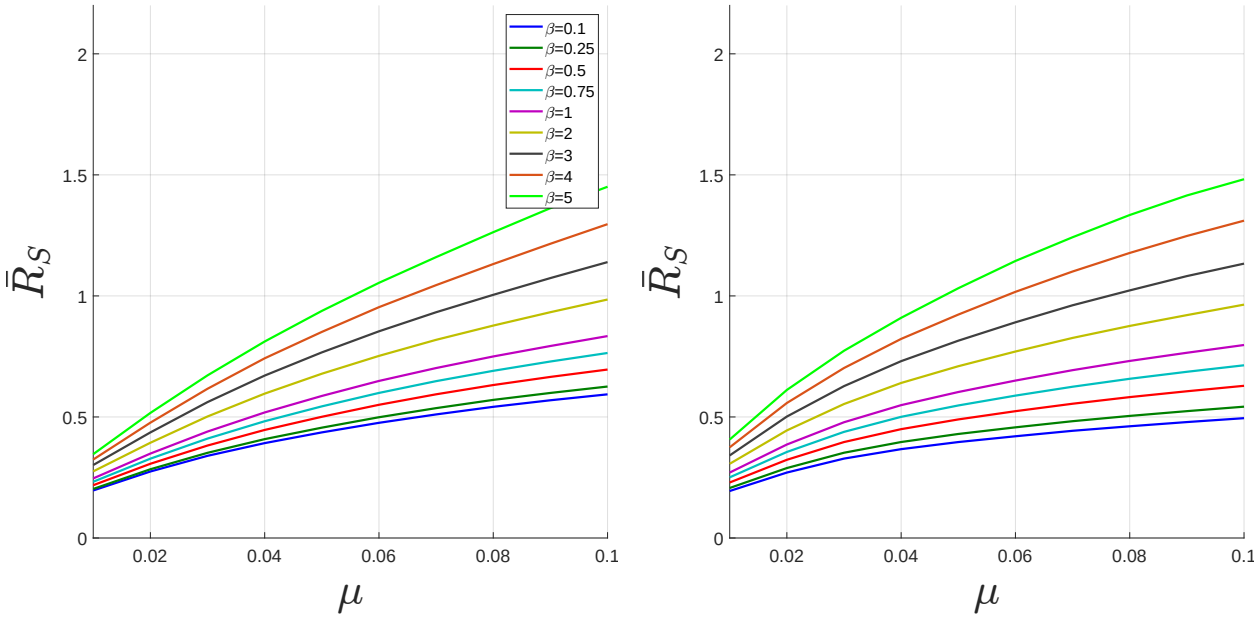

(a) (b)

Figure 5.16: Stroke reduction factors for (a) rock-site and (b) pulse-like ground motion sets.

inertance values leads to poorer performance.

The stroke reduction factor for each ground motion set is shown in Figure 5.16. Based on these figures, the TMDI with the alternative tuning strategy provides reduction in stroke for mass ratios less than 0.05 for the rock-site ground motion set, while reductions are only present for mass ratios less than 0.03 for the pulse-like ground motion set. Moreover, increasing the inertance increases the stroke reduction factor, indicating that the TMDI under the white noise tuning strategy performs better for larger inertance values. This trend is present for both ground motion sets.

For larger mass ratios the stroke reduction factor increases, indicating that the TMDI under white noise tuning performs better. This behavior can be explained by the tuning strategy, where for smaller mass ratios, the spring stiffness would be larger for the alternative tuning strategy as opposed to the white nose tuning strategy. This can be shown when considering the frequency ratio, f, of each tuning strategy (see Figures 5.2a and 5.3a). By considering the overall system response reduction, inertance values less than one are desirable. Moreover,

small mass ratios can be used to achieve significant reductions in all three floors of the structure, while also considerably reducing the stroke.

5.3 Semi-active Tuned Mass Damper with Inerter

In this section, the SATMDI system is incorporated within the three-story structure considered in the prior sections. Similar to the single-story structure equipped with the SATMDI, the SRS is placed in parallel to the spring and damper. The SATMDI is tuned using the alternative tuning strategy presented in Section 5.2.3 since the performance of the TMDI using the alternative tuning strategy was significantly better than that using white noise. Comparisons between the displacement, acceleration, and stroke responses are made between the SATMDI and TMDI systems.

5.3.1 Equations of Motion

The equations of motion for a multi-story structure with SATMDI system is given as

$$\mathbf{M}\ddot{\mathbf{u}} + \mathbf{C}\dot{\mathbf{u}} + (\mathbf{K} + \mathbf{K}_d)\mathbf{u} - \mathbf{K}_d\mathbf{u}_r = -\mathbf{M}_\mathbf{m}\mathbf{r}\ddot{x}_g \tag{5.27}$$

where $\mathbf{M}, \mathbf{M}_m, \mathbf{C}, \mathbf{K}$, and $\mathbf{r}$ are defined in equations (5.2)-(5.6). Using the same spring analogy as before where the SRS is placed parallel to the spring and damper of the TMDI

system, the stiffness matrix associated with the SRS is given by

$$\mathbf{K}_d = \begin{bmatrix} 0 & 0 & 0 & \cdots & \cdots & \cdots & 0 \\ 0 & 0 & 0 & 0 & \cdots & \cdots & 0 \\ 0 & 0 & 0 & 0 & 0 & \cdots & 0 \\ \vdots & \vdots & \ddots & \ddots & \ddots & \cdots & \vdots \\ \vdots & \vdots & \vdots & \ddots & \ddots & \ddots & \vdots \\ 0 & 0 & 0 & \cdots & 0 & k_d & -k_d \\ 0 & 0 & 0 & \cdots & 0 & -k_d & k_d \end{bmatrix}, \tag{5.28}$$

where k_d is the stiffness provided by the SRS. The reset vector $\mathbf{u}_r$ is defined by

$$\text{set } \mathbf{u}_r = \mathbf{u} \text{ whenever } \dot{u}_t - \dot{u}_n = 0 \tag{5.29}$$

Similar to before, the equations of motion in state-space form will be used, that is,

$$\dot{\mathbf{z}} = \mathbf{A}\mathbf{z} + \mathbf{F}\mathbf{z}_r + \mathbf{B}\ddot{x}_g \tag{5.30}$$

where $\mathbf{z}$ is the state vector defined as

$$\mathbf{z} = \begin{bmatrix} \mathbf{u} \\ \dot{\mathbf{u}} \end{bmatrix} \tag{5.31}$$

and $\mathbf{A}$ and $\mathbf{B}$ are the system and input matrices, defined by

$$\mathbf{A} = \begin{bmatrix} \mathbf{0}_{n+1} & \mathbf{I}_{n+1} \\ -\mathbf{M}^{-1}(\mathbf{K} + \mathbf{K}_d) & -\mathbf{M}^{-1}\mathbf{C} \end{bmatrix} \tag{5.32}$$

$$\mathbf{B} = \begin{bmatrix} \mathbf{0}_{n+1} \\ \mathbf{M}^{-1}\mathbf{M_m} \end{bmatrix} \tag{5.33}$$

where $\mathbf{0}_{n+1}$ and $\mathbf{I}_{n+1}$ are the zero and identity matrices, respectively. Two new terms have also been introduced, which accounts for the additional stiffness and reset term, namely, $\mathbf{F}$ and $\mathbf{z}_r$, defined by

$$\mathbf{F} = \begin{bmatrix} \mathbf{0}_{n+1} & \mathbf{0}_{n+1} \\ \mathbf{M}^{-1}\mathbf{K}_d & \mathbf{0}_{n+1} \end{bmatrix} \tag{5.34}$$

and

$$\mathbf{z}_r = \begin{bmatrix} \mathbf{u}_r \\ \dot{\mathbf{u}}_r \end{bmatrix} \tag{5.35}$$

5.3.2 Results

The comparison between the SATMDI and TMDI was done using the response reduction factors presented in the prior section. The structure under consideration was the same three-story structure as before, yet a SATMDI was used instead of the TMDI system. The alternative tuning strategy was considered as it provided greater performance in the TMDI system. In addition, the percent stiffness, denoted by κ, is defined by the percentage of stiffness provided by the SRS device. For this work, κ values range from 0.25 to 1 with increments of 0.25 were considered. Note that for $\kappa < 1$, the SRS and linear spring are both used, while for $\kappa = 1$, the SRS entirely replaces the linear spring.

Figures 5.17-5.20 show the displacement reduction factors for each floor under the rock-site ground motion set. Each figure represents a different κ values corresponding to the

percentage of stiffness provided by the SRS. Figures 5.21-5.24 show the acceleration reduction factor for each κ value selected. Figures 5.25-5.28 show the displacement reduction factors for each floor under the pulse-like ground motion set. Figures 5.29-5.32 show the acceleration reduction factor for each κ value selected. The figures are shown at the end of the chapter.

5.3.3 Discussion

Figures 5.17-5.20 show the displacement reduction factors for $\kappa = 0.25, 0.5, 0.75$ and 1, respectively, under the rock-site ground motion set. Based on these results, incorporating an SRS within a TMDI system provides little to no benefit for κ values less than one, while for $\kappa = 1$, there is a significant decrease in performance. These findings are also present under the pulse-like ground motion set (see Figures 5.25-5.28). For $\kappa = 1$, the SRS replaces the linear spring, which alters the tuning strategy negatively due to the force provided by the SRS vanishing at reset (see Figure 2.2). Since the force in the SRS takes time to increase, the amount of energy transferred from the top-story to the TMDI system is decreased. This in turn causes the decrease in performance. If both the linear spring and SRS are present, there is enough force developed in the linear spring to allow force transfer, which leads to minimal loss in performance, as seen in figures corresponding to $\kappa = 0.25, 0.5$, and 0.75.

When considering the acceleration response in Figures 5.21-5.24 for rock-site and Figures 5.29-5.32 for the pulse-like ground motion set at for various κ values, a similar behavior occurs. Once again, there is little to no benefit in the acceleration response for κ values less than one, while for $\kappa = 1$ there is a significant drop in performance. When considering the stroke reduction factor (Figure 5.33 and 5.34), the SATMDI provides moderate to large reduction for small mass ratios. Yet, increasing the inertance decreases the performance. This implies that a large inerter nullifies the effect of the SRS device due to the significant decrease in the stroke and thereby the amount of energy dissipated by the SRS. For smaller

inertance ratios the SRS provides an additional reduction to the stroke. Moreover, increasing the stiffness percent κ decreases the response, yet similar to the displacement and acceleration responses, $\kappa = 1$ decreases performance. Overall, the SRS should be used within the TMDI system for $\kappa < 1$ since there are no significant losses in the response performance, yet with a significant reduction in stroke. Therefore, the SRS can be used in situations where the footprint of the TMDI system is severely limited.

5.4 Summary

In this chapter the TMDI and SATMDI systems were applied to a multi-story structure. Analysis was performed on a three-story structure with a fundamental period of $T = 0.5$ seconds and a first mode critical damping ratio of $\zeta_1 = 0.02$. For TMDI systems, an alternative tuning strategy based on the work of Sadek et al. [87] was introduced and implemented within a TMDI system. The results showed that the alternative tuning strategy provides superior performance as compared with the white noise tuning strategy. In fact, significant reductions in the displacement, acceleration, and stroke responses were found for small mass ratios and inertance values. Yet, for larger mass ratios, the stroke using the alternative tuning strategy was significantly larger than that of the white noise tuning strategy. Since there is little performance increase in larger mass ratios, these negative effects can be easily avoided.

The SATMDI system was also studied, which incorporated an SRS device within a TMDI system. Due to the superior performance, only the alternative tuning strategy was used. Based on the results of this chapter, the SRS provides little to no benefit in reducing the response of the structure for κ values less than one. Yet, for $\kappa = 1$, there is a sharp decrease in performance as compared with the TMDI system. This was attributed to the control law of the SRS, where the reset sets the device force to zero, negatively affecting the tuning

strategy. The stroke response for κ value was shown to be significantly reduced using an SRS within a TMDI system. From these findings, the SRS can be used as an auxiliary device where the footprint of the TMDI system is limited. Moreover, κ values should always be less than one to avoid the negative effects of incorporating an SRS within a TMDI system.

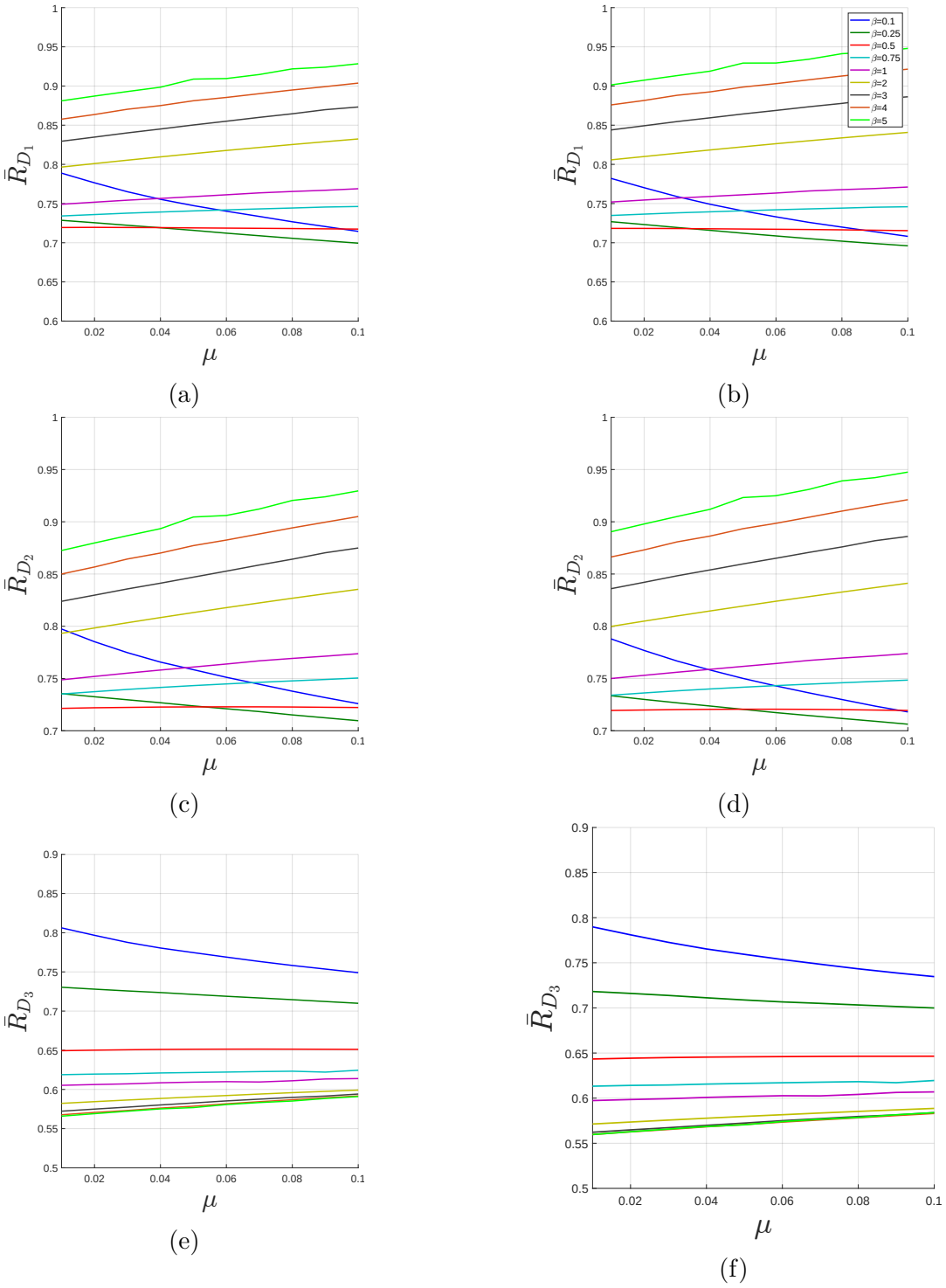

Figure 5.17: First, second, and third floor displacement reduction factors for SATMDI ($\kappa = 0.25$) (a),(c),(e) and TMDI (b),(d),(f) using the rock-site ground motion set.

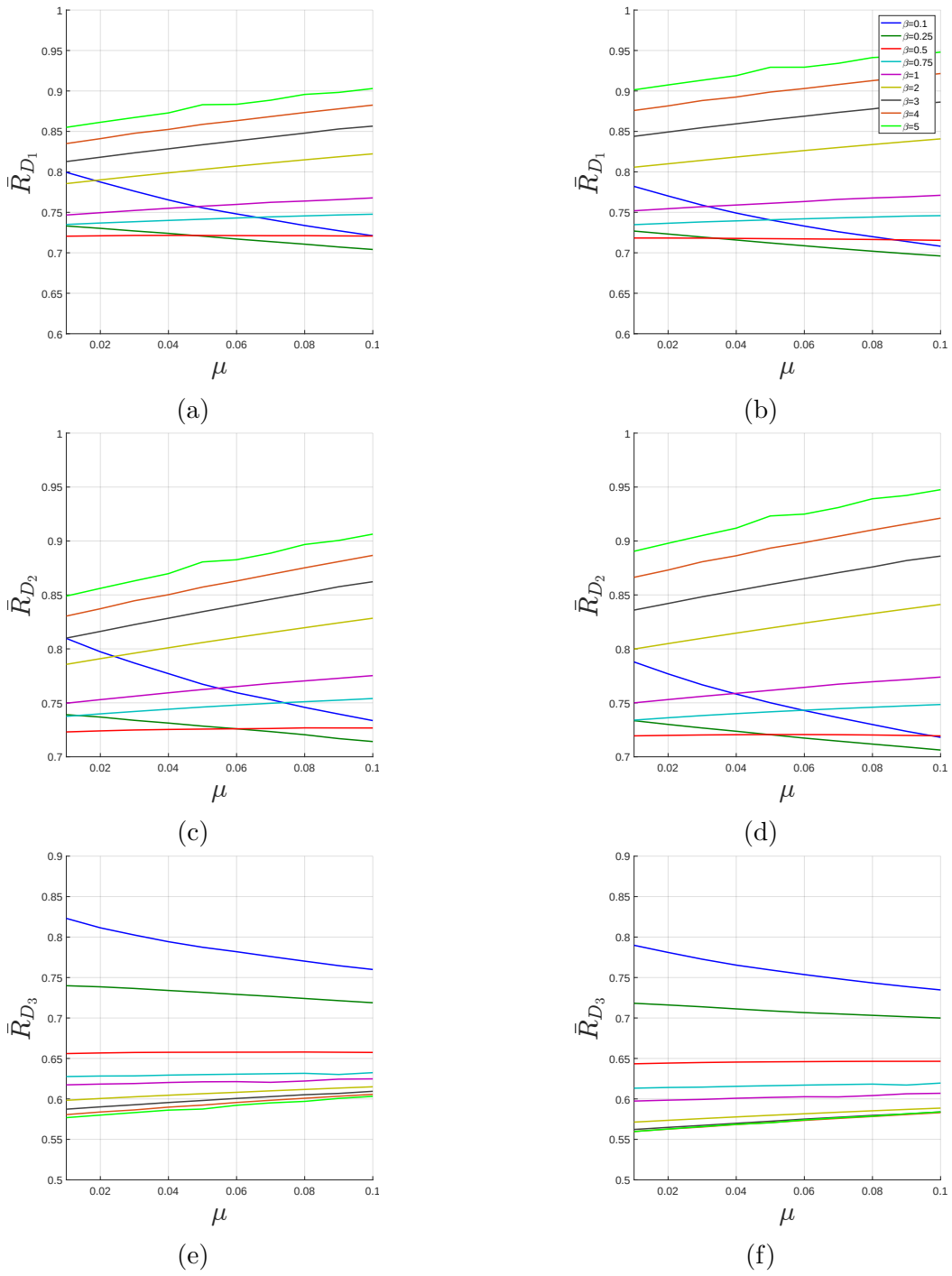

Figure 5.18: First, second, and third floor displacement reduction factors for SATMDI ($\kappa = 0.5$) (a),(c),(e) and TMDI (b),(d),(f) using the rock-site ground motion set.

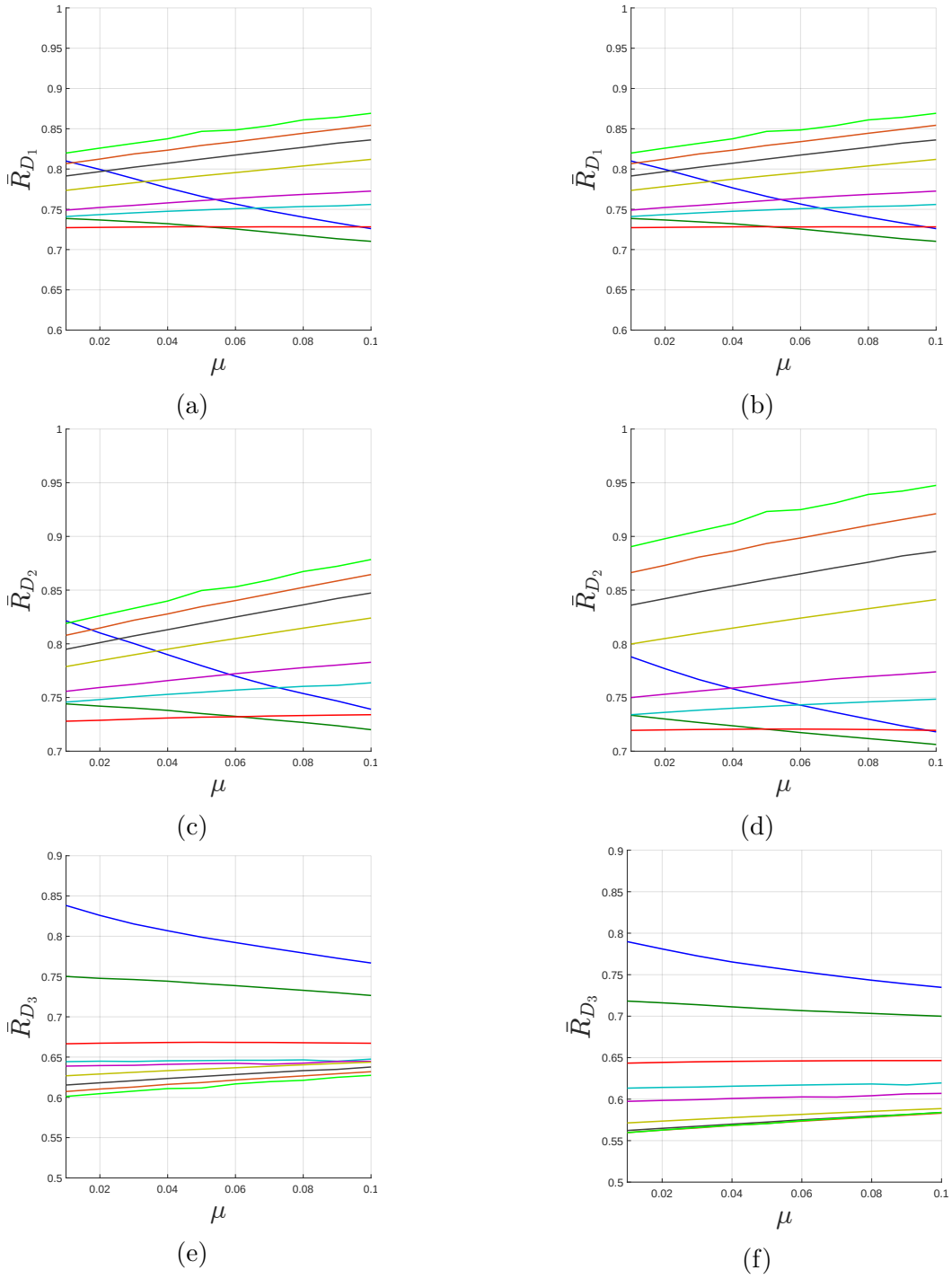

Figure 5.19: First, second, and third floor displacement reduction factors for SATMDI ($\kappa = 0.75$) (a),(c),(e) and TMDI (b),(d),(f) using the rock-site ground motion set.

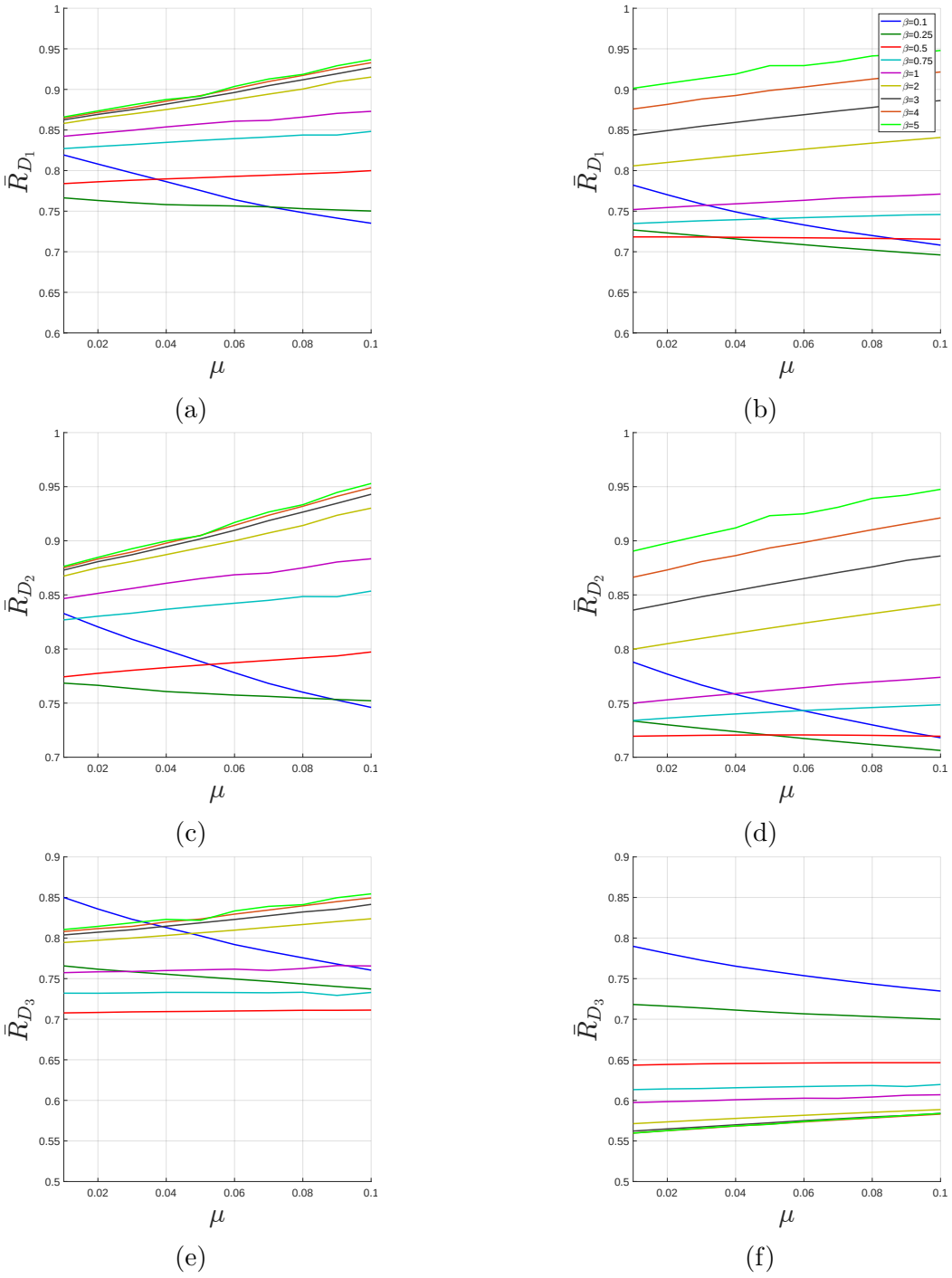

Figure 5.20: First, second, and third floor displacement reduction factors for SATMDI ($\kappa = 1$) (a),(c),(e) and TMDI (b),(d),(f) using the rock-site ground motion set.

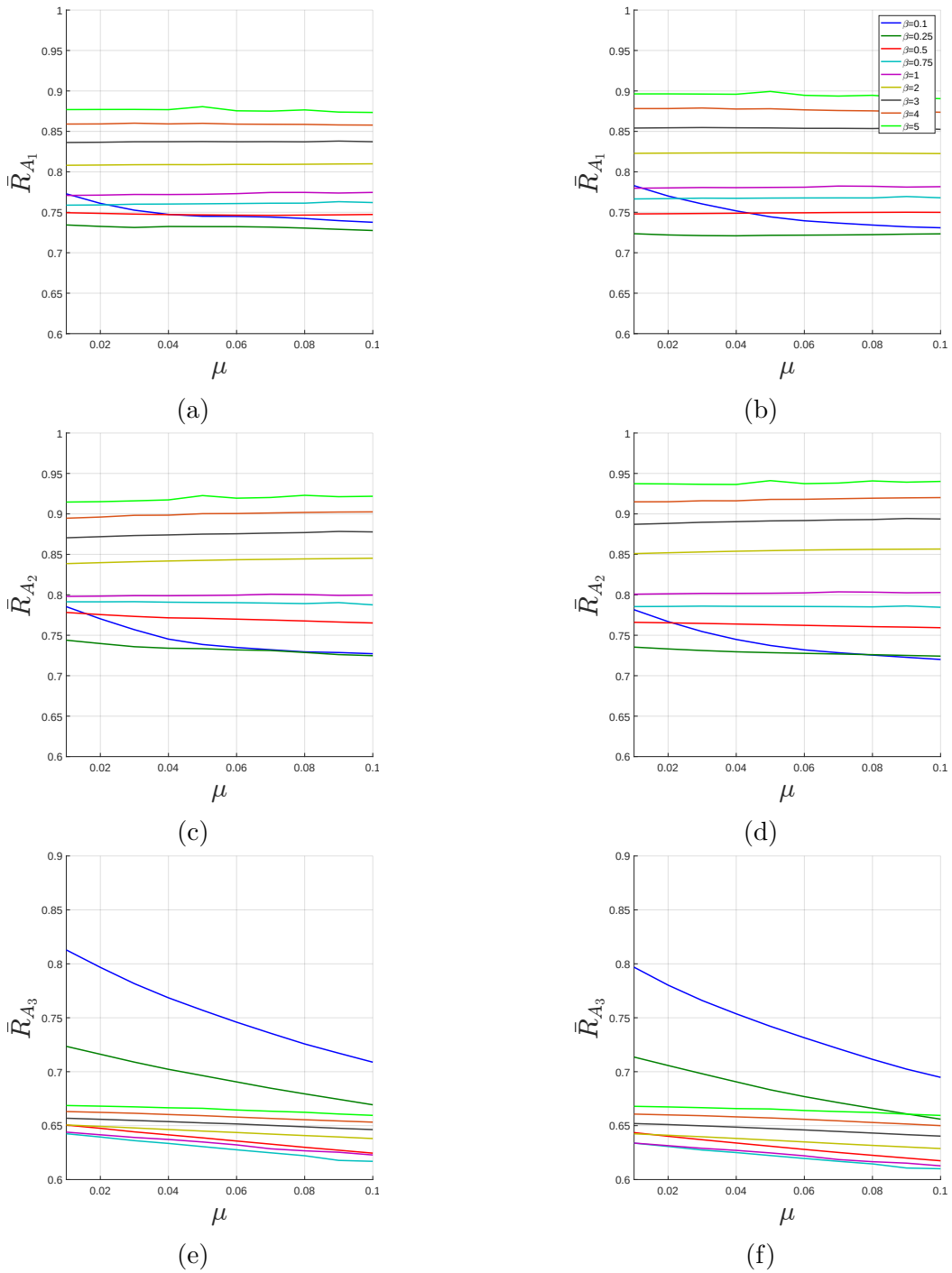

Figure 5.21: First, second, and third floor acceleration reduction factors for SATMDI ($\kappa = 0.25$) (a),(c),(e) and TMDI (b),(d),(f) using the rock-site ground motion set.

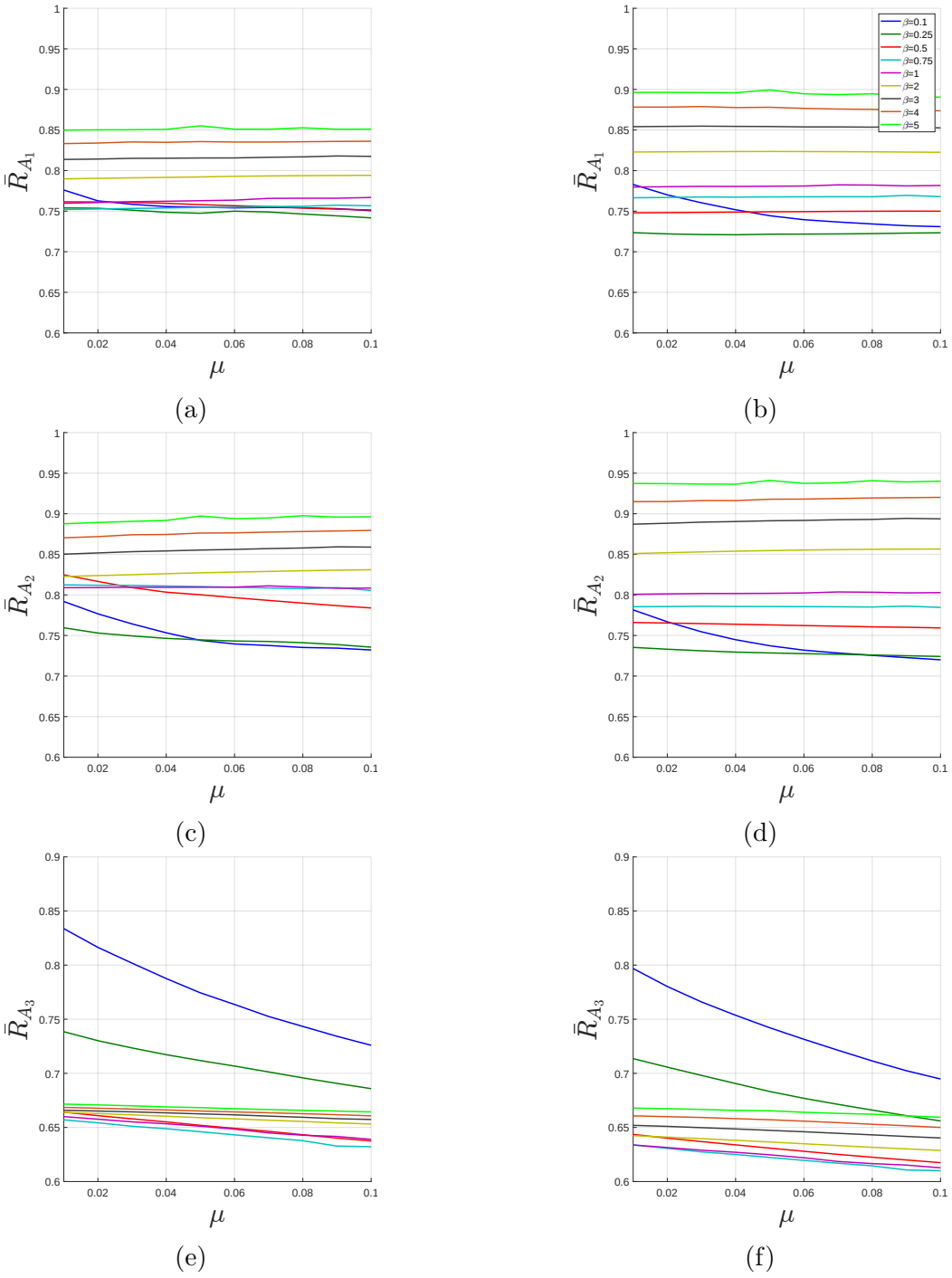

Figure 5.22: First, second, and third floor acceleration reduction factors for SATMDI ($\kappa = 0.5$) (a),(c),(e) and TMDI (b),(d),(f) using the rock-site ground motion set.

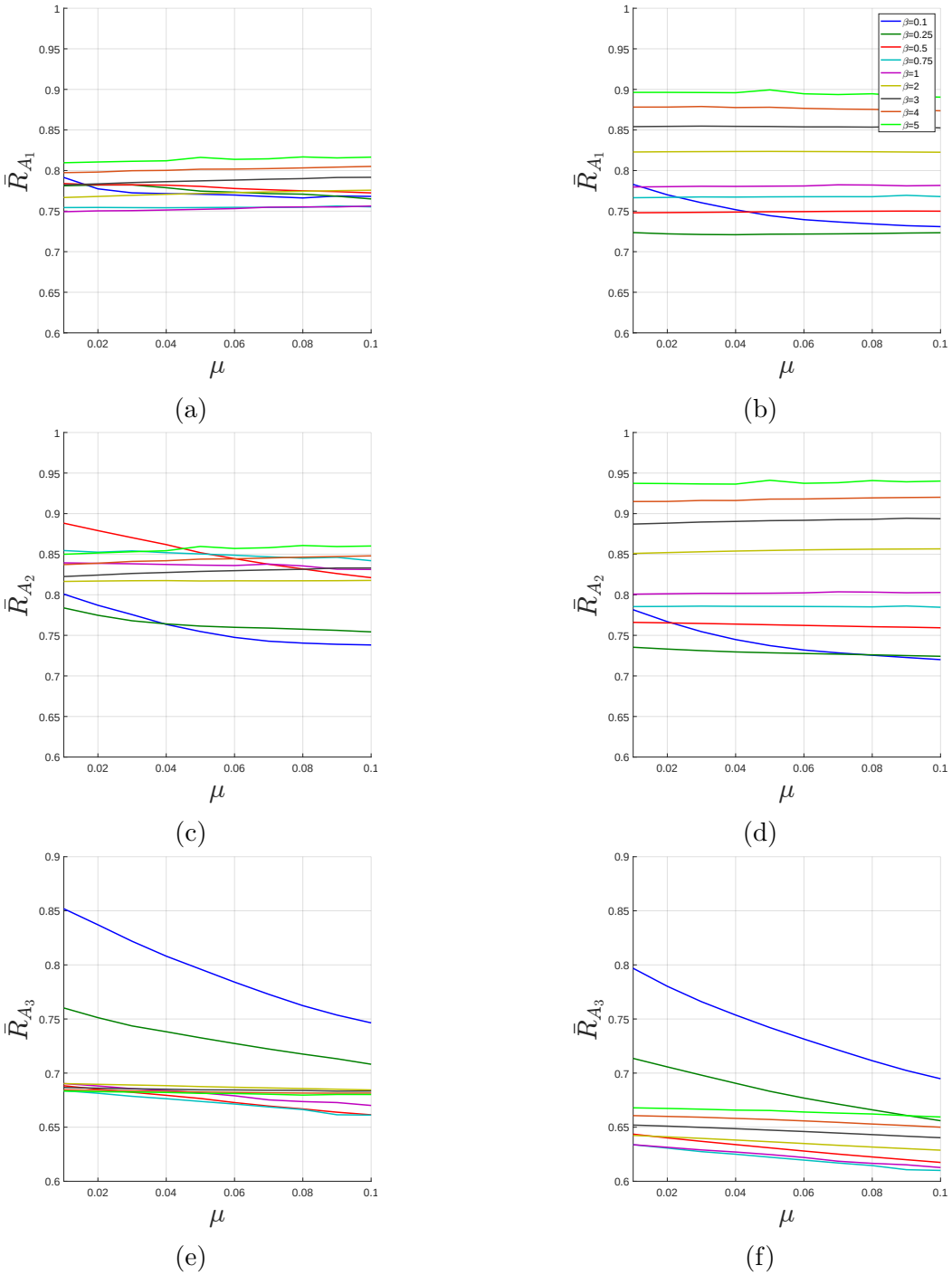

Figure 5.23: First, second, and third floor acceleration reduction factors for SATMDI ($\kappa = 0.75$) (a),(c),(e) and TMDI (b),(d),(f) using the rock-site ground motion set.

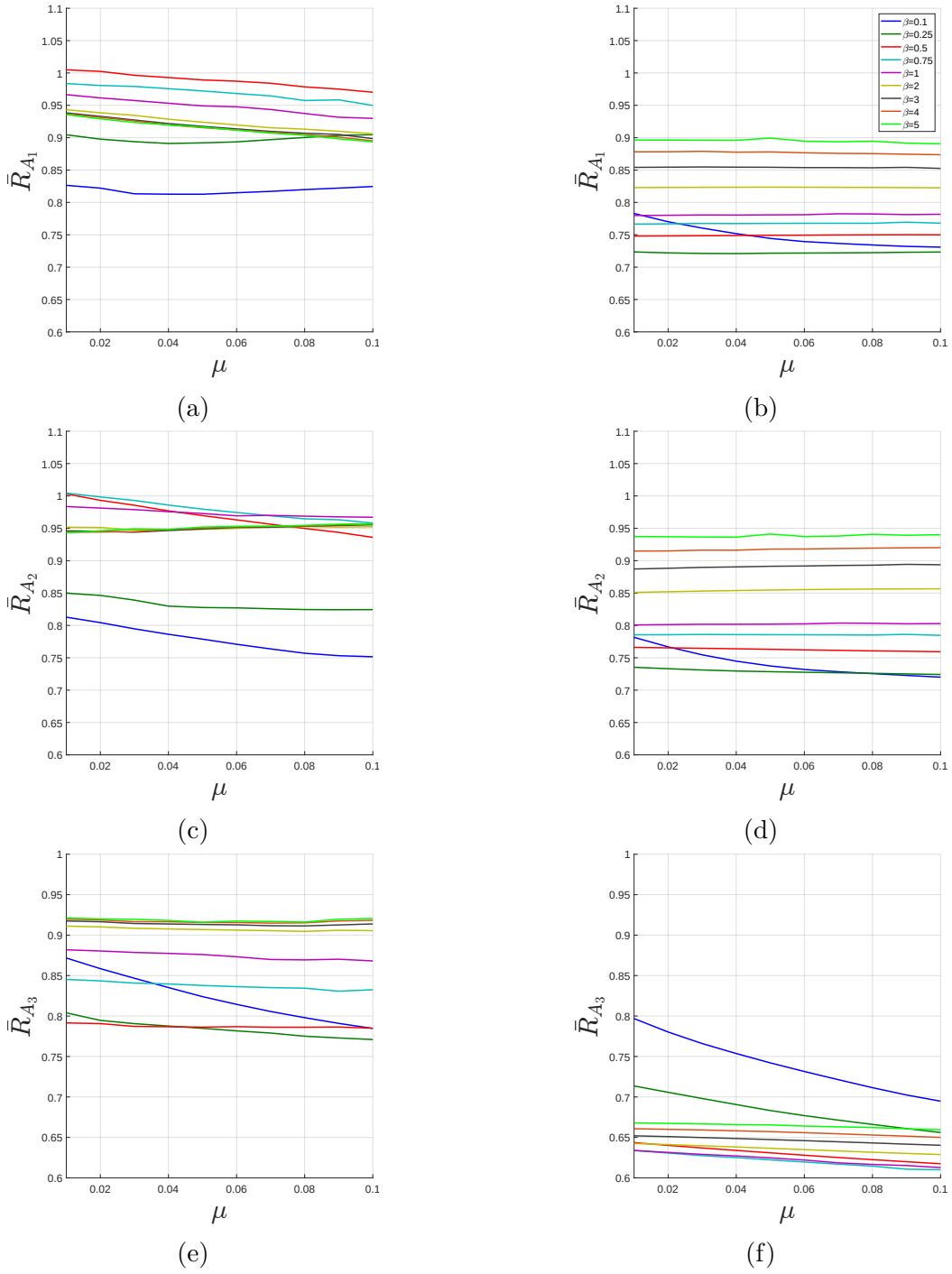

Figure 5.24: First, second, and third floor acceleration reduction factors for SATMDI ($\kappa = 1$) (a),(c),(e) and TMDI (b),(d),(f) using the rock-site ground motion set.

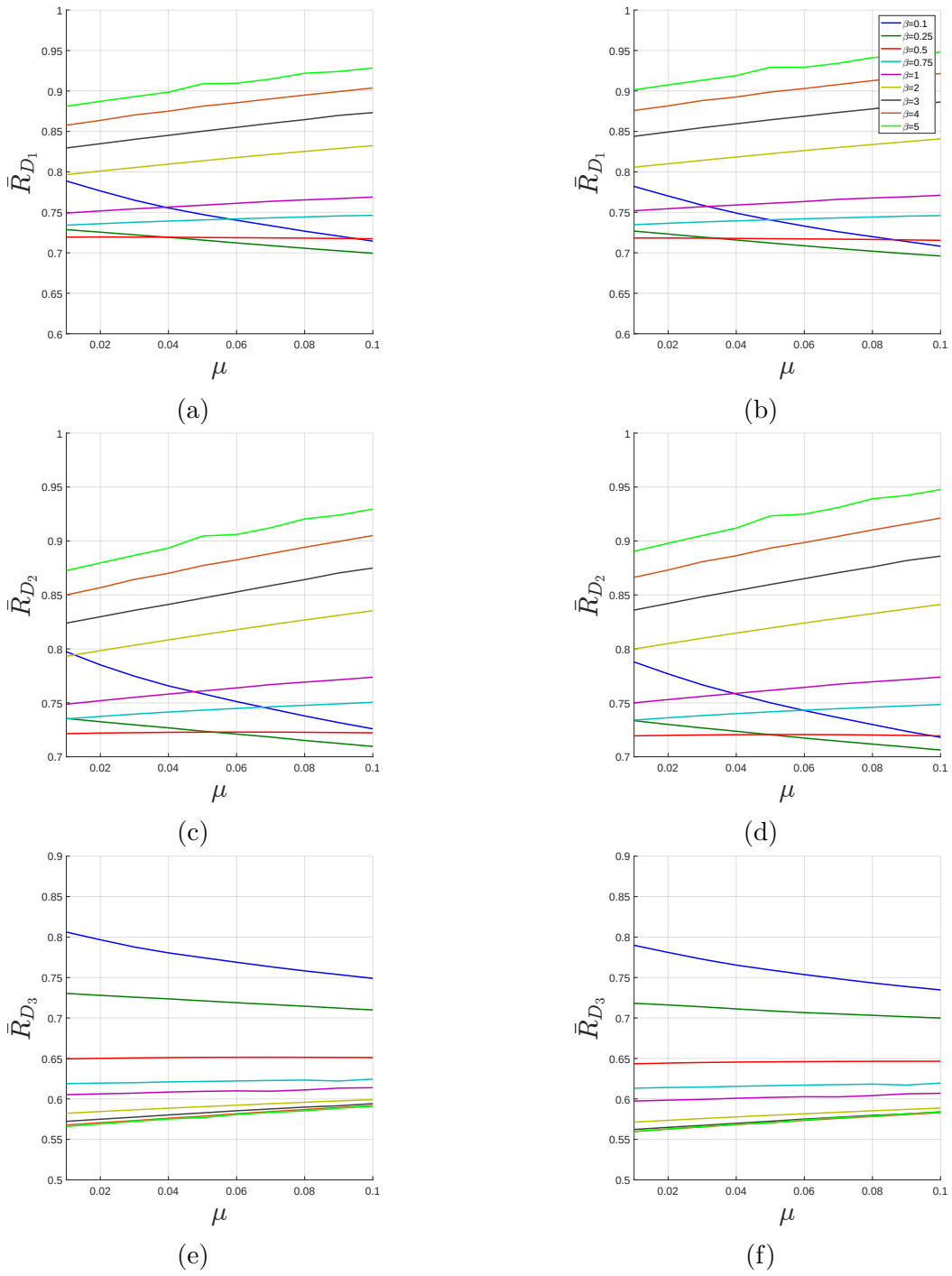

Figure 5.25: First, second, and third floor displacement reduction factors for SATMDI ($\kappa = 0.25$) (a),(c),(e) and TMDI (b),(d),(f) using the pulse-like ground motion set.

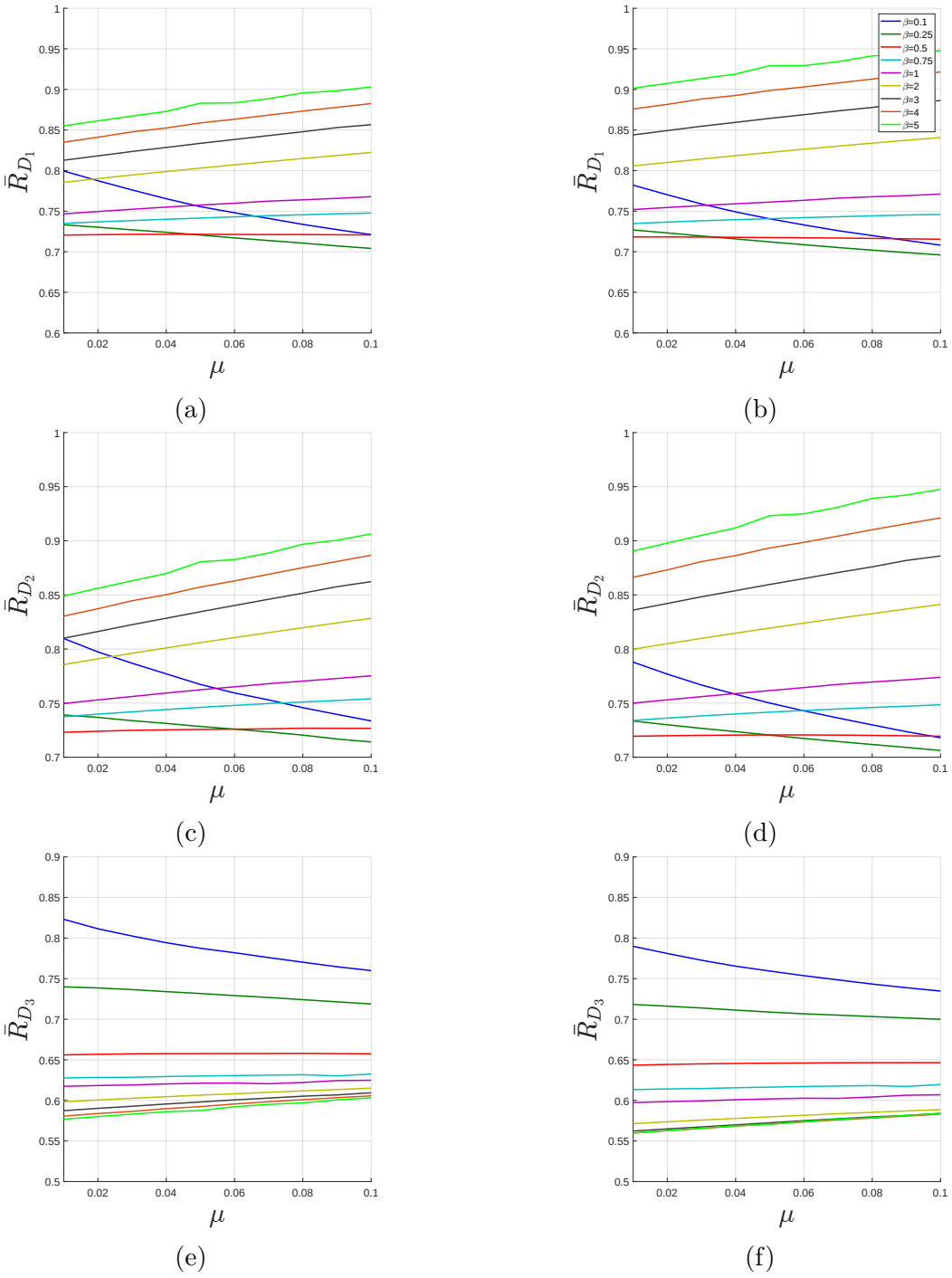

Figure 5.26: First, second, and third floor displacement reduction factors for SATMDI ($\kappa = 0.5$) (a),(c),(e) and TMDI (b),(d),(f) using the pulse-like ground motion set.

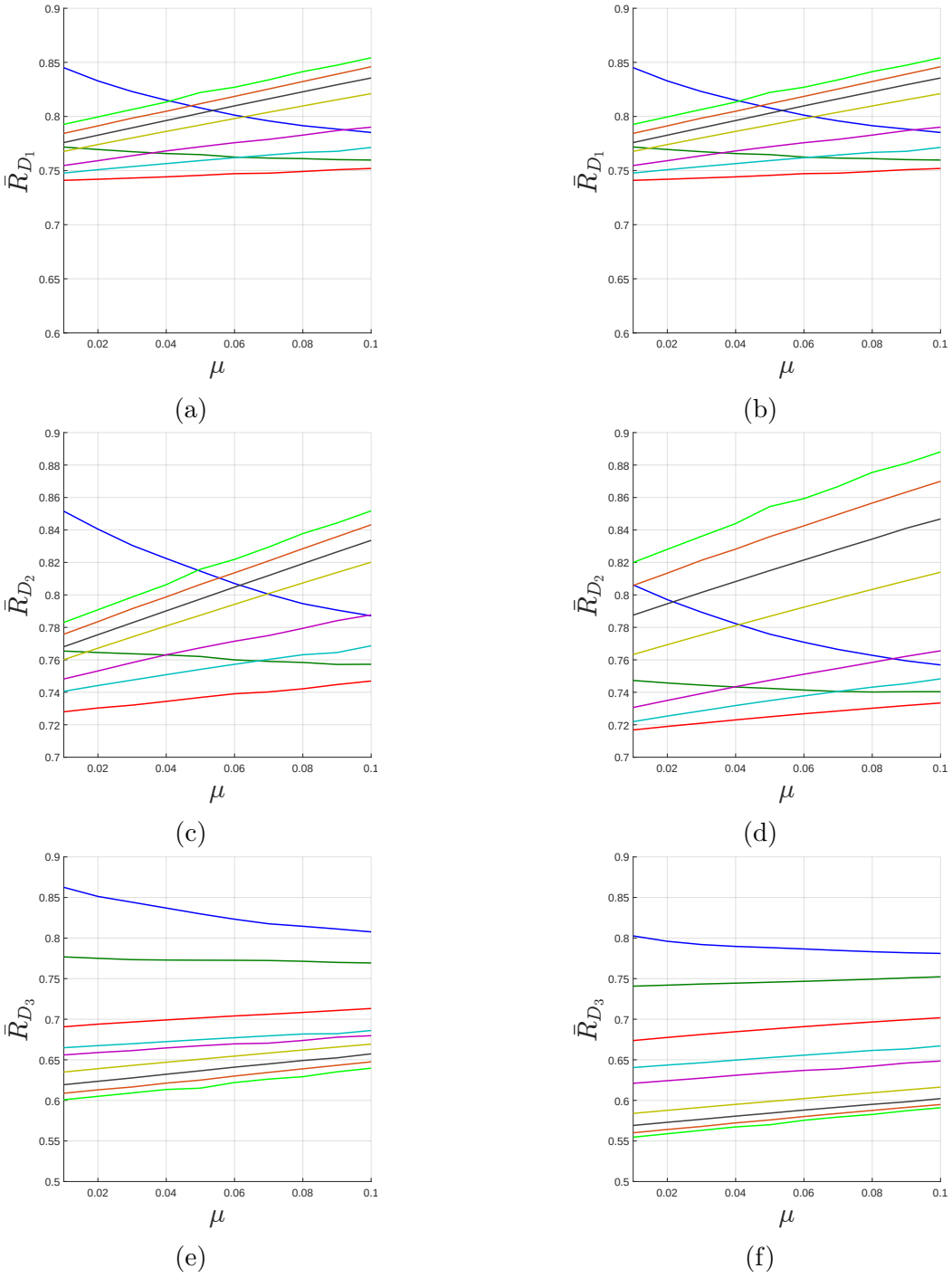

Figure 5.27: First, second, and third floor displacement reduction factors for SATMDI ($\kappa = 0.75$) (a),(c),(e) and TMDI (b),(d),(f) using the pulse-like ground motion set.

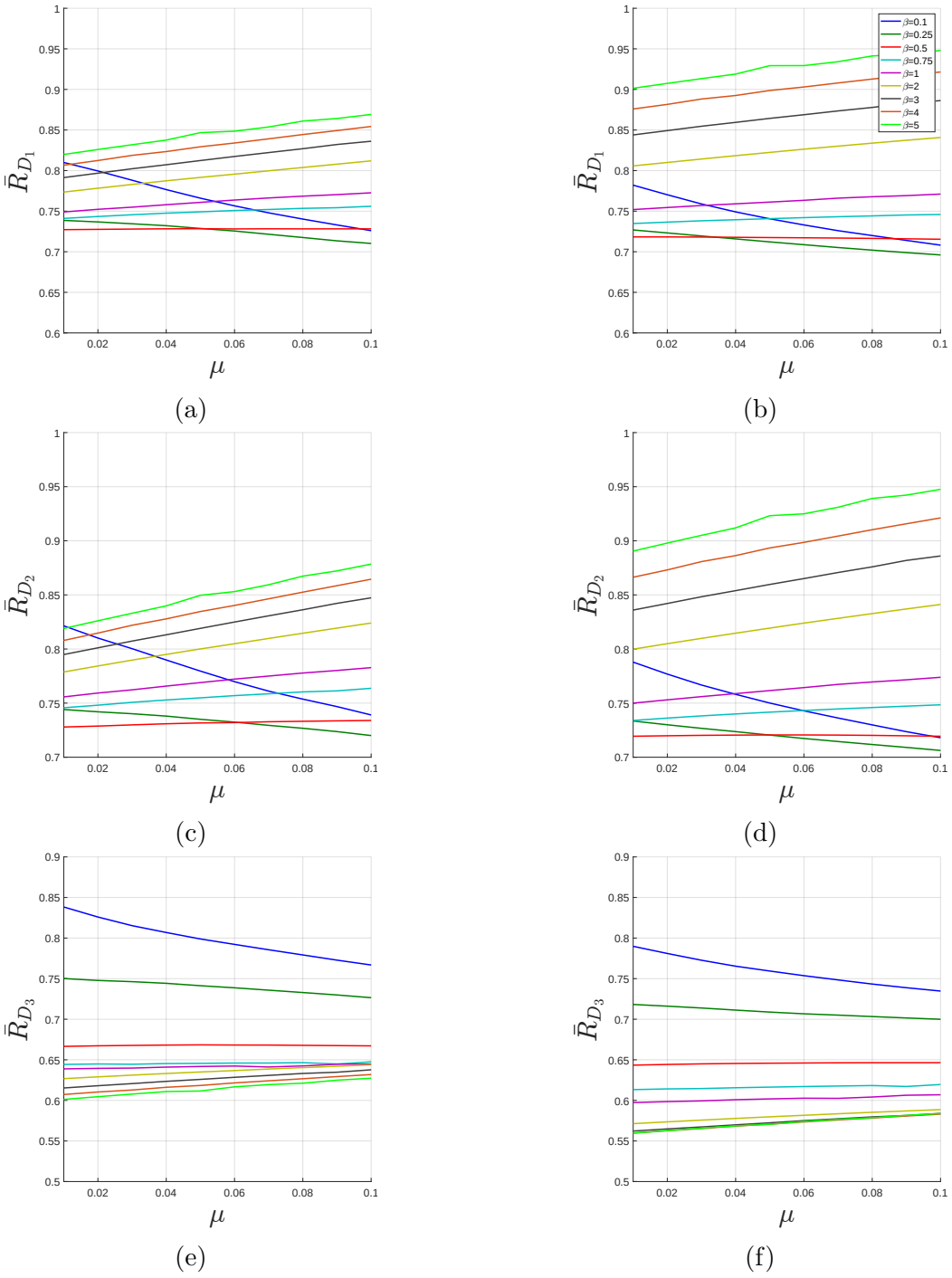

Figure 5.28: First, second, and third floor displacement reduction factors for SATMDI ($\kappa = 1$) (a),(c),(e) and TMDI (b),(d),(f) using the pulse-like ground motion set.

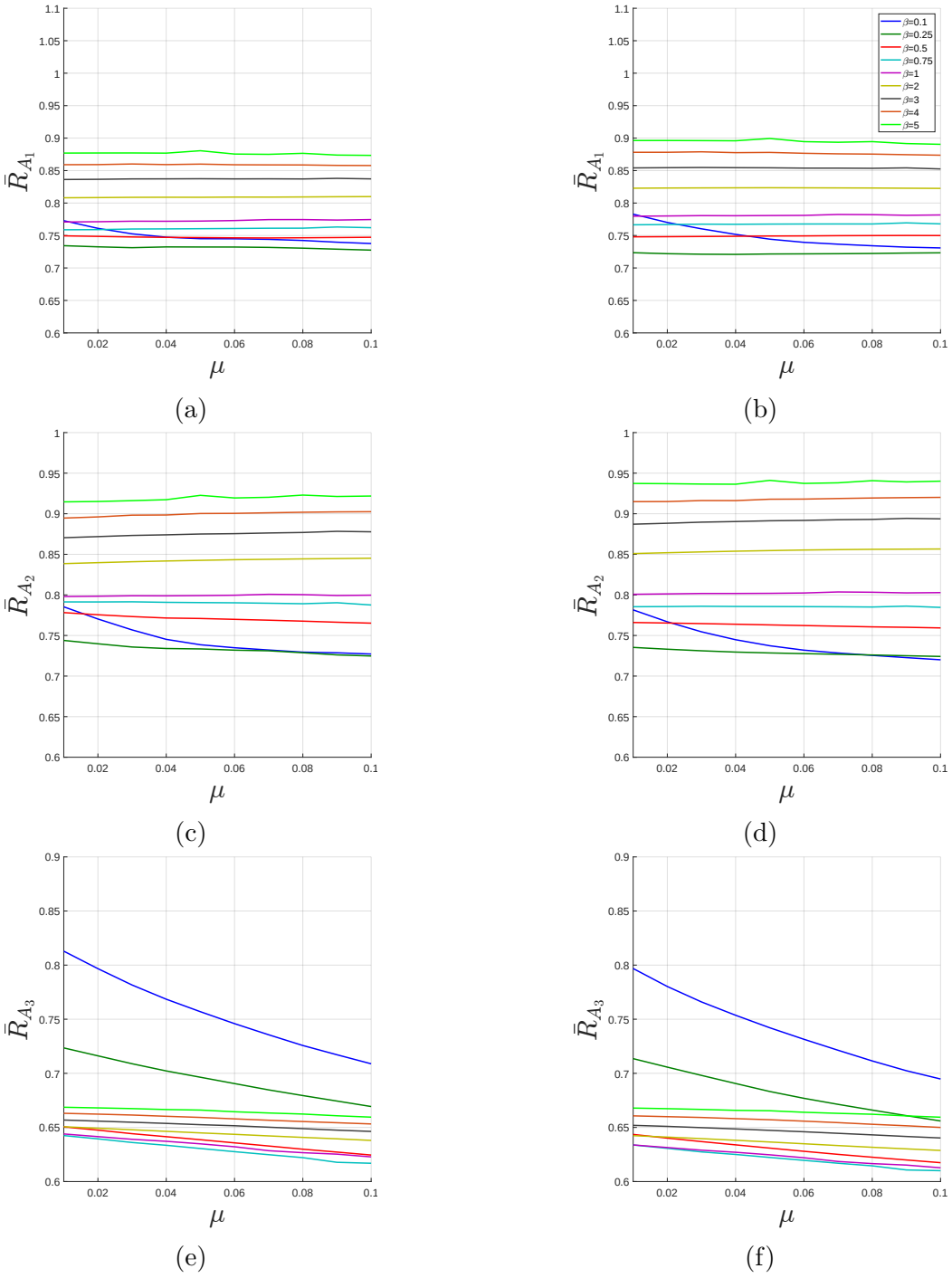

Figure 5.29: First, second, and third floor acceleration reduction factors for SATMDI ($\kappa = 0.25$) (a),(c),(e) and TMDI (b),(d),(f) using the pulse-like ground motion set.

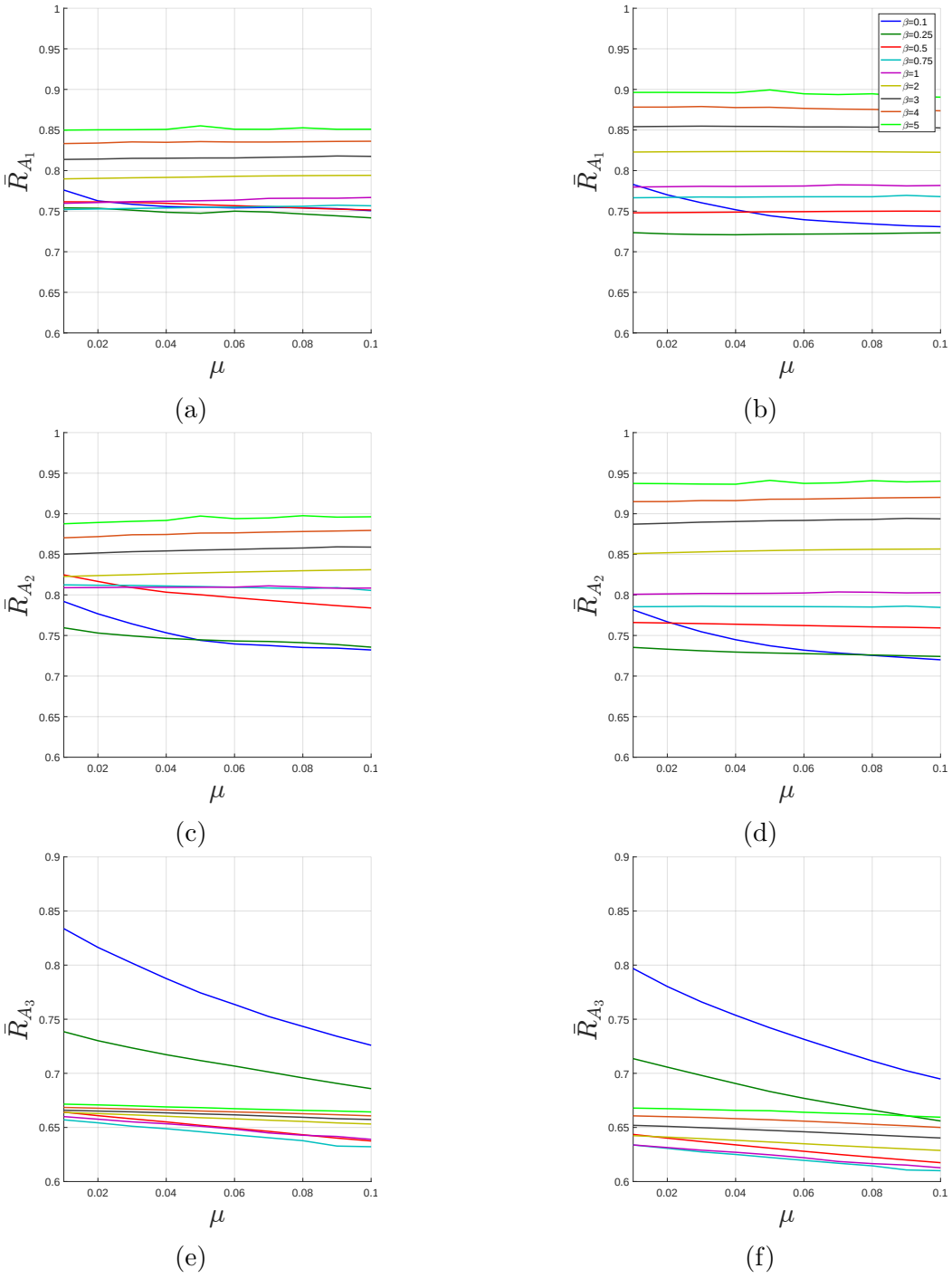

Figure 5.30: First, second, and third floor acceleration reduction factors for SATMDI ($\kappa = 0.5$) (a),(c),(e) and TMDI (b),(d),(f) using the pulse-like ground motion set.

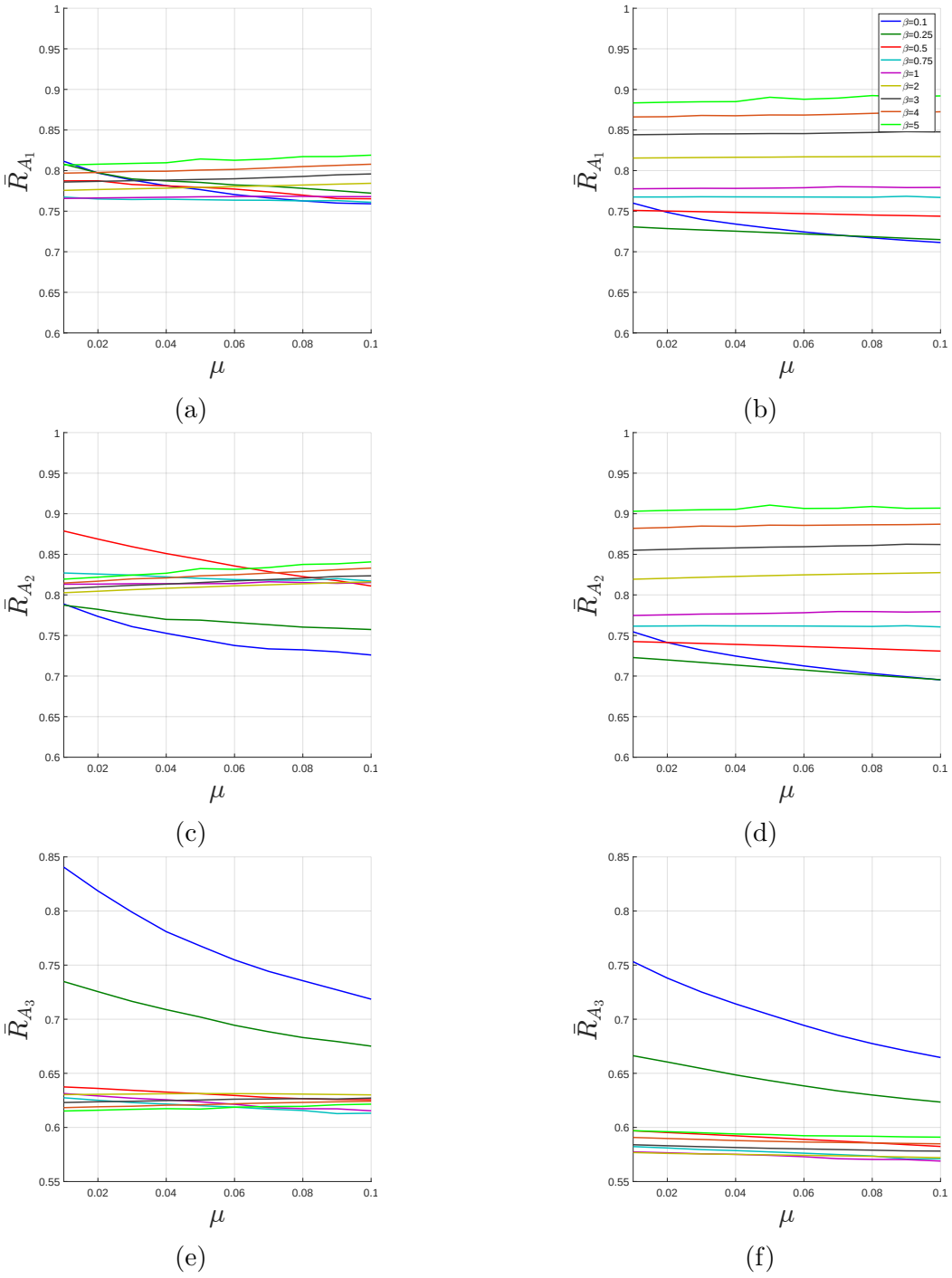

Figure 5.31: First, second, and third floor acceleration reduction factors for SATMDI ($\kappa = 0.75$) (a),(c),(e) and TMDI (b),(d),(f) using the pulse-like ground motion set.

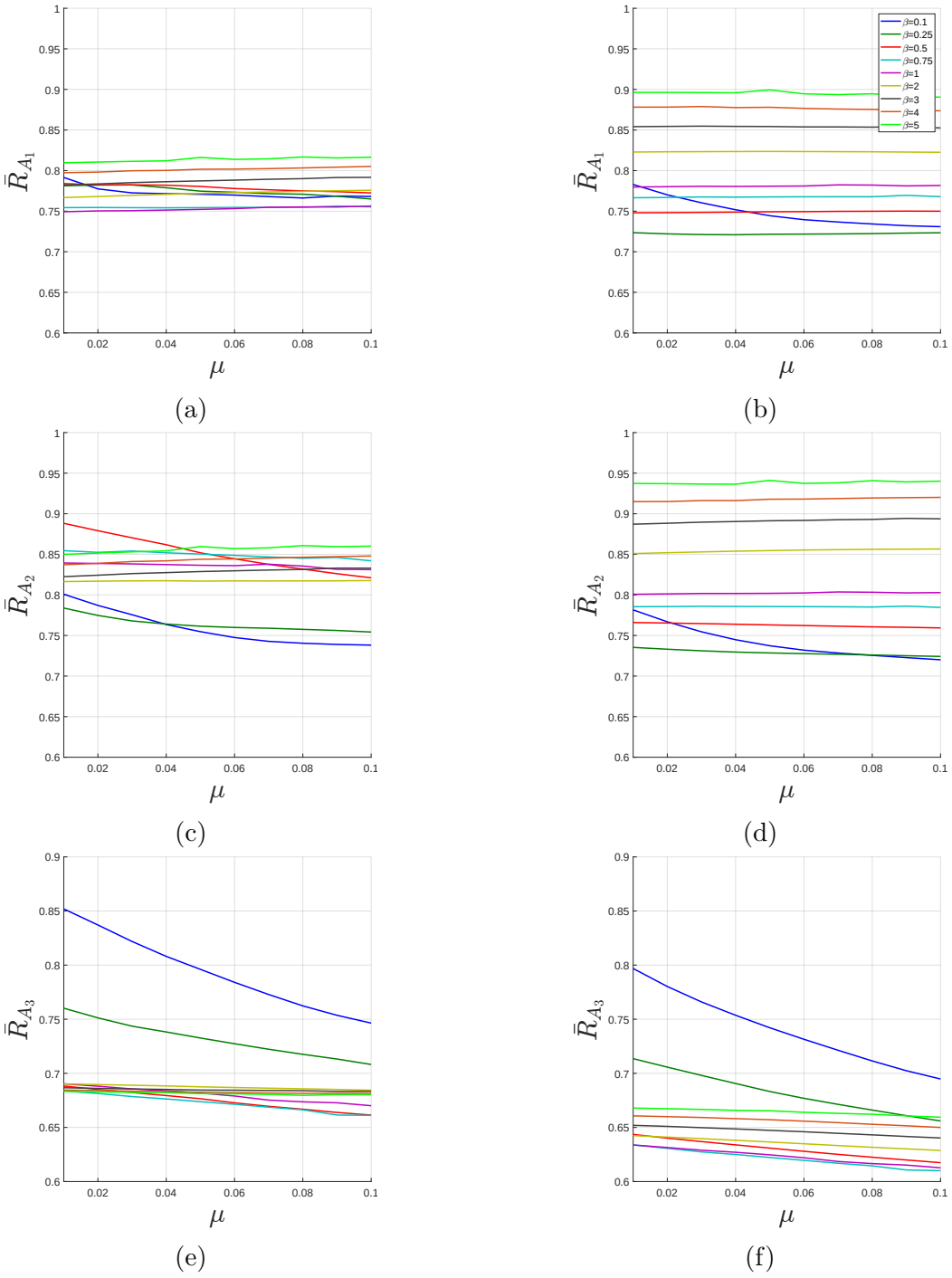

Figure 5.32: First, second, and third floor acceleration reduction factors for SATMDI ($\kappa = 1$) (a),(c),(e) and TMDI (b),(d),(f) using the pulse-like ground motion set.

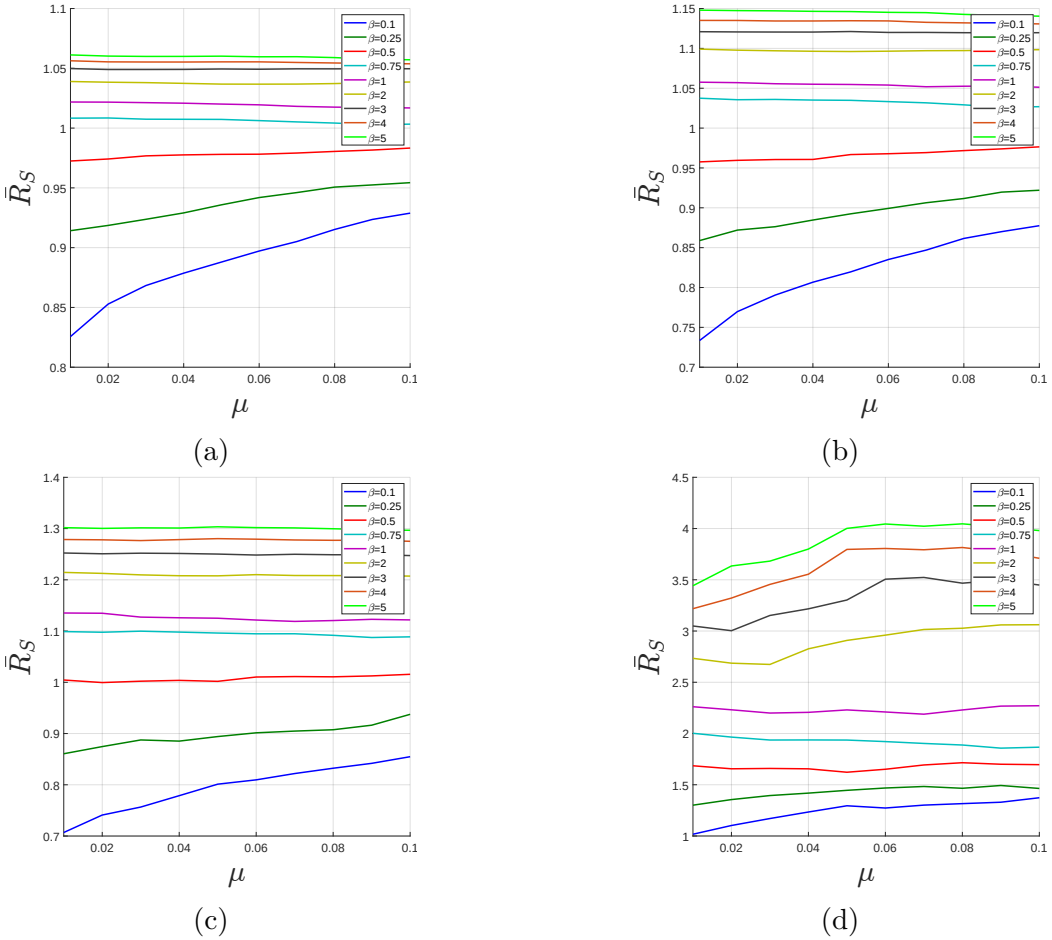

Figure 5.33: Stroke reduction factor for κ values of (a) 0.25, (b), 0.5, (c) 0.75, and (d) 1.0 under the rock-site ground motion set.

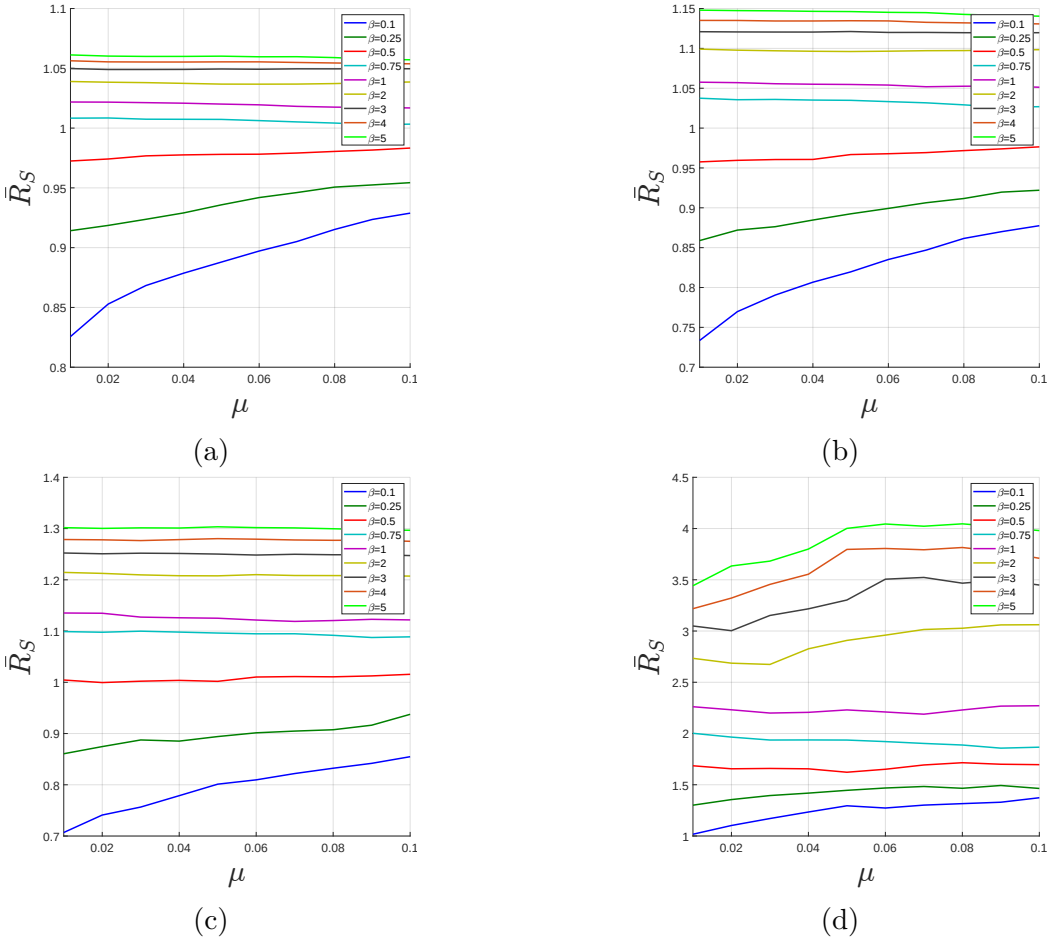

Figure 5.34: Stroke reduction factor for κ values of (a) 0.25, (b), 0.5, (c) 0.75, and (d) 1.0 under the pulse-like ground motion set.

Chapter 6

Asymmetric structures equipped with Semi-active Resettable Springs

6.1 Introduction

Assessment of damage after seismic events has revealed that asymmetry structures have poor performance compared with symmetric structures. Asymmetry arises from uneven distribution of the mass and/or stiffness; it is advised (and promoted) to avoid such circumstances. Architectural, or functional, requirements may force a structural design with eccentricity about one or both horizontal directions. With this backdrop, researchers have focused on mitigation strategies to protect asymmetric structures from damaging seismic torsional response. One approach, summarized herein, is the implementation of supplemental energy dissipating devices to control the response of the structure during seismic excitation.

Several studies have investigated the effectiveness of base isolation [49], active control [17], and passive control [36, 60] for mitigating torsional response of asymmetric buildings. These methods are usually costly and may lead to power or response control restrictions. On the

other hand, semi-active devices are cost effective and provide efficient structural control; they typically require little power to function. The most common semi-active device studied by researchers is magnetorheological (MR) dampers. Several control algorithms have also been introduced to better provide control of the seismic response of asymmetric structures [71, 72, 51]. In contrast with MR dampers, resettable semi-active springs (SRS) [11, 48] have shown superior performance. SRSs focuses on stiffness control rather than viscous damping control in MR dampers. Control algorithms for the utilization SRSs for seismic response reduction of symmetric structures were studied by several research groups (e.g., on SDOFs [30] and on MDOFs [126], among others). A control algorithm for utilizing SRSs towards seismic response mitigation of asymmetric structures is presented herein.

This investigation considers how SRSs affect the seismic response of asymmetric structures. Two recommendations for control strategies using SRSs to mitigate seismic response of asymmetric structures efficiently are recommended. The suggested structural control strategy is general and not geared towards a single structural period and SRS placement [72]. This study aims to identify the key parameters that impact the seismic response of asymmetric structures equipped with SRSs and show how the distribution of SRSs within the structure affects the response. Limitations of each are discussed with suggested implementation guidelines. The analytical and experimental implementation of the proposed methods for the utilization of SRSs towards mitigating torsional response structures is outside the scope of the current research. The intent here is to maintain focus on the control strategies for SRSs.

6.2 Characteristics of semi-active resettable spring

The semi-active resettable spring (SRS) used in this study was first introduced by Bobrow et al. [11]. The device itself is a piston and cylinder with a valve connecting the two sides

of the cylinder and a rod extending through the cylinder to give equal areas on both sides of the piston. The device is used to vary or increase the stiffness of the system in real-time. Fardadi et al. [30] investigated the seismic response of a SDOF system using a SRS whereby the stiffness is added through a bracing system, shown in Figure 6.1. To quantify the amount

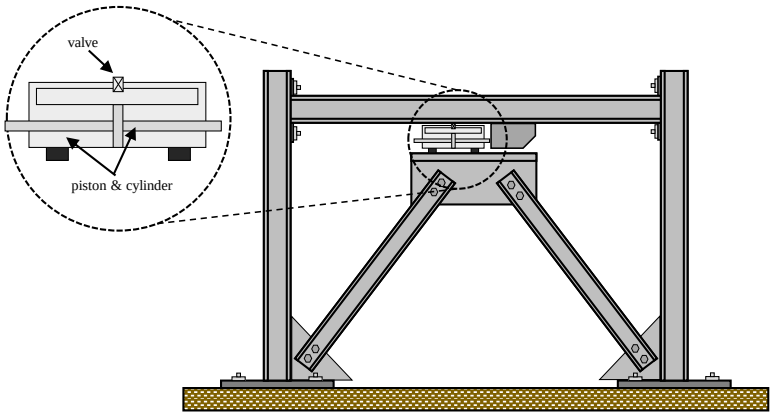

Figure 6.1: Frame with bracing joined by a semi-active resettable spring.

of stiffness provided by the SRS, the brace-to-frame factor is introduced, denoted by BFS, and defined as

$$\text{BFS} = \frac{\text{stiffness of the brace}}{\text{stiffness of the frame}}. \tag{6.1}$$

For BFS = 1, the bracing doubles the stiffness of the frame and when BFS = 0 the SRSs are not been engaged. Since there will be multiple SRSs within the structure, the total stiffness of SRSs in a single direction over the total stiffness of the structure in that same direction is used to compute the BFS factor. The effect the BFS factor has on the response of the structure will be investigated in the proceeding section.

Three control laws were implemented in prior work [30], denoted as 1-4, 1&3, and 2&4, referring to the active quadrant of the figure representing the bracing system's load-displacement curve. From the three control laws, it was found that control law 1-4 was most effective in reducing displacement of the frame. The approach used in control law 1-4 relies on a resetting technique, whereby the energy stored in the device is released when it has reached

its maximum local strain energy, i.e., when the velocity across the device is zero [11, 48]. A physical interpretation of the semi-active resettable device using control law 1-4 is by considering the device as a spring element, and is engaged when the valve is closed. When the device is reset, the valve opens and quickly extracts energy (through heat loss and fluid slushing), which is analogous to resetting the unstretched length of the spring. Since the reset time is short, the valve is closed for much of the seismic event, and so the device continuously adds stiffness to the system. The term reset indicates that the stored energy of the device is dissipated after opening the valve. Using this equivalent spring analogy, the reset locations x_r can be defined by

$$\text{set } x_r = x \text{ whenever } \dot{x} = 0 \tag{6.2}$$

The control law in (6.2) will be modified to account for lateral and rotational motion of the SRSs within the structure.

6.3 System and Equations of Motion

6.3.1 System under consideration

The structural system under consideration is a linearly elastic idealized singly-story building consisting of a rigid deck supported on columns (see Figure 4.8b). The mass of the deck is assumed to be uniformly distributed and thus the center of mass (CM) coincides with the geometric center of the deck. The column stiffness and positions are chosen such that asymmetry is in only one direction, which results in a flexible and stiff edge of the structure (see Figure 6.2a). The center of rigidity (CR) is located at a distance, e_x, from the CM along the x-direction. The structure is asymmetric only in the x-direction and therefore is a two-degree-of-freedom system, namely, lateral displacement and torsional displacement,

denoted as u_y and u_θ, respectively. Similar to the CR, the center of supplemental stiffness (CSS), is selected by choosing the SRS stiffness and positions such that e_{dx} is the distance CSS is away from the CM.

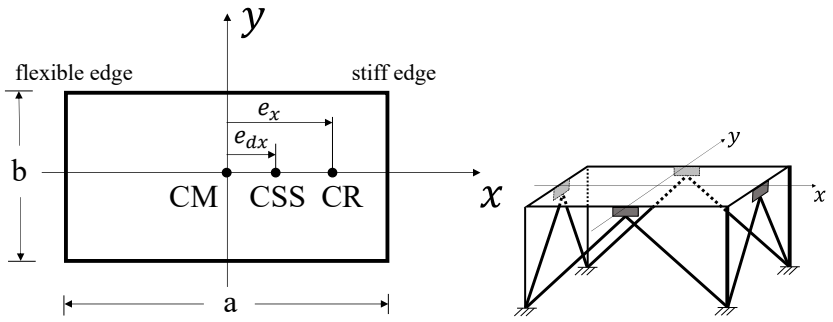

(a) (b)

Figure 6.2: Plan and elevation view of one-way asymmetric structure with SRSs installed.

6.3.2 Equations of Motion

The governing equations of motion of the system are given by

$$\mathbf{M}\ddot{\mathbf{u}} + \mathbf{C}\dot{\mathbf{u}} + \mathbf{K}\mathbf{u} + \mathbf{K}_d\mathbf{u} - \sum_j \mathbf{K}_{dxj}\mathbf{u}_{sxj} - \sum_j \mathbf{K}_{dyj}\mathbf{u}_{syj} = -\mathbf{M}\ddot{\mathbf{u}}_g \tag{6.3}$$

where $\mathbf{M}, \mathbf{C}$, and $\mathbf{K}$ are the mass, damping, and stiffness matrices of the system, respectively. Moreover, $\mathbf{u} = [u_y \, a u_\theta]^T$ is the displacement vector, $\ddot{\mathbf{u}}_g = [\ddot{u}_{gy} \, 0]^T$ is the ground acceleration vector, $\ddot{u}_{gy}$ is the ground acceleration in the y-direction. The mass matrix can be expressed as

$$\mathbf{M} = \begin{bmatrix} m & 0 \\ 0 & m\left(\frac{\rho}{a}\right)^2 \end{bmatrix} \tag{6.4}$$

where m is the lumped mass of the deck and ρ is the radius of gyration about the vertical axis through the CM, that is,

$$\rho = \sqrt{\frac{a^2 + b^2}{12}} = a\sqrt{\frac{1 + \alpha^2}{12\alpha^2}} \tag{6.5}$$

where a and b are the plan dimensions of the building and the aspect ratio $\alpha = a/b$. To construct the stiffness matrix, $\mathbf{K}$, let k_{xi} represent the lateral stiffness and y_i the distance from the CM of the ith column along the x-axis. Let k_{yi} denote the lateral stiffness and x_i the distance from the CM of the ith column along the y-axis. The lateral stiffness along the y-direction is defined as

$$K_y = \sum_i k_{yi} \tag{6.6}$$

and torsional stiffness of the system about the CM is given by

$$K_\theta = \sum_i k_{xi} y_i^2 + \sum_i k_{yi} x_i^2 \tag{6.7}$$

The distance from the CM to the CR in the x-direction, known as the eccentricity, is expressed as

$$e_x = \frac{1}{K_y} \sum_i k_{yi} x_i \tag{6.8}$$

Using the result [41] that $K_\theta = K_{\theta r} + e_x^2 K_y$, where $K_{\theta r}$ is the torsional stiffness about the CR, the stiffness matrix of the system can be expressed as

$$\mathbf{K} = K_y \begin{bmatrix} 1 & \frac{e_x}{a} \\ \frac{e_x}{a} & \left(\frac{e_x}{a}\right)^2 + \frac{1}{a^2}\frac{K_{\theta r}}{K_y} \end{bmatrix} \tag{6.9}$$

Assuming that the system is classically damped, the mass and stiffness matrices, $\mathbf{M}$ and $\mathbf{K}$, can be used to write the damping matrix as

$$C = a_0\mathbf{M} + a_1\mathbf{K} \tag{6.10}$$

where a_0 and a_1 are constants of proportionality. The constants a_0 and a_1 depend on the two damping ratios of the system, denoted as ζ_1 and ζ_2. In a similar fashion to constructing the stiffness matrix of the system, the stiffness matrix associated with the SRSs, $\mathbf{K}_d$, can be expressed as

$$\mathbf{K}_d = K_{dy}\begin{bmatrix} 1 & \left(\frac{e_{dx}}{a}\right) \\ \left(\frac{e_{dx}}{a}\right) & \left(\frac{e_{dx}}{a}\right)^2 + \frac{1}{a^2}\frac{K_{d\theta r}}{K_{dy}} \end{bmatrix} \tag{6.11}$$

where the lateral stiffness provided by the SRSs in the y-direction, K_{dy}, is

$$K_{dy} = \sum_j k_{dyj} \tag{6.12}$$

and semi-active resettable spring (SRS) eccentricity, e_{dx}, is defined as

$$e_{dx} = \frac{1}{K_{dy}}\sum_j k_{dyj}x_{dj} \tag{6.13}$$

The torsional stiffness of the SRSs about the CM is given by

$$K_{d_\theta} = \sum_j k_{dyj}x_{dj}^2 + \sum_j k_{dxj}y_{dj}^2 \tag{6.14}$$

As with the system stiffness matrix, equation (6.11) used the result $K_{d\theta} = e_{dx}^2K_{dy} + K_{d\theta r}$, where $K_{d\theta r}$ is the torsional stiffness of the SRSs about the CSS. Defining the semi-active

resettable spring (SRS) radius of gyration, ρ_d, as

$$\rho_d = \sqrt{\frac{K_{d\theta r}}{K_{dy}}}, \tag{6.15}$$

Note that this naming convention on ρ_d is similar to previous work which used fluid viscous dampers [36] or viscoelastic elements [60]. The stiffness matrix of the SRSs shown in (6.11) can be written as

$$\mathbf{K}_d = K_{dy} \begin{bmatrix} 1 & \left(\frac{e_{dx}}{a}\right) \\ \left(\frac{e_{dx}}{a}\right) & \left(\frac{e_{dx}}{a}\right)^2 + \left(\frac{\rho_d}{a}\right)^2 \end{bmatrix} \tag{6.16}$$

The stiffness matrix associated with the j^{th} device in the x and y-directions are expressed as

$$\mathbf{K}_{dxj} = \begin{bmatrix} 0 & 0 \\ 0 & k_{dxj}\left(\frac{y_{dj}}{a}\right)^2 \end{bmatrix} \quad \text{and} \quad \mathbf{K}_{dyj} = \begin{bmatrix} k_{dyj} & k_{dyj}\left(\frac{x_{dj}}{a}\right) \\ k_{dyj}\left(\frac{x_{dj}}{a}\right) & k_{dyj}\left(\frac{x_{dj}}{a}\right)^2 \end{bmatrix}, \tag{6.17}$$

where k_{dxj} and k_{dyj} are the stiffness provided by the j^{th} device in the x and y-directions, respectively. Also, x_{dj} is the distance of the j^{th} device in the y-direction with respect to the CM and y_{dj} is the distance of the j^{th} device in the x-direction with respect to the CM. Note that the sparsity of $\mathbf{K}_{dxj}$ is a result of having motion only in the y-direction, where the SRSs in the x-direction are only engaged when there is rotation (see Figure 6.2b). Similarly, the reset location vector for the j^{th} device in the x-direction, $\mathbf{u}_{rxj}$, is determined by the control law

$$\text{set } \mathbf{u}_{rxj} = \mathbf{u} \text{ whenever } \dot{u}_\theta = 0. \tag{6.18}$$

The reset location vector for the j^{th} device in the y-direction, $\mathbf{u}_{syj}$, is given by the control law

$$\text{set } \mathbf{u}_{ryj} = \mathbf{u} \text{ whenever } \dot{u}_y + x_{dj}\dot{u}_\theta = 0. \tag{6.19}$$

By normalizing the equations of motion (6.3), the critical system parameters are identified. The normalized system mass, stiffness, damping and SRS stiffness matrices are written as,

$$\mathbf{M} = \begin{bmatrix} 1 & 0 \\ 0 & \frac{1+\alpha^2}{12\alpha^2} \end{bmatrix} \tag{6.20}$$

$$\mathbf{K} = \omega_y^2 \begin{bmatrix} 1 & \bar{e}_x \\ \bar{e}_x & \bar{e}_x^2 + \frac{1+\alpha^2}{12\alpha^2}\Omega^2 \end{bmatrix} \tag{6.21}$$

$$\mathbf{C} = a_0 \begin{bmatrix} 1 & 0 \\ 0 & \frac{1+\alpha^2}{12\alpha^2} \end{bmatrix} + a_1\omega_y^2 \begin{bmatrix} 1 & \bar{e}_x \\ \bar{e}_x & \bar{e}_x^2 + \frac{1+\alpha^2}{12\alpha^2}\Omega^2 \end{bmatrix} \tag{6.22}$$

$$\mathbf{K}_d = \omega_{dy}^2 \begin{bmatrix} 1 & \bar{e}_{dx} \\ \bar{e}_{dx} & \bar{e}_{dx}^2 + \bar{\rho}_d^2 \end{bmatrix} \tag{6.23}$$

where $\alpha = a/b$ is the aspect ratio, $\omega_y = \sqrt{K_y/m}$ is the uncoupled translational natural frequency, $\Omega = \omega_\theta/\omega_y$ is the ratio of uncoupled torsional to translational natural frequency, $\omega_\theta = \sqrt{K_{\theta r}/m\rho^2}$ is the uncoupled torsional frequency, $\bar{e}_x = e_x/a$ is the normalized eccentricity, $\bar{e}_{dx} = e_{dx}/a$ is the normalized SRS eccentricity, and $\bar{\rho}_d = \rho_d/a$ is the normalized SRS radius of gyration. The preceding parameters have been used extensively in prior studies

and their physical interpretation discussed in earlier studies [41]. The mass, damping, and stiffness matrices shown in equations (6.20)-(6.22) are identical to prior studies which studied one-way asymmetric structures equipped with fluid viscous dampers [36, 68] or viscoelastic dampers [60]. For this study, equations (6.11)-(6.19) were introduced to account for the SRSs within the structure. Their development was analogous to that of using a fluid viscous damper [36], instead accounting for the addition stiffness provided by the SRSs.

Equations (6.20)-(6.23) show that there are two sets of parameters to consider. The first is for the uncontrolled system, which includes the aspect ratio, α, the uncoupled natural frequency ω_y, the normalized eccentricity, $\bar{e}_x$, and the ratio of the torsional to lateral natural the frequencies, Ω. The final parameter, Ω, has a useful physical interpretation, namely, for $\Omega < 1$, the structure is considered torsionally-flexible, while for $\Omega > 1$, the structure is torsionally-stiff. For $\Omega = 1$, both the uncoupled natural frequencies are equal, and the structure is considered strongly coupled.

The second set of parameters correspond to the semi-active resettable spring (SRS), which comprise of the uncoupled natural frequency of the SRSs, ω_{dy}, the normalized SRS eccentricity, $\bar{e}_{dx}$, and the normalized SRS radius of gyration, $\bar{\rho}_d$. The parameter $\bar{e}_{dx}$ indicates how the SRSs are distributed within the structure. A zero value indicates they are evenly distributed, while a negative or positive value indicates most of the additional stiffness is distributed toward the flexible or stiff edges, respectively (see Figure 6.2). Since the SRSs are only located within the plan of the structure, the limiting values of $\bar{e}_{dx}$ are -0.5 and 0.5. These values correspond to all of the SRSs located on the flexible or stiff edges. The SRS radius of gyration, $\bar{\rho}_d$, indicates how far apart the SRSs are located from the CSS. When all the SRSs are placed at the CSS, they provide zero resistance to rotation, since $K_{d\theta r} = 0$, while for positive values the SRSs provide resistance to rotation. Note that to study various cases, the locations of columns and SRSs in this study are not restricted to the structure edges.

6.4 Parametric study

6.4.1 System parameters

The values for $T_y = 2\pi/\omega_y$ were selected to range from 0.05-3 seconds to represent many low and mid-rise structures. The aspect ratio was selected as $\alpha = 2$. The normalized eccentricity was taken to be $\bar{e}_x = 0.2$, representing an eccentricity that is 20% of the horizontal plan dimension. The three cases of Ω to represent torsionally-flexible ($\Omega = 0.5$), strongly coupled ($\Omega = 1$), and torsionally-stiff ($\Omega = 2$) structures were also considered. The constants a_0 and a_1 were selected so that the damping ratios in the two modes were 5% of the critical damping, that is, $\zeta_1 = \zeta_2 = 0.05$.

The additional stiffness provided by the SRSs in the y-direction is taken to be equal to that of the uncontrolled structure, that is, $K_{dy} = K_y$. In terms of the brace-to-frame factor, BFS = 1. In Section 6.4.5, the effect the BFS factor has on the response of the structure is investigated for $T_y = 1$ and the three Ω values. Three values of the normalized SRS eccentricity are considered, $\bar{e}_{dx} = 0, 0.2, -0.2$. The first corresponds to one where the stiffness is equally distributed. The second and third values of $\bar{e}_{dx}$ are for when the normalized SRS eccentricity is equal in magnitude yet being either on the same or opposite sides of the normalized eccentricity $\bar{e}$. For each of the aforementioned three cases, the normalized SRS radius of gyration was fixed at $\bar{\rho}_d = 0.2$. In addition, several values of $\bar{\rho}_d$ are also considered to represent small, medium, and large layouts of the SRSs within the structure for a fixed normalized SRS eccentricity $\bar{e}_{dx} = -0.2$.

6.4.2 Response parameters

For asymmetric structures, larger deformations will be present at the edges, as opposed to the CM, since the peak lateral and rotational displacements may not occur simultaneously. Thus, the flexible and stiff edge responses are examined. To measure the effectiveness of using SRSs within an asymmetric structure, the following normalized response parameters for the flexible and stiff edges are introduced:

$$R_f = \frac{\text{Peak flexible edge displacement (controlled)}}{\text{Peak flexible edge displacement (uncontrolled)}} \tag{6.24}$$

$$R_s = \frac{\text{Peak stiff edge displacement (controlled)}}{\text{Peak stiff edge displacement (uncontrolled)}} \tag{6.25}$$

The controlled system refers to a structure with SRSs installed, whereas the uncontrolled refers to the corresponding structure without any SRSs. Since each set of ground motions (pulse and rock-site) comprise of 40 fault-normal ground motion records, the mean values of the normalized reduction parameters are compared and are denoted by $\bar{R}_f$ and $\bar{R}_s$. This study investigated both rock-site and pulse-like ground motions, the forthcoming figures show only the rock-site responses and the pulse-like responses were left out for brevity. Although the results are not explicitly shown, the coming discussion for rock-site responses also applies to pulse-like.

6.4.3 Semi-active resettable spring eccentricity

Figure 6.3 shows the normalized response parameters, $\bar{R}_f$ and $\bar{R}_s$, versus the structure period, T_y, for $\bar{e}_{dx} = 0, 0.2$ and -0.2. The normalized SRS radius of gyration for each case is $\bar{\rho}_d = 0.2$ and where $\Omega = 0.5$. Figures 6.4 and 6.5 show the same results for $\Omega = 1$ and

$\Omega = 2$, respectively. The results show that adding SRSs within an asymmetric structure can significantly reduce the edge displacements. Yet, the amount of reduction depends on the period of the structure and the normalized SRS eccentricity, $\bar{e}_{dx}$. There is a common trend among all the figures where for very stiff structures ($T_y < 0.15$ seconds) that the addition of the SRS provides considerably less reduction as compared with more flexible structures ($T_y > 0.15$ seconds). This can be due to the high column stiffness required to achieve such low fundamental periods where the additional stiffness provided by the SRSs has less of an impact on the reduction of the edge displacements.

For strongly coupled ($\Omega = 1$) and torsionally-stiff ($\Omega = 2$) system, the flexible edge has the largest reductions when $\bar{e}_{dx} = -0.2$ and the smallest reductions for $\bar{e}_{dx} = 0.2$. This trend in $\bar{e}_{dx}$ is reversed for the stiff edge. For laterally stiff structures, that is, when $T_y < 0.25$ seconds, the stiff edge displacements are larger than the uncontrolled asymmetric structure. For a torsionally-flexible system ($\Omega = 0.5$), a similar trend in $\bar{R}_f$ occurs for various $\bar{e}_{dx}$, yet for $\bar{R}_s$ with the symmetric distribution of SRSs ($\bar{e}_{dx} = 0$), leads to the largest reductions. Overall, increasing the normalized SRS eccentricity leads to larger reductions. For positive values of $\bar{e}_{dx}$, the stiff edge is most benefited, while for negative values of $\bar{e}_{dx}$ the flexible edge is. A similar result is found when incorporating fluid viscous dampers in asymmetric structures [36]. It is worth noting that as the structure becomes more torsionally stiff, the effects of the $\bar{e}_{dx}$ on reducing edge displacements becomes less pronounced.

6.4.4 Semi-active resettable spring radius of gyration

Figures 6.6-6.8 show the normalized reduction parameters, $\bar{R}_f$ and $\bar{R}_s$, versus the structure period, T_y, for increasing values of SRS radius of gyration $\bar{\rho}_d$. The normalized SRS eccentricity is fixed at $\bar{e}_{dx} = -0.2$. It is clear from observing the figures that larger values of $\bar{\rho}_d$ leads to greater reductions in the edge displacements. The effect of increasing $\bar{\rho}_d$ is most

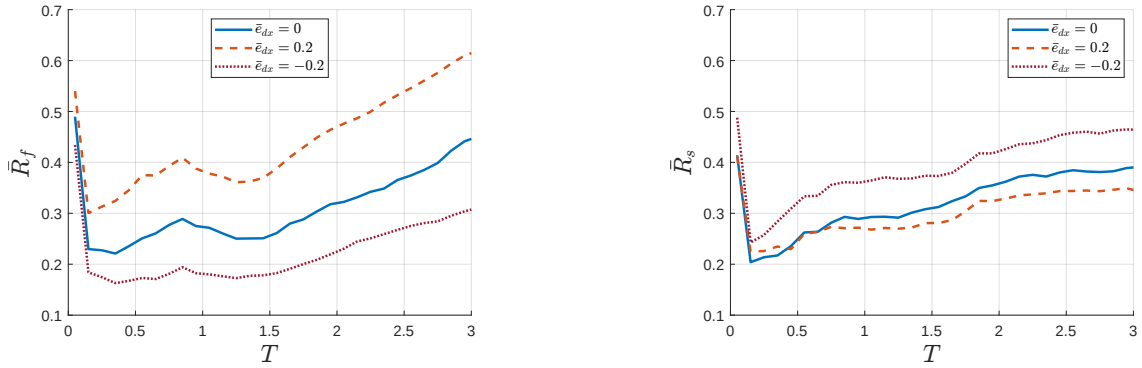

(a) (b)

Figure 6.3: Mean normalized flexible (a) and stiff (b) edge displacements for various $\bar{e}_{dx}$ values and $\Omega = 0.5$.

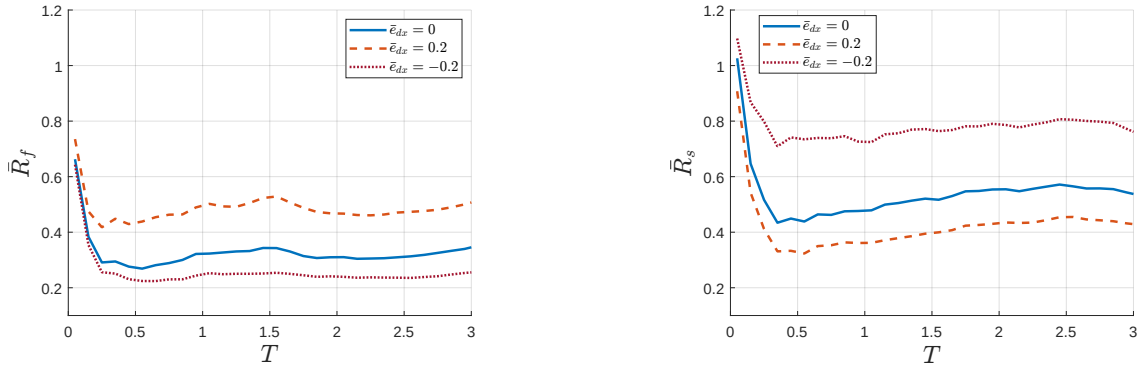

(a) (b)

Figure 6.4: Mean normalized flexible (a) and stiff (b) edge displacements for various $\bar{e}_{dx}$ values and $\Omega = 1$.

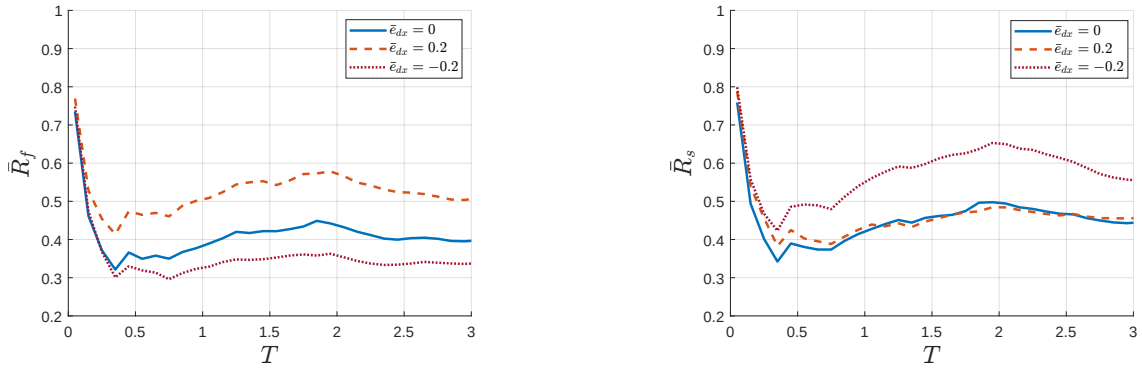

(a) (b)

Figure 6.5: Mean normalized flexible (a) and stiff (b) edge displacements for various $\bar{e}_{dx}$ values and $\Omega = 2$.

pronounced for torsionally-flexible structures ($\Omega = 0.5$) with decreasing effects as Ω is increased. When the structure is torsionally-stiff ($\Omega = 2$), the benefit to increasing $\bar{\rho}_d$ of the SRSs is negligible. This can partly be due the small rotations present whereby much of the structure motion is translational. When using SRSs along the y-direction, it may arise that

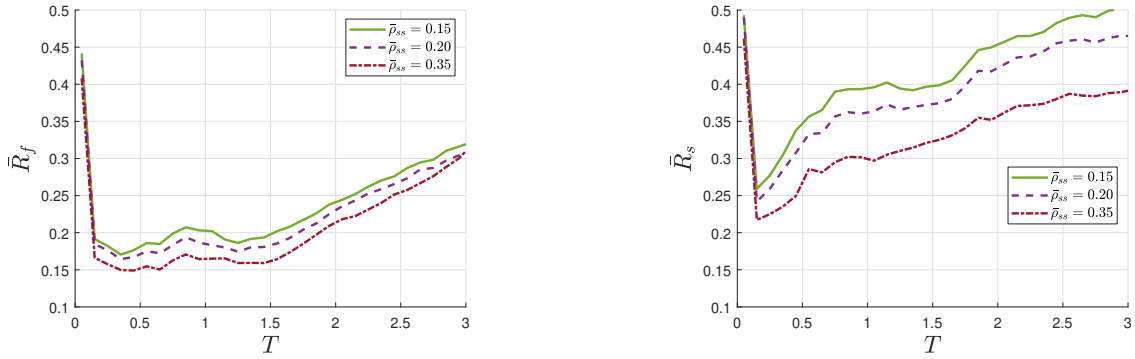

(a) (b)

Figure 6.6: Mean normalized flexible (a) and stiff (b) edge displacements for various $\bar{e}_{dx}$ values and $\Omega = 0.5$.

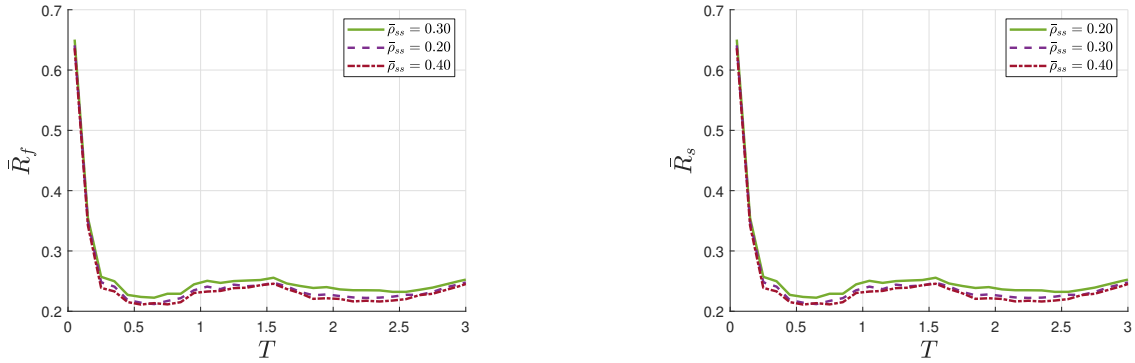

(a) (b)

Figure 6.7: Mean normalized flexible (a) and stiff (b) edge displacements for various $\bar{e}_{dx}$ values and $\Omega = 1$.

the SRS location is restricted by architectural demands. In this case, it will be beneficial to include SRSs along the direction perpendicular to the lateral direction. Although, adding these SRSs will not change $\bar{e}_{dx}$ it will lead to larger $\bar{\rho}_d$. When including SRSs in the perpendicular direction, care must be taken to not introduce eccentricities since the stiffness of the system is being changed. This can be accomplished by distributing the total additional

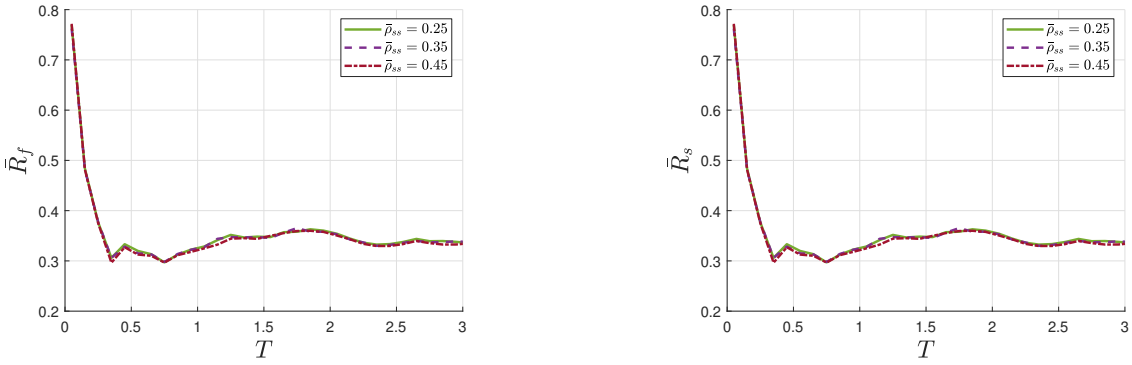

(a) (b)

Figure 6.8: Mean normalized flexible (a) and stiff (b) edge displacements for various $\bar{e}_{dx}$ values and $\Omega = 2$.

stiffness evenly between SRS on opposite side of the CM.

6.4.5 Brace-to-frame factor

Figures 6.9 shows the normalized reduction parameters $\bar{R}_f$ and $\bar{R}_s$, versus the brace-to-frame factor, BFS, for $\Omega = 1$. The figure shows results for $\bar{e}_{dx} = 0, 0.2, -0.2$ where $\bar{\rho}_{sd} = 0.2$ and $T_y = 1$ second. The results show that in increasing the BFS factor has a decreasing effect on the flexible and edge responses. A general trend occurs where much of the reduction in the response is due to the initial 20% additional stiffness provided by the SRSs, while increasing the BFS factor from 20% to 100% provides little additional improvement. A similar trend is also present for $\Omega = 0.5$ and 2. These results are similar to those found using fluid viscous dampers [36] where increasing the damping constant reduces the response.

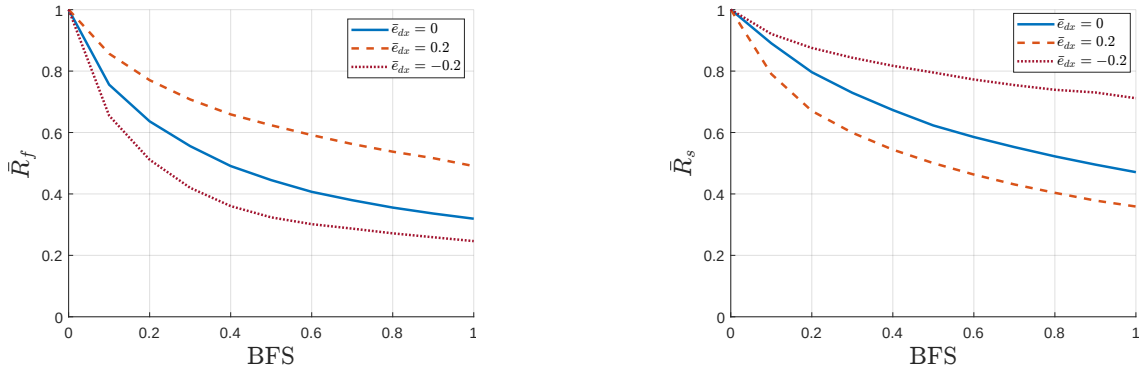

(a) (b)

Figure 6.9: Mean normalized flexible (a) and stiff (b) edge displacements for various $\bar{e}_{dx}$ values and $\Omega = 1$.

6.5 Towards an optimal distribution

6.5.1 Semi-active resettable spring eccentricity and radius of gyration

There is a general trend in the response of the flexible edge, namely, the largest reductions in the flexible edge occur when $\bar{e}_{dx}$ is negative. Increasing the SRS radius of gyration, $\bar{\rho}_d$, also decreases the flexible edge displacement. These findings are similar to those found when using fluid viscous dampers [36, 60]. Due to geometric constraints, both the normalized SRS eccentricity and SRS radius of gyration cannot simultaneously take their respective maximum values.

The stiffness distribution can be selected such that both the normalized SRS eccentricity and SRS radius of gyration are the largest possible under the column layout constraints. To demonstrate this process, consider two SRSs placed on opposite ends of the structure in the y-direction. Define the stiffness distribution, denoted by κ, to be the percent of stiffness provided to the stiff side SRS, and where $1 - \kappa$ is the percent provided by the flexible side SRS. For $\kappa = 0$, all the additional stiffness is provided by the flexible side SRS and where

$\kappa = 1$, the stiff side SRS provides all the additional stiffness. By varying κ, both the SRS eccentricity and SRS radius of gyration can be changed.

To determine the optimal stiffness distribution, one can plot $\bar{e}_{dx}^2$ and $\bar{\rho}_d^2$ against κ. The squared quantities are considered since the normalized SRS eccentricity is negative, while the SRS radius of gyration can only take on positive values. Figures 6.10 show the two

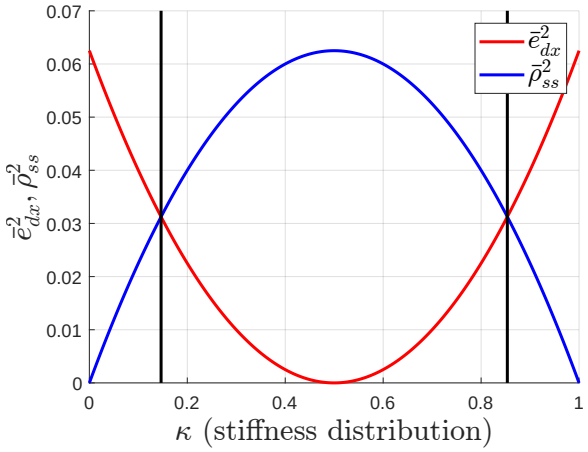

Figure 6.10: Plot of $\bar{e}_{dx}^2$ (red) and $\bar{\rho}_d^2$ (blue) versus the stiffness distribution κ.

points of intersection of $\bar{e}_{dx}^2$ and $\bar{\rho}_d^2$. Values of $\kappa < 0.5$ corresponds to negative normalized SRS eccentricity whereas $\kappa > 0.5$ corresponds to positive eccentricity, and $\kappa = 0$ for when $\bar{e}_{dx} = 0$. For two SRSs, one can show analytically (see Sections 6.5.2) that the two intersection points occur at $\kappa = (1 \pm \sqrt{0.5})/2$ for any Ω. Using this distribution value leads to $\bar{e}_{dx}^* = -0.177$ for $\Omega = 0.5$, $\bar{e}_{dx}^* = -0.255$ for $\Omega = 1$, and $\bar{e}_{dx}^* = -0.354$ for $\Omega = 2$. The flexible and stiff edge displacement responses using this strategy are shown in Figures 6.11-6.13. Based on these results, selecting the normalized SRS eccentricity to be $\bar{e}_{dx}$ leads to moderately better performance for $\Omega = 1$ and $\Omega = 2$, while being slightly worse for $\Omega = 0.5$. This approach significantly reduces the flexible edge displacements, yet it comes at the cost of larger displacements for the stiff edge.

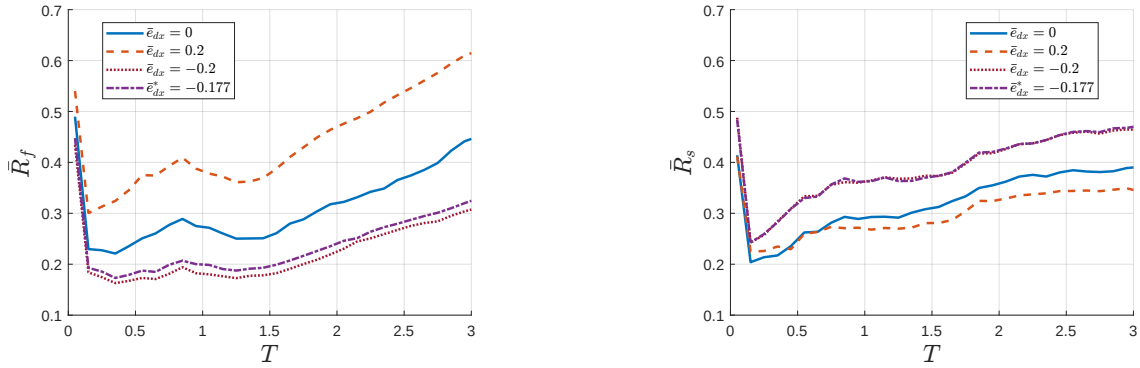

(a) (b)

Figure 6.11: Mean normalized flexible (a) and stiff (b) edge displacements for various $\bar{e}_{dx}$ values and $\Omega = 0.5$

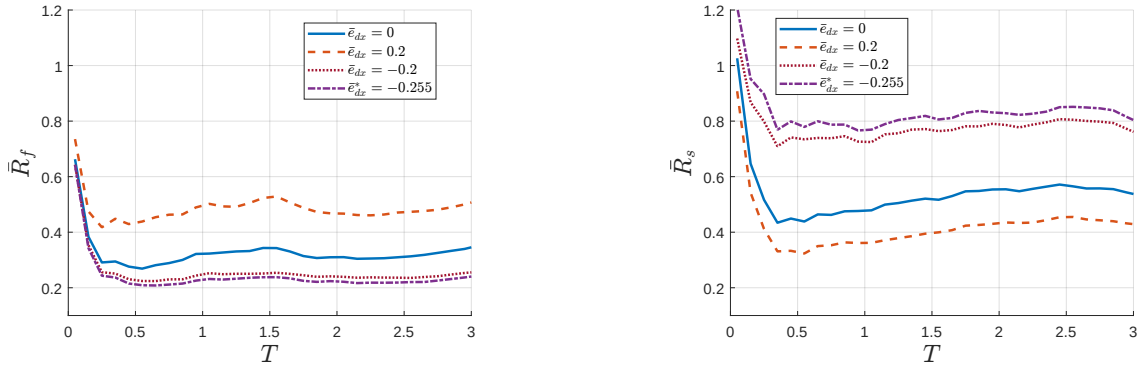

(a) (b)

Figure 6.12: Mean normalized flexible (a) and stiff (b) edge displacements for various $\bar{e}_{dx}$ values and $\Omega = 1$

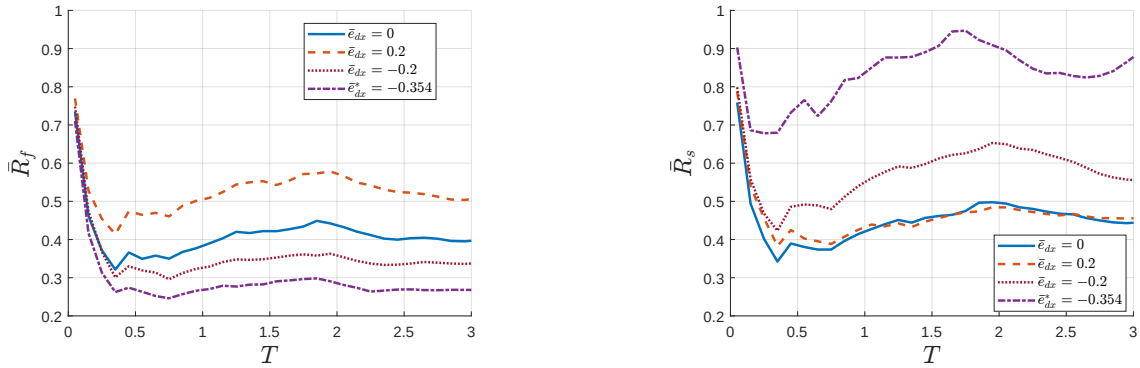

(a) (b)

Figure 6.13: Mean normalized flexible (a) and stiff (b) edge displacements for various $\bar{e}_{dx}$ values and $\Omega = 2$

6.5.2 Establishing $\kappa = (1 \pm \sqrt{0.5})/2$

Consider the structure shown in Figure 4.8b where two SRSs are equal distance from the CM, but on opposite sides of the structure. The SRSs are placed only in the y-direction. Let κ be the stiffness distribution of the available stiffness K_{dy}. For this case, take $K_{dy} = K_y$, that is, where BFS = 1. Then $k_{d1} = (1-\kappa)K_y$ and $k_{d2} = \kappa K_y$. The normalized SRS eccentricity is now

$$\begin{aligned} \bar{e}_{dx} = \frac{e_{dx}}{a} &= \sum_j k_{dyj} x_{dj} \\ &= \frac{1}{aK_y}\left(-(1-\kappa)K_y(\gamma a) + \kappa K_y(\gamma a)\right) \end{aligned} \tag{6.26}$$

where the factor γ is in $(0, 0.5]$. Simplifying the above equation gives

$$\bar{e}_{dx} = \gamma(2\kappa - 1) \tag{6.27}$$

Similarly, the normalized SRS radius of gyration is given by

$$\begin{aligned} \bar{\rho}_d^2 = \left(\frac{\rho}{a}\right)^2 &= \frac{K_{dt} - e_{dx}^2 K_y}{K_y}\frac{1}{a^2} \\ &= \frac{(1-\kappa)K_y(\gamma a)^2 + \kappa K_y(\gamma a)^2 - e_{dx}K_y}{K_y}\frac{1}{a^2} \\ &= \gamma^2 - \bar{e}_{dx}^2 \\ &= \gamma^2\left(1 - (2\kappa - 1)^2\right) \end{aligned} \tag{6.28}$$

Setting $\bar{e}_{dx}^2 = \bar{\rho}_d^2$ gives $\kappa = (1 \pm \sqrt{0.5})/2$.

6.5.3 N-number of SRSs along the lateral direction

Consider n SRSs placed along the y-direction with stiffness values defined by

$$\begin{aligned} k_{d1} &= \kappa_1 K_y \\ k_{d2} &= \kappa_2 K_y \\ &\vdots \\ k_{dn} &= \kappa_n K_y \end{aligned} \tag{6.29}$$

where $\sum \kappa_i = \text{BFS}$ and $K_{dy} = \text{BFS}K_y$. Then we can write the normalized SRS eccentricity as

$$\bar{e}_{dx} = \frac{1}{aK_y}\left(\kappa_1 K_y \gamma_1 a + \cdots + \kappa_n K_y \gamma_n a\right) = \sum \kappa_i \gamma_i \tag{6.30}$$

where $\gamma_i \in [-0.5, 0.5]$ are provided. The normalized SRS radius of gyration is also given by

$$\begin{aligned} \bar{\rho}_d^2 &= \frac{1}{a^2}\frac{\kappa_1 K_y (\gamma_1 a)^2 + \cdots + \alpha_n K_y (\gamma_n a)^2 - e_{dx}^2 K_y}{K_y} \\ &= \sum \kappa_i \gamma_i^2 - \left(\sum \kappa_i \gamma_i\right)^2. \end{aligned} \tag{6.31}$$

Setting $\bar{e}_{dx}^2 = \bar{\rho}_d^2$ leads to following equation in $\kappa_1, \ldots, \kappa_n$,

$$\sum \kappa_i \gamma_i^2 - 2\left(\sum \kappa_i \gamma_i\right)^2 = 0 \tag{6.32}$$

Solving for the roots $\kappa_1, \ldots, \kappa_n$ provides the optimal distribution of stiffness given each SRS placement location γ_i. It is worth noting that since we have an underdetermined system, i.e., 1 equation with $n-1$ unknowns, there may be several or no choices of κ_i given $\gamma_1, \ldots, \gamma_n$ that satisfy the above equation. This means that based on layout of the columns and SRSs the finding the optimal distribution from finding the intersection of $\bar{e}_{dx}^2$ and $\bar{\rho}_d^2$ is not unique or may not be possible.

6.5.4 Modal characteristics

It has been shown in prior work that the flexible edge modal displacement is largest in the first mode, while the stiff edge modal displacement is largest in the second mode [68]. Due to the eccentricity, both the lateral and rotation components are coupled. In fact, increasing the eccentricity leads to a stronger degree of coupling [60]. Since the SRS provides additional stiffness to the system, the mode shapes can be altered. The concept of mode shapes can be used due to the homogeneity [46] property of these class of nonlinear devices, that is, the additional stiffness is continuously provided. For a symmetric system, the flexible and stiff edges would have equal displacement since no rotation occurs. With this in mind, the stiffness provided by the SRS is selected such that the first modal displacements of the stiff and flexible edges are equal. By varying the stiffness distribution, the normalized SRS eccentricity, $\bar{e}_{dx}$, is changed. Figure 6.14 shows the modal displacements of the flexible and stiff edges for $\Omega = 0.5, 1$, and 2. For each system, the intersection of the modal displacements

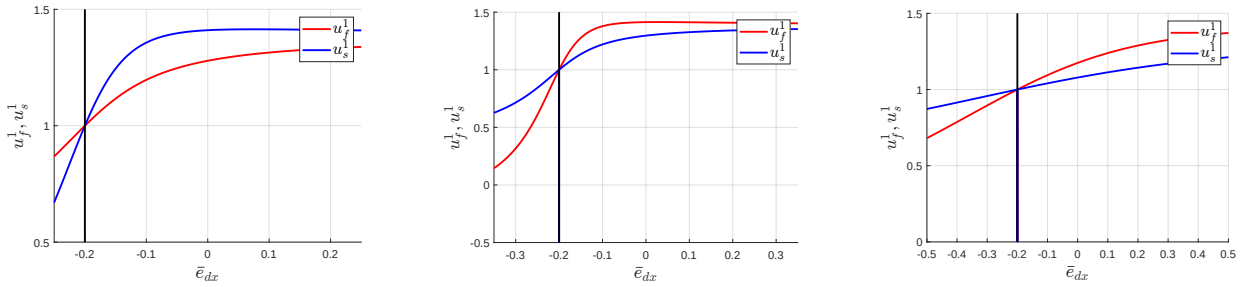

(a) (b) (c)

Figure 6.14: Modal displacements of flexible and stiff edges for (a) $\Omega = 0.5$ (torsionally flexible), (b) $\Omega = 1$ (strongly coupled), and (c) $\Omega = 2$ (torsionally stiff).

of the flexible and stiff edges occurs at $\bar{e}_{dx} = -0.2$. This result should not come as a surprise, since it is precisely the normalized SRS eccentricity which decouples the stiffness matrix (see equations (6.3), (6.21), and (6.23)). The results shown prior that this choice in normalized SRS eccentricity leads to significant reductions in both the flexible and stiff edges for the three cases of Ω.

6.6 Limitations and guidelines

In the prior sections, two approaches to determine the optimal distribution of SRSs were proposed. Both approaches lead to similar results for the flexible edge displacements. Yet, each approach has limitations. For the first method which selected the point of intersection of the curves $\bar{e}_{dx}^2$ and $\bar{\rho}_d^2$ it was shown that an optimal stiffness distributed was found to be $\kappa = (1 - \sqrt{0.5})/2$ for the stiff side SRS and $1 - \kappa$ for the flexible side SRS. Although this method did produce satisfactory results, the approach may become cumbersome or impossible when the number of SRS increases. It can be shown (see Section 6.5.3), that for n number of SRSs in the y-direction, to solve for the optimal stiffness distribution requires solving for the roots of

$$\sum \kappa_i \gamma_i^2 - 2\left(\sum \kappa_i \gamma_i\right)^2 = 0 \tag{6.33}$$

where γ_i is between $[-0.5, 0.5]$ and $\gamma_i a$ is the distance the i^{th} SRS is from the CM. Note that the roots of the equation are κ_i where $\sum \kappa_i = 1$. The above equation can be treated as an underdetermined system of $n - 1$ equations, which can have several or no solutions. Thus, incorporating several SRSs in the direction of interest can pose difficulties if the architectural restrictions (i.e., the choices of γ_i) prevent a feasible distribution of stiffness.

The second method instead considered the modal displacement of the edges. The idea of mode shapes can only be considered for elastic structures. For this approach, the first mode flexible and stiff edge displacements were made equal by varying the normalized SRS eccentricity $\bar{e}_{dx}$. It was found that this occurred when $\bar{e}_{dx} = -0.2$. It was stated earlier that this choice of $\bar{e}_{dx}$ leads to decoupling the stiffness matrix of the system, namely, $\mathbf{K} + \mathbf{K}_{dy}$, which occurs because $\omega_y^2 \bar{e}_x = \omega_{dy}^2 \bar{e}_{dx}$. This result was also a consequence on the brace-to-frame (BFS) factor equaling one, since $\omega_{dy}^2 = \text{BFS}\omega_y^2$. Note that the selection of the BFS factor and $\bar{e}_{dx}$ is not unique, and any combination will be sufficient as long as the product

equals (or is close to) $\bar{e}_x$. Note that $\bar{e}_{dx} > -0.5$ otherwise all the SRSs would be concentrated on the flexible side, leading to detrimental effects in the stiff edge displacements. Moreover, the closer $\bar{e}_{dx}$ is to zero and/or for larger eccentricities $\bar{e}_x$, leads to large BFS factors to decouple the stiffness matrices. Thus, if limitations exist on the bracing system housing the SRS, the uncontrolled structure eccentricity may be large enough such that an optimal value of $\bar{e}_{dx}$ cannot be selected. If there is no restriction the sizing of the bracing system, then no matter the degree of eccentricity of the structure, a optimal distribution of stiffness can be achieved.

Based on the prior discussion, some guidelines are as follows: (1) use as few SRSs as allowed in the lateral direction of interest, (2) select the $\bar{e}_{dx}$ to be equal to, and opposite the side of the normalized eccentricity, $\bar{e}_x$, (3) if proper selection of $\bar{e}_{dx}$ is not possible, select the largest value of $\bar{e}_{dx}$ possible and consider using SRSs in the x-direction, since increasing the normalized SRS radius of gyration reduces edge displacements.

6.7 Summary

In this investigation several parameters were identified which relate to the added stiffness provided by the SRS and the stiffness distribution. From these, the normalized SRS eccentricity and normalized SRS radius of gyration played a key role in the response of the flexible edge displacements. The effects of these parameters on the edge displacements were investigated. It was shown that including SRSs in a one-way asymmetric structure leads to reduced edge displacements. Significant reductions were possible, but depend on the distribution of the SRSs.

Two approaches for determining the optimal distribution of semi-active resettable springs (SRSs) in a one-way asymmetric structure were proposed. The first approach was to de-

termine the maximum value the normalized SRS eccentricity and normalized SRS radius of gyration can take on accounting for geometric and column layout constraints. The second was based on modal analysis. Both approaches lead to finding an appropriate distribution of SRSs within the structure. However, each approach had its own limitations. The results of this study are summarized as follows:

1. The addition of the SRSs in an elastic one-way asymmetric structure provided upwards to 80% reductions in edge displacements for structures that are torsionally-flexible, strongly coupled, and torsionally-stiff with fundamental periods $T_y > 0.15$ seconds. For laterally-stiff structures ($T_y < 0.15$ seconds) the reductions are moderate.

2. Reductions in the flexible edge occur when the normalized SRS eccentricity is on the opposite side of the normalized eccentricity, and vice versa for the stiff edge. Increasing the normalized SRS eccentricity leads to further reductions in the edge displacement.

3. Distributing the SRSs such that they are farthest away from the CSS leads to greater reductions. In other words, increasing the normalized SRS radius of gyration leads to larger reductions in the edge displacements, yet the improvement is not as pronounced for strongly coupled and torsionally-stiff systems. For one-way asymmetric structures, additional reductions can be achieved by incorporating SRSs in the direction perpendicular to the lateral motion.

4. The first approach to distribute the SRSs was based on the observation that increasing the normalized SRS eccentricity or normalized SRS radius of gyration leads to larger reductions in edge displacement. Due to column layouts restrictions, $\bar{e}_{dx}$ and $\bar{\rho}_d$ cannot both take on their respective maximum values simultaneously. By introducing the stiffness distribution κ, it was shown that the intersection of the curves $\bar{e}_{dx}^2$ and $\bar{\rho}_d^2$ leads to the maximum value both parameters can be simultaneously. This approach leads to the greatest reductions in the flexible edge displacement, yet it comes at

significantly increasing the stiff edge displacement. The results of this approach are akin to that found for fluid viscous dampers [36].

5. The second approach used modal analysis. The additional stiffness provided by the SRSs allowed altering the mode shapes of the system. The stiffness distribution was selected so that the modal displacements of the flexible and stiff edges were equal in the first mode. This approach led to decoupling the stiffness matrix of the system. Although this approach performed slightly worse in reducing the flexible edge displacement, it also provides considerable reductions in reducing the stiff edge displacement. In other words, this approach leads to an overall reduction in both edges as opposed to only the flexible edge.

Chapter 7

Conclusion and Future Work

7.1 Summary of Thesis

In this thesis, existing control devices were implemented in a variety of settings to provide further reduction of the response of civil structures. Two sets of ground motion having broad-band and pulse-like characteristics were used as inputs. For a single-story structure, a semi-active resettable spring (SRS) and inerter were used within a TMD system and were called semi-active tuned mass damper inerter (SATMDI) and tuned mass damper inerter (TMDI). The tuning strategy for the TMDI used closed-form equations based on having a white noise input. The results showed that for large inertance values, the SATMDI provides moderate reduction in the displacement response, while providing significant reduction in the acceleration and stroke responses. It was shown that a SATMDI system whereby the inerter replaced the TMD mass entirely provided the highest performance among the three mass ratios selected.

Base-isolation enhancement of a single-story structure was also presented. A novel configuration of a SRS and TMD was proposed. In this new configuration, the SRS grounds the TMD

mass instead of being parallel to the spring and damper. This new configuration was called a non-traditional semi-active tuned mass damper (NT-SATMD) and was compared against a traditional (T-TMD) and non-traditional (NT-TMD) tuned mass dampers. The NT-TMD configuration is where the damper grounds the TMD mass instead of being parallel to the spring. An ad-hoc tuning strategy was proposed for the NT-SATMD which combined tuning strategies from the T-TMD and NT-TMD systems. The results of the study showed that the NT-SATMD provided equal or better performance in reducing the base and superstructure displacements for a significantly smaller mass ratio. Yet, the NT-SATMD increased the relative displacement between $1-5\%$ yet due to the base-isolation system (BIS) providing significant reductions, this increase was deemed acceptable. The acceleration responses were mildly improved using the NT-SATMD, yet were still inferior to the NT-TMD under pulse-like ground motions.

Multi-story structures equipped with a TMDI and SATMDI were also considered. For a TMDI system, an alternative tuning strategy was proposed which involved selecting the stiffness and damping of the TMDI system based on the first and second modes natural frequencies and damping ratios. The alternative tuning strategy was compared with one based on white noise input. The system considered was a three-story structure with a fundamental period of $T = 0.5$ seconds and having a first mode critical damping ratio of $\zeta_1 = 0.02$. The results showed that the alternative tuning strategy provides significant improvement in reducing the top-story displacement and acceleration. For the lower stories, smaller inertance values produced better results as opposed to larger inertance. In addition, the alternative tuning strategy provided better performance for small mass ratios as compared with the white noise tuning strategy. As for the stroke response, it was shown that for small mass ratios a significant reduction in the stroke was achieved across all inertance values. Yet, increasing the mass ratio led to worse performance.

Asymmetric structures equipped with SRSs were also considered in this study. The structure

considered was single-story structure having a stiffness eccentricity producing a flexible and stiff edge. A parametric study over a wide range of structure periods was considered. In addition, torsionally stiff, flexible, and strongly coupled structures were also studied. Two strategies for determining the optimal placement of the SRSs were proposed, both leading to roughly the same performance. The first approach found that selecting a SRS distribution so that the SRS eccentricity was opposite in sign to the structure's eccentricity and largest as possible in magnitude. In addition, by increasing the SRS radius of gyration, better performance was found. These two quantities cannot both take on simultaneously maximum values due to geometric constraints. The optimal stiffness distribution was chosen that produced the largest possible SRS eccentricity and SRS radius of gyration. An analytical result was found for two SRSs in a single directions. The second approach led to decoupling the stiffness matrix by selecting the SRS stiffness distribution so that the modal displacements of the stiff and flexible edges were equal. This lead to selecting a SRS eccentricity that was equal in magnitude to the structure's eccentricity, but opposite in sign. Guidelines and limitations on the selection of the stiffness distribution were also provided for design purposes.

7.2 Further work and Other Applications

7.2.1 Further Explore Alternative Tuning Strategy for TMDI

An alternative tuning strategy for a TMDI system was introduced which showed significant reductions in the top-story displacement and acceleration responses. It was found that smaller mass ratios provided better performance as compared with the TMDI using the white noise tuning strategy. In addition, for smaller mass ratios, the stroke was also considerably reduced. For the investigation shown prior, only a single three-story structure was studied. It will be beneficial to investigate how the alternative tuning strategy will perform over a

wide range of fundamental periods. Moreover, the modal properties and how they affect the tuning strategy will also been investigated. This is inspired by the work done by Sadek et al. [87] where the mode shape played a role in the selection of the frequency and critical damping ratio of the TMD. Closed-form equations similar to those found in the prior study will be sought for. This may or may not be possible depending on how the frequency and critical damping ratios will change shape as the modal characteristics of the structure change.

7.2.2 Equipment or Artifact Isolation

Damage to delicate scientific equipment or historical artifacts in structures has been observed in many cases during severe ground motions. This type of damage can cause considerable monetary costs or irreparable loss to historical and artistic heritage. For this reason, there has been increased attention in recent years to mitigate equipment and artifact damage under seismic events. Previous studies [108] have implemented base isolation and active control to mitigate (or eliminate) damage to artifacts with promising results. Yet, due to the high-power requirements of active control, and the potential for power outages during seismic events, this control strategy may not be sufficient or practical. To address this issue, we will investigate the use of a SRS within base isolation to reduce damage to equipment or artifacts under seismic events. We suspect to have promising results, since the use of SRS within a BIS system has been shown to be effective in reducing the response of buildings. Preliminary analysis has been performed on a four-story structure where the equipment is isolated on the first floor. An SRS device is placed in series to the parallel spring and damper representing the stiffness and damping provided by the BIS. Figure 7.1 shows a schematic of the system analyzed. The control laws considered were the 1&3, 2&4, and 1-4, which were introduced in Section 2.2.1. For this preliminary analysis, the SAC Phase 2 Project [95] ground motion suites were used. Each suite has ten different histories (five in each orthogonal direction) of recorded and generated ground motions. The suites were selected to

represent the magnitude and distance characteristics of the seismic hazard in Los Angeles, CA. The first suite (low) represents ground motions having a 50% probability of exceedance in 50 years, the second suite (medium) represents a 10% probability of exceedance in 50 years, and the third suite (high) a 2% probability of exceedance in 50 years. This study only evaluated fault-normal ground motions.

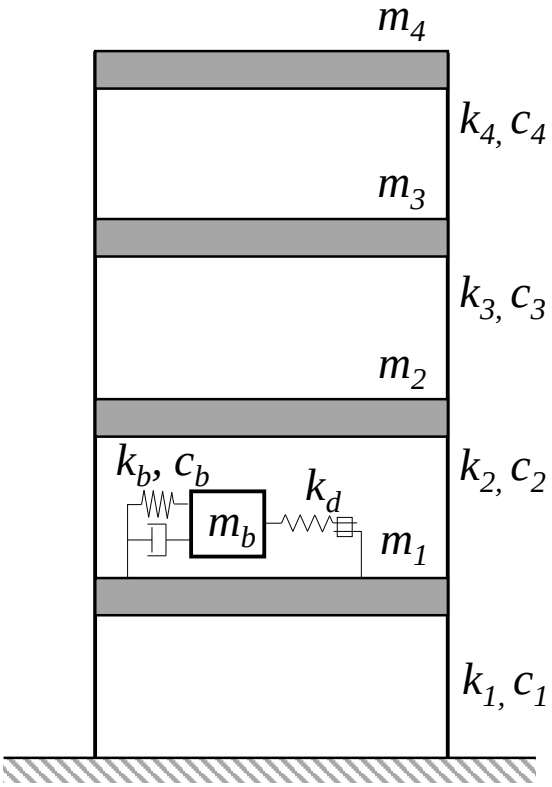

Figure 7.1: Four-story structure with equipment isolated using a BIS and SRS device.

Figures 7.2, 7.3, and 7.4 show the displacement and absolute acceleration normalized by the corresponding BIS responses over all twenty-five ground motions using control laws 1-4, 2&4, and 1&3, respectively. The horizontal axis represents the percent stiffness provided by the SRS device. To avoid excessive outliers, the median values were considered. Based on these preliminary results, control law 1-4 (Figure 7.2) provides the greatest amount of displacement reduction but provide negligible absolute acceleration reduction. For equipment isolation, it is the absolute acceleration which is of more concern [32]. When considering control

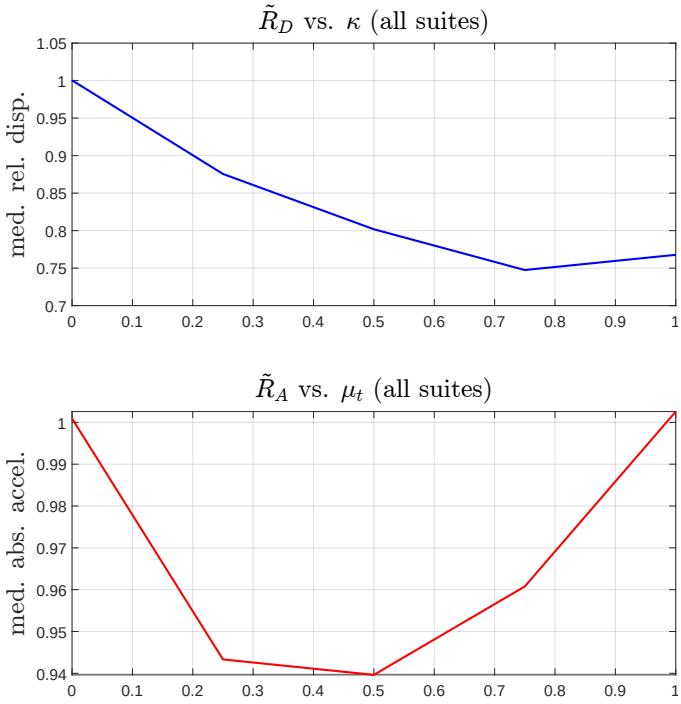

Figure 7.2: Median reduction factors for the displacement and absolute maximum acceleration under all ground motion suites using control law 1-4.

law 2&4 (Figure 7.3) there is considerable reduction in the acceleration, yet nearly none for displacement. When the SRS provides all the stiffness of the BIS system, it causes an significant increase in the displacement response and thus should be avoided. For control law 1&3 (Figure 7.4), there is more of balance between the displacement and absolute acceleration reduction. In fact, the greatest reductions occur when the SRS replaces the the BIS stiffness.

Based on these preliminary findings, the alternative control laws for the SRS when incorporated in the BIS can yield large reductions in the displace or absolute acceleration. A more thorough parametric study is warranted to gain insight into the best performance using the various control laws. Moreover, hazard analysis can be performed based on the SAC 2 ground motions used. A reliability analysis can also be done to study how variation in the stiffness, damping, or stiffness percent can affect the performance of the isolation system.

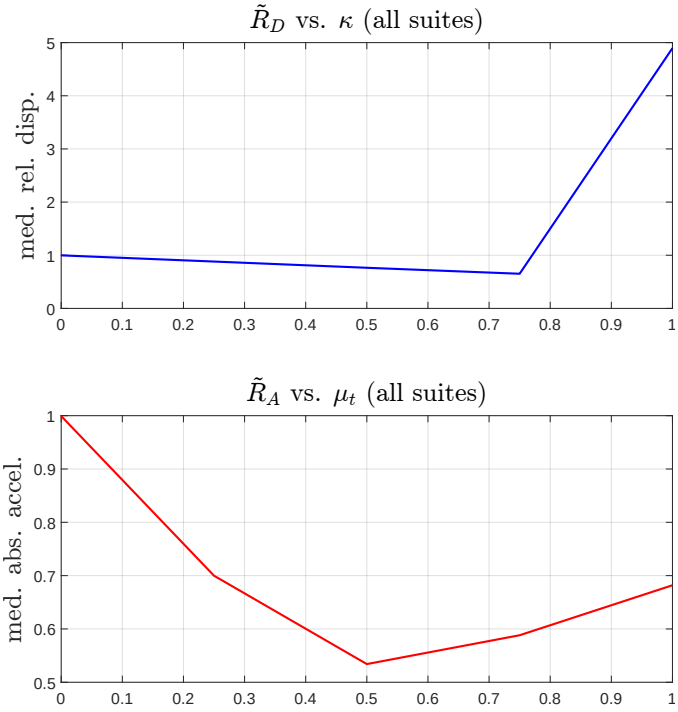

Figure 7.3: Median reduction factors for the displacement and absolute maximum acceleration under all ground motion suites using control law 2&4.

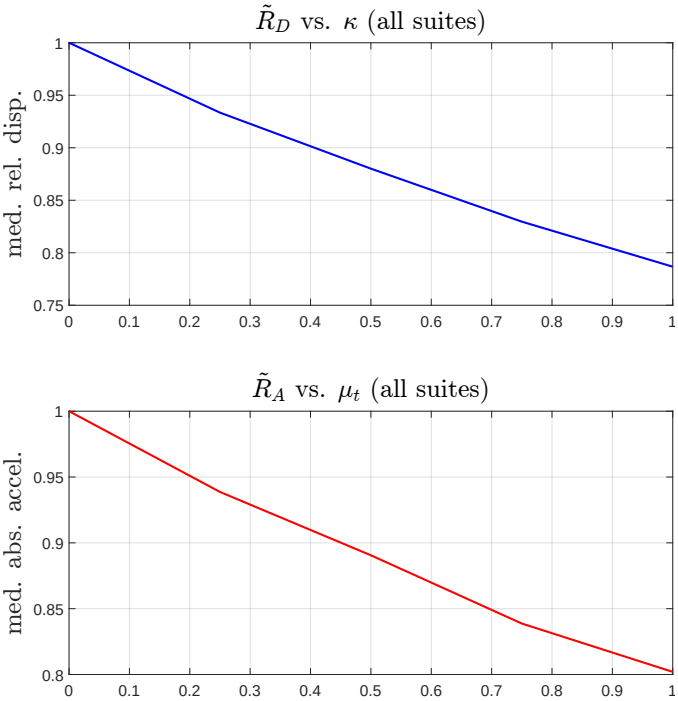

Figure 7.4: Median reduction factors for the displacement and absolute maximum acceleration under all ground motion suites using control law 1&3.

Bibliography

[1] Z. Akbay and H. Aktan. Intelligent energy dissipation devices. In *Proc. of the Fourth*, 1990.

[2] Z. Akbay and H. M. Aktan. Actively regulated friction slip devices. In *Proc. of the Fourth*, 1991.

[3] M. AlHamaydeh, M. A. Jaradat, M. Serry, L. Sawaqed, and K. S. Hatamleh. Structural control of mr-dampers with genetic algorithm-optimized quasi-bang-bang controller. In *2017 7th International Conference on Modeling, Simulation, and Applied Optimization (ICMSAO)*, pages 1–6, 2017.

[4] S. A. Anagnostopoulos and K. V. Spiliopoulos. An investigation of earthquake induced pounding between adjacent buildings. *Earthquake Engineering & Structural Dynamics*, 21(4):289–302, 1992.

[5] J. Arrigan, V. Pakrashi, B. Basu, and S. Nagarajaiah. Control of flapwise vibrations in wind turbine blades using semi-active tuned mass dampers. *Structural Control and Health Monitoring*, 18(8):840–851, 2011.

[6] T. Asai, K. Ikago, and Y. Araki. Outrigger tuned viscous mass damping system for high-rise buildings subject to earthquake loadings. In *In: 6AESE/11ANCRiSST joint conference, Urbana, IL*, 2015.

[7] H. Bachmann, W. J. Ammann, F. Deischl, J. Eisenmann, I. Floegl, G. H. Hirsch, G. K. Klein, G. J. Lande, O. Mahrenholtz, H. G. Natke, et al. *Vibration problems in structures: practical guidelines*. Birkhäuser, 2012.

[8] J. W. Baker. Quantitative Classification of Near-Fault Ground Motions Using Wavelet Analysis. *Bulletin of the Seismological Society of America*, 97(5):1486–1501, 10 2007.

[9] S. V. Bakre and R. S. Jangid. Optimum parameters of tuned mass damper for damped main system. *Structural Control and Health Monitoring*, 14(3):448–470, 2007.

[10] J. E. Bobrow and F. Jabbari. A new approach to shock isolation and vibration suppression using resettable actuators. *ASME J. Dyn. Syst., Meas., Control*, pages 570–573, 2000.

[11] J. E. Bobrow, F. Jabbari, and K. Thai. An active truss element and control law for vibration suppression. *Smart Materials and Structures*, 4(4):264–269, dec 1995.

[12] B. A. Bolt. *The Nature of Earthquake Ground Motion*, pages 1–45. Springer US, Boston, MA, 2001.

[13] J. E. Brock. A Note on the Damped Vibration Absorber. *Journal of Applied Mechanics*, 13(4):A284–, 03 1946.

[14] California Safety Commission. *Findings and Recommendations from the Ridgecrest Earthquake Sequence of July 2019*. California Safety Commission, 2019.

[15] B. Carpani. Base isolation from a historical perspective. 01 2017.

[16] C. M. Casado, I. M. Díaz, J. de Sebastián, A. V. Poncela, and A. Lorenzana. Implementation of passive and active vibration control on an in-service footbridge. *Structural Control and Health Monitoring*, 20(1):70–87, 2013.

[17] J. C. Chang and T. T. Soong. Structural control using active tuned mass dampers. *Journal of the Engineering Mechanics Division*, 106(6):1091–1098, 1980.

[18] L. Chen, Y. Shen, Y. Liu, X. Zhang, and X. Yang. Optimized modeling and experiment test of a fluid inerter. *Journal of Vibroengineering*, 18(5):2789–2800, aug 2016.

[19] M.-H. Chey, J. G. Chase, J. B. Mander, and A. J. Carr. Semi-active tuned mass damper building systems: Design. *Earthquake Engineering & Structural Dynamics*, 39(2):119–139, 2010.

[20] K.-M. Choi, S.-W. Cho, H.-J. Jung, and I.-W. Lee. Semi-active fuzzy control for seismic response reduction using magnetorheological dampers. *Earthquake engineering & structural dynamics*, 33(6):723–736, 2004.

[21] A. Coburn and R. Spence. *Earthquake Protection*. John Wiley and Sons, Chichester, 2003.

[22] A. W. Coburn, R. J. Spence, and A. Pomonis. Factors determining human casualty levels in earthquakes: mortality prediction in building collapse. In *Proceedings of the tenth world conference on earthquake engineering*, volume 10, pages 5989–5994. Balkema Rotterdam, 1992.

[23] W. Cousins, W. Robinson, and G. McVerry. Recent developments in devices for seismic isolation. *Bulletin of the New Zealand Society for Earthquake Engineering*, 25(3):167–174, 1992.

[24] M. Cutfield, K. Ryan, and Q. Ma. A case study cost-benefit analysis on the use of base isolation in a low-rise office building. *NCEE 2014 - 10th U.S. National Conference on Earthquake Engineering: Frontiers of Earthquake Engineering*, 01 2014.

[25] D. De Domenico, P. Deastra, G. Ricciardi, N. D. Sims, and D. J. Wagg. Novel fluid inerter based tuned mass dampers for optimised structural control of base-isolated buildings. *Journal of the Franklin Institute*, 356(14):7626–7649, 2019. Special Issue on Inerter-based Systems.

[26] D. De Domenico and G. Ricciardi. Optimal design and seismic performance of tuned mass damper inerter (tmdi) for structures with nonlinear base isolation systems. *Earthquake Engineering & Structural Dynamics*, 47(12):2539–2560, 2018.

[27] J. Den Hartog. *Mechanical Vibrations*. Civil, Mechanical and Other Engineering Series. Dover Publications, 1985.

[28] S. J. Dyke, B. F. Spencer, M. K. Sain, and J. D. Carlson. Modeling and control of magnetorheological dampers for seismic response reduction. *Smart Materials and Structures*, 5(5):565–575, oct 1996.

[29] A. Elnashai and L. Sarno. *Fundamentals of Earthquake Engineering From Source to Fragility*. John Wiley and Sons, Chichester, 2015.

[30] M. Fardadi, F. Jabbari, and F. Zareian. Effectiveness of resettable energy dissipating devices in seismic response modification of elastic sdof systems. *Earthquake Engineering & Structural Dynamics*, 45(15):2571–2588, 2016.

[31] H. Frahm. Device for damping vibration bodies, 1911. U.S. patent No.989958.

[32] H. P. Gavin and A. Zaicenco. Performance and reliability of semi-active equipment isolation. *Journal of Sound and Vibration*, 306(1):74–90, 2007.

[33] A. Giaralis and L. Marian. Use of inerter devices for weight reduction of tuned mass-dampers for seismic protection of multi-story building: the Tuned Mass-Damper-Interter (TMDI). In G. Park, editor, *Active and Passive Smart Structures and Integrated Systems 2016*, volume 9799, pages 415 – 424. International Society for Optics and Photonics, SPIE, 2016.

[34] A. Giaralis and L. Marian. Use of inerter devices for weight reduction of tuned mass-dampers for seismic protection of multi-story building: the tuned mass-damper-interter (tmdi). page 97991G, 04 2016.

[35] A. Giaralis and F. Petrini. Wind-induced vibration mitigation in tall buildings using the tuned mass-damper-inerter. *Journal of Structural Engineering*, 143(9):04017127, 2017.

[36] R. K. Goel. Effects of supplemental viscous damping on seismic response of asymmetric-plan systems. *Earthquake engineering & structural dynamics*, 27(2):125–141, 1998.

[37] H.-M. Gutmann. A radial basis function method for global optimization. *Journal of Global Optimization*, 19:201–207, 2001.

[38] J. F. Hall, T. H. Heaton, M. W. Halling, and D. J. Wald. Near-source ground motion and its effects on flexible buildings. *Earthquake Spectra*, 11(4):569–605, 1995.

[39] T. Hashimoto, K. Fujita, M. Tsuji, and I. Takewaki. Innovative base-isolated building with large mass-ratio tmd at basement for greater earthquake resilience. *Fut Cit & Env*, 1(9), 2015.

[40] T. H. Heaton, J. F. Hall, D. J. Wald, and M. W. Halling. Response of high-rise and base-isolated buildings to a hypothetical ¡i¿m¡/i¿¡sub¿w¡/sub¿ 7.0 blind thrust earthquake. *Science*, 267(5195):206–211, 1995.

[41] R. Hejal and A. K. Chopra. Earthquake response of torsionally coupled, frame buildings. *Journal of Structural Engineering*, 115(4):834–851, 1989.

[42] G. W. Housner, L. A. Bergman, T. K. Caughey, A. G. Chassiakos, R. O. Claus, S. F. Masri, R. E. Skelton, T. T. Soong, B. F. Spencer, and J. T. P. Yao. Structural control: Past, present, and future. *Journal of Engineering Mechanics*, 123(9):897–971, 1997.

[43] D. Hrovat, P. Barak, and M. Rabins. Semi‐active versus passive or active tuned mass dampers for structural control. *Journal of Engineering Mechanics*, 109(3):691–705, 1983.

[44] K. Ikago, K. Saito, and N. Inoue. Seismic control of single-degree-of-freedom structure using tuned viscous mass damper. *Earthquake Engineering & Structural Dynamics*, 41(3):453–474, 2012.

[45] K. Ikago, Y. Sugimura, K. Saito, and N. Inoue. Modal response characteristics of a multiple-degree-of-freedom structure incorporated with tuned viscous mass dampers. *Journal of Asian Architecture and Building Engineering*, 11(2):375–382, 2012.

[46] J. A. Inaudi, G. Leitmann, and J. M. Kelly. Single‐degree‐of‐freedom nonlinear homogeneous systems. *Journal of Engineering Mechanics*, 120(7):1543–1562, 1994.

[47] *Development of V-Shaped Hybrid Mass Damper and its Application to High-Rise Buildings*, volume Volume 3C: 15th Biennial Conference on Mechanical Vibration and Noise — Vibration Control, Analysis, and Identification, 09 1995.

[48] F. Jabbari and J. E. Bobrow. Vibration suppression with resettable device. *Journal of Engineering Mechanics*, 128(9):916–924, 2002.

[49] R. S. Jangid and T. K. Datta. Nonlinear response of torsionally coupled base isolated structure. *Journal of Structural Engineering*, 120(1):1–22, 1994.

[50] L. M. Jansen and S. J. Dyke. Semiactive control strategies for mr dampers: Comparative study. *Journal of Engineering Mechanics*, 126(8):795–803, 2000.

[51] L. M. Jansen and S. J. Dyke. Semiactive control strategies for mr dampers: Comparative study. *Journal of Engineering Mechanics*, 126(8):795–803, 2000.

[52] E. A. Johnson, J. C. Ramallo, B. F. Spencer Jr, and M. K. Sain. Intelligent base isolation systems. In *Proceedings of the Second World Conference on Structural Control*, volume 1, pages 367–76, 1998.

[53] H.-J. Jung, K.-S. Park, B. F. Spencer Jr, and I.-W. Lee. Hybrid seismic protection of cable-stayed bridges. *Earthquake Engineering & Structural Dynamics*, 33(7):795–820, 2004.

[54] B. JW, T. Lin, S. Shahi, and N. Jayaram. New ground motion selection procedures and selected motions for the peer transportation research program. Technical report, 03 2011.

[55] M. Kasagi, K. Fujita, M. Tsuji, and I. Takewaki. Automatic generation of smart earthquake-resistant building system: Hybrid system of base-isolation and building-connection. *Heliyon*, 2(2):e00069, 2016.

[56] J. Kelly. *Earthquake-resistant design with rubber*. Springer Publications, 1993.

[57] J. M. Kelly. Base isolation: Linear theory and design. *Earthquake Spectra*, 6(2):223–244, 1990.

[58] M. Khan. *Earthquake-Resistant Structures: Design, Build, and Retrofit*. Elsevier Science, 2013.

[59] H. Kida, Y. Watanabe, S. Nakaminami, H. Tanaka, Y. Sugimura, K. Saito, K. Ikago, and N. Inoue. Full-scale dynamic tests of tuned viscous mass damper with force restriction mechanism and its analytical verification. *Journal of Structural and Construction Engineering (Transactions of AIJ)*, 76:1271–1280, 07 2011.

[60] J. Kim and S. Bang. Optimum distribution of added viscoelastic dampers for mitigation of torsional responses of plan-wise asymmetric structures. *Engineering Structures*, 24(10):1257–1269, 2002.

[61] F. Krimgold. Economic and social impacts of armenia earthquake. In *Proceedings of Tenth World Conference of Earthquake Engineering*, pages 7011–7015, 1992.

[62] I. F. Lazar, S. Neild, and D. Wagg. Using an inerter-based device for structural vibration suppression. *Earthquake Engineering & Structural Dynamics*, 43(8):1129–1147, 2014.

[63] J. Leavitt, J. E. Bobrow, and F. Jabbari. Design of a 20,000 pound variable stiffness actuator for structural vibration attenuation. *Shock and Vibration*, pages 1070–9622, 2008.

[64] J. Leavitt, J. E. Bobrow, F. Jabbari, and J. N. Yang. Application of a high-pressure gas semi-active resettable damper to the benchmark smart base-isolated building. *Structural Control and Health Monitoring*, 13(2-3):748–757, 2006.

[65] A. Leung and H. Zhang. Particle swarm optimization of tuned mass dampers. *Engineering Structures*, 31(3):715–728, 2009.

[66] Y. Li, C. Howcroft, S. A. Neild, and J. Z. Jiang. Using continuation analysis to identify shimmy-suppression devices for an aircraft main landing gear. *Journal of Sound and Vibration*, 408:234–251, 2017.

[67] Y. Li, J. Z. Jiang, and S. Neild. Inerter-based configurations for main-landing-gear shimmy suppression. *Journal of Aircraft*, 54(2):684–693, 2017.

[68] W. Lin and A. Chopra. Understanding and predicting effects of supplemental viscous damping on seismic response of asymmetric one-story systems. *Earthquake Engineering & Structural Dynamics*, 30:1475 – 1494, 10 2001.

[69] N. Makris. Notice of aseismatic arrangements, adapted to structures in countries subject to earthquake shocks. *Transaction of the Royal Scottish Society of Arts*, 7:557–566, 1868.

[70] L. Marian and A. Giaralis. Optimal design of a novel tuned mass-damper–inerter (tmdi) passive vibration control configuration for stochastically support-excited structural systems. *Probabilistic Engineering Mechanics*, 38:156–164, 2014.

[71] S. Mevada and R. Jangid. Seismic response of asymmetric structures with variable dampers. *International Journal of Civil and Structural Engineering*, 3:31–43, 07 2012.

[72] S. Mevada and R. Jangid. Seismic response of torsionally coupled building with passive and semi-active stiffness dampers. *International Journal of Advanced Structural Engineering*, 7, 02 2015.

[73] A. Mokha, M. C. Constantinou, A. M. Reinhorn, and V. A. Zayas. Experimental study of friction‐pendulum isolation system. *Journal of Structural Engineering*, 117(4):1201–1217, 1991.

[74] F. Naeim and J. Kelly. *Design of Seismic Isolated Structures*. John Wiley & Sons, Ltd, 1999.

[75] S. Nagarajaiah and N. Varadarajan. Smart variable stiffness control systems. In S.-C. Liu, editor, *Smart Structures and Materials 2001: Smart Systems for Bridges, Structures, and Highways*, volume 4330, pages 345 – 353. International Society for Optics and Photonics, SPIE, 2001.

[76] I. Nishimura, T. Kobori, M. Sakamoto, N. Koshika, K. Sasaki, and S. Ohrui. Active tuned mass damper. *Smart Materials and Structures*, 1(4):306–311, dec 1992.

[77] A. Okumura, Japan Patent Koukai, H09-177875, 11 July 1997.

[78] J. Ormondroyd and J. D. Hartog. The theory of the dynamic vibration absorber. *Journal of Applied Mechanics*, 50:9–22, 1928.

[79] B. Palazzo, L. Petti, and M. de Ligio. Response of base isolated systems equipped with tuned mass dampers to random excitations. *Journal of Structural Control*, 4(1):9–22, 1997.

[80] L. Petti, G. Giannattasio, M. De Iuliis, and B. Palazzo. Small scale experimental testing to verify the effectiveness of the base isolation and tuned mass dampers combined control strategy. *Smart Structures and Systems*, 6, 01 2010.

[81] D. Pietrosanti, M. De Angelis, and M. Basili. Optimal design and performance evaluation of systems with tuned mass damper inerter (tmdi). *Earthquake Engineering & Structural Dynamics*, 46(8):1367–1388, 2017.

[82] D. C. K. Poon, S. Shieh, L. M. Joseph, and C.-C. Chang. Structural design of taipei 101, the world's tallest building. 2004.

[83] R. Rana and T. Soong. Parametric study and simplified design of tuned mass dampers. *Engineering Structures*, 20(3):193–204, 1998. Structural Control.

[84] A. Reggio and M. De Angelis. Combined primary–secondary system approach to the design of an equipment isolation system with high-damping rubber bearings. *Journal of Sound and Vibration*, 333(9):2386–2403, 2014.

[85] M. Ren. A variant design of the dynamic vibration absorber [3]. *Journal of Sound and Vibration - J SOUND VIB*, 245:762–770, 08 2001.

[86] W. H. Robinson. Lead-rubber hysteretic bearings suitable for protecting structures during earthquakes. *Earthquake Engineering & Structural Dynamics*, 10(4):593–604, 1982.

[87] F. Sadek, B. Mohraz, A. W. Taylor, and R. M. Chung. A method of estimating the parameters of tuned mass dampers for seismic applications. *Earthquake Engineering & Structural Dynamics*, 26(6):617–635, 1997.

[88] K. Saito, Y. Sugimura, S. Nakaminami, H. Kida, and N. Inoue. Vibration tests of 1-story response control system using inertial mass and optimized soft spring and viscous element. 01 2008.

[89] J. Salvi and E. Rizzi. Optimum tuning of tuned mass dampers for frame structures under earthquake excitation. *Structural Control and Health Monitoring*, 22(4):707–725, 2015.

[90] S. Sedhain and A. Giaralis. Enhanced optimal tuned mass-damper-inerter performance for seismic protection of multi-storey buildings via top-storey softening. 09 2019.

[91] A. Shaw, S. Neild, D. Wagg, P. Weaver, and A. Carrella. A nonlinear spring mechanism incorporating a bistable composite plate for vibration isolation. *Journal of Sound and Vibration*, 332(24):6265–6275, 2013.

[92] W. Shen, A. Niyitangamahoro, Z. Feng, and H. Zhu. Tuned inerter dampers for civil structures subjected to earthquake ground motions: optimum design and seismic performance. *Engineering Structures*, 198:109470, 2019.

[93] M. Smith. Synthesis of mechanical networks: the inerter. *IEEE Transactions on Automatic Control*, 47(10):1648–1662, 2002.

[94] M. Smith. Force-controlling mechanical device., US Patent 7,316,303, 2001.

[95] P. Somerville, S. NF, S. Punyamurthula, and S. JI. Development of ground motion time histories for phase 2 of the fema/sac steel project. 01 1997.

[96] T. Soong and M. Costantinou. Passive and active structural vibration control in civil engineering. Springer-Verlag:Wien, 2014.

[97] B. F. Spencer and S. Nagarajaiah. State of the art of structural control. *Journal of Structural Engineering*, 129(7):845–856, 2003.

[98] Y. Sugimura, W. Goto, H. Tanizawa, T. Nagasaku, K. Saito, T. Ninomiya, and K. Saito. Response control effect of hi-rised steel building structure using tuned viscous mass dampers. *AIJ Journal of Technology and Design*, 18:441–446, 06 2012.

[99] N. Swift and D. Wagg. A fluid inerter with variable inertance properties. In *6th European Conference on Structural Control*, 2016.

[100] S. J. Swift, M. C. Smith, A. R. Glover, C. Papageorgiou, B. Gartner, and N. E. Houghton. Design and modelling of a fluid inerter. *International Journal of Control*, 86(11):2035–2051, 2013.

[101] M. D. Symans, F. A. Charney, A. S. Whittaker, M. C. Constantinou, C. A. Kircher, M. W. Johnson, and R. J. McNamara. Energy dissipation systems for seismic applications: Current practice and recent developments. *Journal of Structural Engineering*, 134(1):3–21, 2008.

[102] M. D. Symans and M. C. Constantinou. Semi-active control systems for seismic protection of structures: a state-of-the-art review. *Engineering Structures*, 21(6):469–487, 1999.

[103] I. Takewaki, S. Murakami, S. Yoshitomi, and M. Tsuji. Fundamental mechanism of earthquake response reduction in building structures with inertial dampers. *Structural Control and Health Monitoring*, 19(6):590–608, 2012.

[104] T. Taniguchi, A. Der Kiureghian, and M. Melkumyan. Effect of tuned mass damper on displacement demand of base-isolated structures. *Engineering Structures*, 30(12):3478–3488, 2008.

[105] J. Touaillon. Device for damping vibration bodies, Feb. 15 1870. U.S. patent No. 99,973.

[106] H.-C. Tsai. The effect of tuned-mass dampers on the seismic response of base-isolated structures. *International Journal of Solids and Structures*, 32(8):1195–1210, 1995.

[107] United States Geological Survey. *USGS Fact Sheet 068-03: Reducing Earthquake Losses Throughout the United States*. U.S. Department of the Interior, U.S. Geological Survey, Virgina, 2003.

[108] I. Venanzi, L. Ierimonti, and A. Materazzi. Active base isolation of museum artifacts under seismic excitation. *Journal of Earthquake Engineering*, 24, 03 2018.

[109] R. Villaverde. Reduction seismic response with heavily-damped vibration absorbers. *Earthquake Engineering & Structural Dynamics*, 13(1):33–42, 1985.

[110] R. Villaverde. *Fundamental Concepts of Earthquake Engineering*. 1st Edition, CRC Press., 2009.

[111] R. Villaverde and L. A. Koyama. Damped resonant appendages to increase inherent damping in buildings. *Earthquake Engineering & Structural Dynamics*, 22(6):491–507, 1993.

[112] F.-C. Wang, M.-F. Hong, and C.-W. Chen. Building suspensions with inerters. *Proceedings of the Institution of Mechanical Engineers, Part C: Journal of Mechanical Engineering Science*, 224(8):1605–1616, 2010.

[113] F.-C. Wang, M.-F. Hong, and T.-C. Lin. Designing and testing a hydraulic inerter. *Proceedings of the Institution of Mechanical Engineers, Part C: Journal of Mechanical Engineering Science*, 225(1):66–72, 2011.

[114] F.-C. Wang, C.-H. Lee, and R.-Q. Zheng. Benefits of the inerter in vibration suppression of a milling machine. *Journal of the Franklin Institute*, 356(14):7689–7703, 2019. Special Issue on Inerter-based Systems.

[115] F.-C. Wang, M.-K. Liao, B.-H. Liao, W.-J. Su, and H.-A. Chan. The performance improvements of train suspension systems with mechanical networks employing inerters. *Vehicle System Dynamics*, 47(7):805–830, 2009.

[116] J.-F. Wang, C.-C. Lin, and C.-H. Lian. Two-stage optimum design of tuned mass dampers with consideration of stroke. *Structural Control and Health Monitoring*, 16(1):55–72, 2009.

[117] Y.-P. Wang, M.-C. Teng, and K.-W. Chung. Seismic isolation of rigid cylindrical tanks using friction pendulum bearings. *Earthquake Engineering & Structural Dynamics*, 30(7):1083–1099, 2001.

[118] G. B. Warburton. Optimum absorber parameters for various combinations of response and excitation parameters. *Earthquake Engineering & Structural Dynamics*, 10(3):381–401, 1982.

[119] Y. Wen, Z. Chen, and X. Hua. Design and evaluation of tuned inerter-based dampers for the seismic control of mdof structures. *Journal of Structural Engineering*, 143(4):04016207, 2017.

[120] N. Wongprasert and M. D. Symans. Experimental evaluation of adaptive elastomeric base-isolated structures using variable-orifice fluid dampers. *Journal of Structural Engineering*, 131(6):867–877, 2005.

[121] P. Xiang and A. Nishitani. Optimum design for more effective tuned mass damper system and its application to base-isolated buildings. *Structural Control and Health Monitoring*, 21(1):98–114, 2014.

[122] Z. Xu, A. K. Agrawal, and J. N. Yang. Semi-active and passive control of the phase i linear base-isolated benchmark building model. *Structural Control and Health Monitoring*, 13(2-3):626–648, 2006.

[123] L. Y. *Probabilistic Theory of Structural Dynamics*. McGraw-Hill, New York, 1967.

[124] J. Yang, A. Danielians, and S. Liu. Aseismic hybrid control system for building structures under strong earthquake. *Journal of Intelligent Material Systems and Structures*, 1(4):432–446, 1990.

[125] J. N. Yang, J. Bobrow, F. Jabbari, J. Leavitt, C. P. Cheng, and P. Y. Lin. Full-scale experimental verification of resetable semi-active stiffness dampers. *Earthquake Engineering & Structural Dynamics*, 36(9):1255–1273, 2007.

[126] J. N. Yang, J.-H. Kim, and A. K. Agrawal. Resetting semiactive stiffness damper for seismic response control. *Journal of Structural Engineering*, 126(12):1427–1433, 2000.

[127] H. Yoshioka, J. C. Ramallo, and B. F. Spencer. “smart” base isolation strategies employing magnetorheological dampers. *Journal of Engineering Mechanics*, 128(5):540–551, 2002.

[128] N. Youssef. Supertall buildings with tuned mass damper. *The Structural Design of Tall Buildings*, 3(1):1–12, 1994.

[129] R. Zhang, Z. Zhao, and K. Dai. Seismic response mitigation of a wind turbine tower using a tuned parallel inerter mass system. *Engineering Structures*, 180:29–39, 2019.

[130] S. Y. Zhang, J. Z. Jiang, and S. Neild. Passive vibration suppression using inerters for a multi-storey building structure. *Journal of Physics: Conference Series*, 744:012044, sep 2016.

[131] S. Y. Zhang, J. Z. Jiang, and S. Neild. Optimal configurations for a linear vibration suppression device in a multi-storey building. *Structural Control and Health Monitoring*, 24(3):e1887, 2017. e1887 STC-16-0018.R2.